The Formulation of a Novel Control Framework for Regulation of an Active Low Voltage Network

Prepared by:

Mobolaji Oladipupo Windapo

WNDMOB001

Department of Electrical Engineering

University of Cape Town

Supervised by:

Dr. David Oyedokun

Department of Electrical Engineering

University of Cape Town

A dissertation submitted in fulfilment of the requirements for the Degree of Master of Philosophy (MPhil) in Electrical Engineering

Declaration

I know the meaning of plagiarism and declare that all the work in the document, save for the properly acknowledged and the normal guidance of my supervisor, is my own.

Signature of the author:

Mobolaji Oladipupo Windapo

Department of Electrical Engineering,
University of Cape Town,
South Africa
April 2022

ABSTRACT

The low voltage (LV) Network has become more complex due to the addition of loads like Electric Vehicles (EVs) and generation from Renewable Energy Sources (RES). These additions will result in power quality issues arising from excess supply or load unbalance. As LV networks and power systems were not designed with these entities in mind, scalable and flexible mitigation strategies will be needed to tackle these problems. This general conclusion was determined in the literature.

This dissertation presents the implementation of a novel framework established to solve these problems. The proposed framework consists of a Multi-Agent Control System (MAS) to coordinate the various independent entities (agents) and a Thévenin Equivalent Impedance (TEI) based estimator to measure real-time load unbalance towards determining optimal currents in real-time and adjust supply/demand optimally to minimize losses.

A test network was developed to compare systems making use of the same MAS-generated charging scheme (for the ESS and EV) but with different modes of phase power injection, BPI (Balanced Power Injection), and OPI (Optimal Power Injection).

The study reveals OPI minimizes transmission losses by exploiting the transmission lines with lower impedance. Also, the impact of OPI on the network voltage is minimal as seen in phase voltage unbalance rate (%PVUR) figures, this means the extra unbalance introduced by OPI is negligible. Based on the findings the study concludes that the integration of MAS and OPI (guided by TEI parameter estimations) is a feasible combination and an improvement on the existing frameworks as it minimizes losses.

ACKNOWLEDGEMENTS

I want to thank my supervisor **Dr David Oyedokun** for guiding me in my research, **Dr Simona Ruggeri for her** assistance in conducting research, **Mr George Gabriels** for assisting, contributing, and working together on various experiments, Dr Oludamilare Adewuyi for helping me proof read my document and finally, Prof Abimbola Windapo for giving me the opportunity to conduct this research.

Contents

Figures

Tables

Nomenclature

- MAS - Multi-Agent Systems
- ACL – Agent Communication Language
- FIPA – Foundation for Intelligent Physical Agents.
- DG - Distributed Generation
- DGs – Distributed Generators
- EV - Electric Vehicles
- PEC - Plug-in Electric Vehicle
- PCC – Point of Common Coupling
- ESS - Energy Storage Systems
- DSO - Distributed System Operator
- AD - Active Demand
- PV - Photo Voltaic
- RES - Renewable Energy Source
- MGCC - Microgrid Central Controller
- LV - Low Voltage
- MV - Medium Voltage
- HV - High Voltage
- LC - Local Controllers
- EI-DG - Electronically Interfaced Distributed Generation
- PVUR - Phase Voltage Unbalance Rate
- PF – Power Factor
- OPI – Optimal Power Injection
- BPI – Balanced Power Injection

1 Introduction

1.1 Background

Due to the effects of climate change and the exponential increase in carbon emissions within the last century, there has been a push to rely less on fossil fuel as the primary source of energy, resulting in an increased demand for renewable energy-based power generation.

The increased electrical demand and distributed generation at the LV level has resulted in the LV network dealing with a situation it was not designed for, and as a result, there could be voltage variation that could negatively affect the quality of supply and increases technical losses. The combination of renewable energy source (RES) intermittency and variability increases problems related to power quality and reliability that in the past could be resolved through costly measures like reinforcing grid assets or preventing the connection of new power plants [1]. Conventional LV networks could reach performance limits due to voltage surges or voltage increases leading from increased power generation. Considering this, the best way to deal with the rapid growth of inverter driven distributed power generation and minimize losses is to adopt a suitable control strategy to optimally inject and draw currents from a multi-phase power system. [2].

Most existing networks were built with centralized generation in mind, with the notion of electricity flowing in one direction only, from large generation plants to passive consumers. Distributed generators typically connect to the LV grid rather than the transmission network (HV/MV). Therefore, a change in control philosophy would entail seeing distributed networks no longer as passive appendages to the larger transmission network but as an active network with two-way flows of electricity that will need its management strategy [2].

More sophisticated control allows for the LV network distributed generation to be scalable and more complex, and improve its performance, notably by maximizing the return on the capital-intensive investment [2]. By optimizing utilization of infrastructure capacity, control drives up output volume and performance and lowers the unit cost of production. Rather than producing the traditional economies of scale, speed, and scope, effective control contributes to the economies of the system [2].

1.2 Objective

The objective of this research is to:

- Investigate and implement a control strategy that will inject and extract optimal energy contribution from PV-based renewable energy sources, electric vehicles (EVs), and energy storage systems (ESSs) into or from various independent nodes.

1.3 Scope and Limitations

- The study was limited to the LV network.
- ESSs and PVs were only considered as alternative energy sources to the 3-phase voltage source. Other energy sources such as diesel generators were not considered.
- The unbalance of transmission lines and unbalanced loads are considered.
- Communication technology and techniques between agents were not given focus.
- Power from the MV/LV transformer is uni-directional.

1.4 Problem Statement

As the global community becomes increasingly reliant on non-fossil fuels for power generation, the penetration of LV PV generation and non-carbon transportation (EVs specifically) will increase. The LV network, however, was not designed with this in mind. This poses a problem for Distributed System Operators (DSOs). The result is that there can be an under-voltage due to too much current being drawn (for example, multiple EVs charging simultaneously) and not enough supply, or there can be an over-voltage from the PV contributions because there is not enough demand or the time coincidence of PV generation in a local area is very high, this could overwhelm the LV network.

It is possible to either reinforce the LV grid, which is costly, or to manage the resources to ensure there is consistent power that meets the expected demand and can deal with variations caused by the Active Demand (AD). Therefore, this research investigated the solutions available using intelligent resource management.

1.5 Hypothesis

A Multi-Agent System (MAS) enabled by Thevenin parameter estimations is a feasible solution for the regulation/control of a distributed and unbalanced LV network to minimize losses in an unbalanced network with multiple independent entities

1.6 Research Questions

The five research questions listed provided a framework for the literature review and the research towards addressing the hypothesis.:

1. What are the similarities and differences between centralized system control and decentralized (MAS) power control?
2. What kind of design strategies has been used for proactive power control using MAS in an LV network?
3. What are the costs of using proactive agents (cognitive) and reactive agents (reflective) in a MAS, and which ones are needed for this task?
4. What are the impacts of network unbalance?
5. What is the impact of trying to determine the Thevenin Equivalent Impendence at different nodes simultaneously?

1.7 Plan of Development

The Problem Statement is stated, which is used to develop a hypothesis. Some relevant theory is discussed, and the literature studied is reviewed and presented. The methodology derived from this literature review is discussed, and a simulation protocol is formed. Results from this simulation are presented and discussed, based on which conclusions are made.

2 Literature Review

A literature review was conducted on various concepts such as distributed generation, centralized and decentralized control systems, Multi-Agent Systems (MAS), Multi-agent organization, MAS Infrastructure, Unbalanced systems, and Thevenin Equivalent circuits.

2.1 Distributed Generation

Distributed Generation (DG), also known as embedded generation, dispersed generation, and embedded generation, is an electric power source connected directly to the distribution network or on the customer side of the meter. The category of distributed generation does not define the rating of the generation source (meaning it is not absolute), as the maximum rating depends on the local distribution network conditions (voltage rating, for example) [3].

Technology like solar panels and battery storage are becoming cheaper to manufacture, making them a more economically viable alternative to generate and store power. This pushes their distribution at dispersed points of interest on a network, including at the point of consumption (LV level) [4], ESSs are used more in power systems where RESs are integrated. ESSs are needed since, between production and consumption, there is a gap in time between where the energy is produced and where the energy is required. This is because the issues of power generation volatility (because of their intermittency) of RESs and the variability of consumer demands (across the day) can be mitigated with increased ESS use. ESSs can participate in frequency control and represents a flexible solution to supply the demands in power systems [5], meaning ESSs can be used as sources of backup power, ensure the voltage is within DSO limits, by storing excess power from RES stations and discharge at a later point of higher demand.

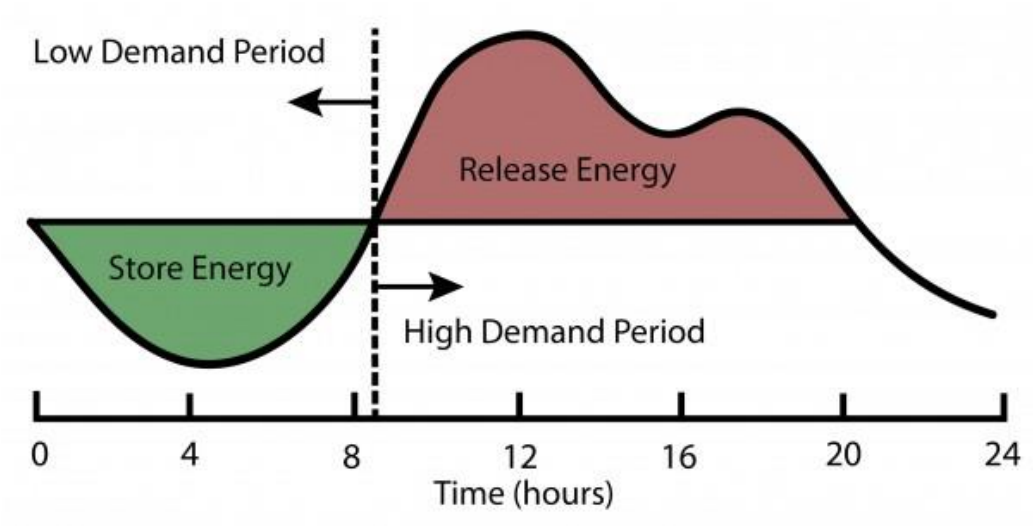

Figure 2-1: Daily load levelling and energy storage. [6]

Figure 2-1 shows a load demand curve and PV generation curve over 24 hours. It shows the excess energy generated by the PV can be stored by ESSs and used in the evening.
Integration of ESSs has economic benefits as they siphon excess power from RESs (that were not considered during the development of LV network infrastructure) and reduce the strain on the LV network transmission line, which helps reduce I^2R losses due to excess current (which causes the transmission lines to experience heat) and prevents costly infrastructure expenditure [5].

While there is existing literature that covers the utilization of MAS to manage LV networks and microgrids, there has not been any literature surrounding the use of converters/chargers that transfer power with Thévenin parameter estimation as an enabler. Therefore, answering the last question was done via experiment since the converter in question was built at UCT. Also, the fifth research question, what is the impact of trying to determine the Thévenin Equivalent Impedance (TEI) at different nodes simultaneously, was answered in the methodology and it affected how the MAS design was done.

Since more users are choosing to be prosumers (energy producers and consumers) and are changing the behaviour of the formerly passive LV network, making it more active like a smart grid/microgrid

2.2 Differences between centralized and decentralized systems

The challenge of future networks is the increasing complexity of the LV networks, with increased penetration of DERs (which can result in voltage unbalance due to the emergence of independent distributed entities [7]), energy storage systems, and Electric vehicles (EVs). This increased complexity requires regulators to engage in more complex control, and the organization of that control is essential. There are two main methods of network control/management, which are decentralized and centralized control architecture (note that this is not a binary but a spectrum of implementation, an adequate solution would make use of the strengths and weaknesses of both methods) [8]. A decentralized system is one where entities on a lower rung of a system hierarchy make use of information within their immediate vicinity (local information) to achieve broader system objectives (global). A centralized system is where both local and global information is sent to a singular entity to solve both local and global problems [8] and [9].

The following section discusses the computational costs and engineering complexity, as these are the most significant distinctions between the two main methods of network control.

2.2.1 Computational costs

The key computational differences between decentralized and centralized system management are the level of computational responsibility allotted to a central entity and the level of independence that entities on a lower rung of the network hierarchy are given. This divergence emerges in how quickly the control system can solve a given problem and how quickly it can adapt to changes in the environment.

In [10], a decentralized system (MAS) is compared to a centralized system in a laboratory experiment. The task assigned to the management system is to effectively charge a large population of EVs. The equipment used for both approaches was not the same; the centralized system makes use of a CPU with a 3.1 GHz clocking speed and a RAM of 8 GB, while the decentralized system (MAS) has each EV charging unit (agent) with a CPU that has 400 MHz clocking speed and a RAM of 64 MB. This means the centralized unit has 7.75 times the processing speed and 128 times the memory of a single unit in the decentralized system.

Both approaches give similar solutions to the power management of the population of EVs. Still, the distinctions emerge when examining how long it took for the system to determine that optimal answer. The results of this experiment are shown in Figure 2-2.

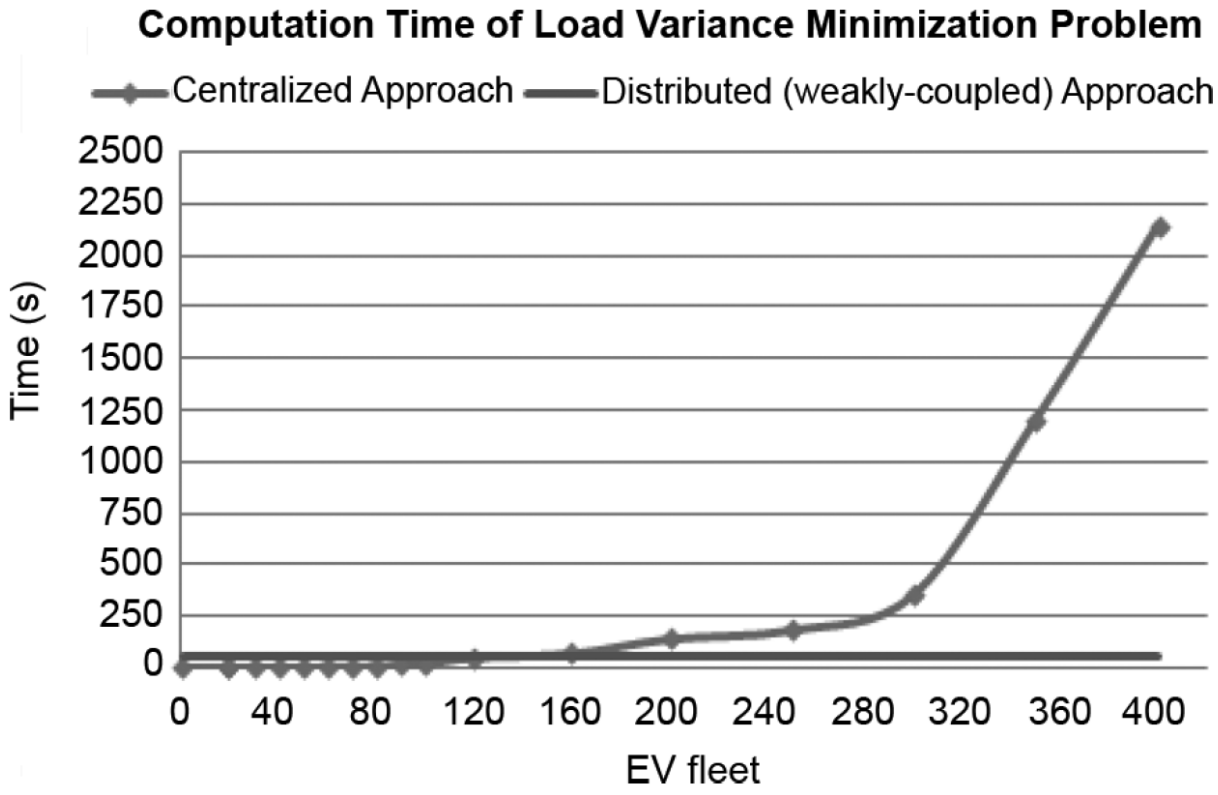

Figure 2-2: A chart comparing the computation time of a centralized and decentralized system [10]

Figure 2-2 shows that the centralized system had better performance initially but became exponentially more inefficient when compared to the distributed approach. It is worth noting that more advanced hardware would easily improve the performance of the centralized system (the same can be said for a decentralized system). However, the fact remains that the centralized system would still depend on the number of EVs in the system, meaning the point at which the two graphs cross is just shifted to a later point across the X-axis. The more distributed approach is far less dependent on the number of EVs and shows a significant level of scalability that decentralized systems offer. Another reason for this difference is that centralized management platforms suffer from an information processing bottleneck [8]. This is also in part due to the magnitude of information having to be received, processed, and optimized [11] all by a single entity instead of the decentralized approach limits data exchange (between entities) to only the most essential parameters, which can help limit the cost of communication infrastructure [11] and [12].

The literature review reveals that a more distributed system fairs much better than a centralized one since it is a more scalable system and more cost-effective system, which would require smaller computation and communication overhead.

2.2.2 Engineering Complexity

When it comes to implementing a centralized and decentralized system, the critical difference is how the various parameters of the system are modeled, hardware cost , and user integration. These factors determine how scalable and robust each approach is, which is necessary to deal with the current challenges being faced by LV networks.

The modeling of an environment for distributed and centralized systems are not necessarily different from each other (provided the environment is constant), with a good example being the systems in [10] and [13], what changes are how detailed each approach is and how many parameters can be considered and optimized. In a centralized system with only one intelligent singularity exists to analyze all the available data (global and local) [9] in a network (an example would be the current through lines, harmonics, the voltage at buses, or ESS/EV battery charge levels). In contrast, a more decentralized system can consist of more autonomous entities at lower levels to handle local data and a possible singularity to handle global data [10]. This would be a complex issue for a centralized system. If the network were to be modified, expanded, or separate independent entities were to be added to it (for example, the increasing network demand and the addition of another feeder), it will be necessary to implement modifications to the centralized database and software code [9]. A system with more local autonomous entities can identify a failure (due to immediate access of its local data) and react accordingly and possibly even replicate itself (due to the redundancy present in MAS) [14].

In a centralized approach, all information is communicated to a central entity for analysis requiring more powerful and expensive hardware (as seen in [10]). In comparison, a decentralized system would require lighter computational resources that are distributed at a much lower cost than the centralized system, which can be observed in [10] [9]. To minimize the cost of a centralized control architecture, an option is to create a simplified description of the system and obtain results that would probably be suboptimal [11].

Note that all the centralized proposals assume that the charging of EVs, ESSs, or any other entity in the network is a public utility, meaning all entities in the network are under network ownership which is very unlikely [15]. In a centralized system, network control usually means assessing the capacity of the system to supply electricity to its users. In a disaggregated system with multiple independent power producers (IPPs), control requirements were far more complex, owing to many involved parties with conflicting interests [2]. This is most visible with EVs, which will be under more fragmented ownership due to cars being owned by individuals, owners who are reluctant to allow an outside entity to control how their EV charges (or share their data with a public source). The key issue for independent users is that centralized control is very closed off and a more open distributed approach allows users of EVs, ESSs and DER units to attach their programmable units that can operate within a decentralized control system [11].

2.2.3 Section Summary

The literature reinforces a preference for a more distributed approach (for this thesis problem) as this approach allows for a system that is flexible and open to consumers and meets their requirements that can vary widely. It is very robust and scalable as it would not require too much modification from a hardware and software point if there are to be modifications to the system, allowing it to handle a more complex active network that is very likely subject to change.

2.3 Multi-Agent Systems Overview

This section will give a brief discussion of MAS basic concepts and approaches. It will go into the benefits of MAS in power engineering and its application to DGs in a LV network-like environment (microgrids).

2.3.1 Concepts: Terminology and Definitions

A multi-agent system (MAS) comprises two or more agents. There is no overall system goal, simply the local goals of each separate agent. The system designer's intentions can only be realized by including multiple agents, with local goals corresponding to subparts of that intention [14]. While the definition of a MAS is solid, the definition of the components that make up the system, *agents*, is not as straightforward.

2.3.1.1 A Definition of Agency

The computer science community has generated many definitions for what an *agent* is. The existence of various definitions shows the difficulty in defining the notion of agency. While the multiple explanations of what an agent is differs, they share a basic set of concepts: the idea of an *agent*, its *environment* (everything external to the agent), and the property of *autonomy*. [14]

It is essential to note the separation of the agent (like a power converter) and its environment (a LV network in the case of this research) in the conceptualization since agents are the entities changing the environment. This makes it clear that moving an agent or placing multiple agents in a particular environment does not alter its (local) goals it needs to meet or the type of reasoning it will be acting under but will only affect its observations (input from the environment) and its response (output) [14]. An example would be the varying power demands on different feeders in an LV network or the different cable power ratings on other feeders in an LV network. This means an agent can operate so long as it is in the right environment [14].

An *agent* is operating in an *environment* when it can observe a part of it (being able to determine the Thevenin equivalent of an LV network, observing the nodal voltage at a PCC, for example) and/or is changeable by the agent (for example power flow in an LV network, demand in a network). An *environment* can be physical (like the LV network), or it may be the computing environment (data sources, yellow pages containing a list of agents for the system) [14].

An *agent*, according to Wooldridge, is an entity that reacts *autonomously* in a changing *environment* [14], but autonomy is not a well-defined term. The broadest definition of autonomy is the ability of an entity to exercise control over its actions in response to a change in its environment and not due to the entity (agent) in-built (preprogrammed) knowledge, from Wooldridge, Norvig, and Russell. Therefore, autonomy is the ability to schedule action based on environmental observations [14].

2.3.1.2 Definition of an Intelligent Agent

The issue with this definition of agency, from an engineering perspective (and a source for confusion in this project), is that many existing entities already meet the requirements that determine they have agency and can be classified as an *agent* [14]. An example would be a home-based inverter power supply (a system that uses mains supply to charge up deep cycle batteries and, in the case of a power outage, automatically backs up power in the home with little interruption): it is operating within an *environment* (the house), it can observe the environment (detect if there is power coming from mains or not), and change the state of that environment (give power if power quality from mains is bad or act a back-up power completely) without interference, exhibiting *autonomy*. Renaming existing entities as agents offer nothing new. It is crucial to make this distinction since it will help highlight how MAS varies from already existing systems [14]. These differences and their advantages help justify MAS as a solution to the research problem.

To create this distinction, Wooldridge extends his concept of an *agent* to an *intelligent agent* by expanding the definition of *autonomy* to *flexible autonomy* [14]. *Flexible autonomy* has the following three characteristics:

1. **Reactivity**: an *intelligent agent* can take inputs from the environment and will promptly output for it.
2. **Pro-activeness**: An intelligent agent will show goal-directed behaviour. Goal-directed behaviour means the intelligent agent will dynamically adjust its behaviour to achieve its goal [14]. An example would be two battery-charging stations on a feeder, and one of them went offline. The remaining station would adjust its power consumption to meet its charge requirement.
3. **Social ability**: intelligent agents interacting with each other [14]; this does not simply mean communication (data transfer) but also the cooperation of intelligent agents with other intelligent agents within an environment to change that environment. An example would be the buying and selling of energy between two nodes in an LV network.

To surmise, *intelligent agents* distinguish themselves through their *cognitive* behaviours such as *Pro-activeness* and *Social ability*, while *agents* (many hardware and software entities that already exist) only exhibit reactivity. This distinction between intelligent agents and agents helps to highlight the value of MAS compared to other systems.

2.3.2 The Benefits of MAS Technology and Motivation for application in Power Engineering.

The motivation and means for utilizing MAS in power engineering require a basic understanding of the fundamental ways MAS can be exploited. MAS is usually used in two ways: as an approach to building flexible and extensible hardware/software systems and as a modelling approach (which is not the focus of this dissertation) [14].

2.3.2.1 A. MAS as an Approach to the Construction of Robust, Flexible, and Extensible Systems

There are many power engineering application areas for which flexible and extensible solutions are beneficial.

Flexibility means the ability to react accordingly to changing situations. While the characteristics of agency (autonomy) mean an entity can schedule its actions, flexibility relates to having several possible steps to select the most correct. An example of flexible behaviour is if an agent cannot reach a local goal within a set of constraints and/or a set amount of time; then the agent's local goals can be relaxed to meet global goals for the MAS.

Extensibility connotes the ability to easily add new features to a system, augmenting or upgrading existing functionality [14]. Suppose the charging of an ESS in an LV network does not consider battery degradation as a constraint or temperature as a factor. This feature can be added to the intelligent agent charging the ESS, or the agent can be replaced with an updated agent without affecting the rest of the MAS. Notably, a truly extensible system will allow new functionality to be added without the need to re-implement the existing functionality [14].

Fault tolerance is also a requirement for many power engineering applications. If a portion of a designed system should fail, the system should still meet its design objective.

MAS can provide a way of building such systems. The ability of MAS to be flexible, extensible, and fault-tolerant is often part of the justification for their use [14]. However, for that justification to be valid, how does a MAS provide flexibility, extensibility, and fault tolerance.

The properties of agents and MAS that produce these qualities are examined in the following section.

2.3.2.2 Benefits of Autonomy and Agent Encapsulation

The autonomy of intelligent agents in a MAS encapsulates a particular function similar to object-oriented programming [14]. This means the agent can take requests or messages, through a standard ACL, from other agents in the MAS while the other agent(s) are oblivious of the agents' internal workings or goals. A MAS consists of a service agent(s) (Directory Facilitator) that acts as a yellow page, with information on other agents present in the MAS that can be accessed by the agents. This is beneficial because:

- The agent autonomy that results in no direct link between agents allows for flexibility and scalability.
- It allows for easy integration of extra functionality simply by deploying new agents who can use the service agent(s) to access other agents in the MAS.
- The flexibility allows for deploying a diverse mix of agents to deal with individual situations, while flexible handling of messages will enable the system to self-configure.
- Legacy/existing systems can be integrated with the MAS by covering legacy functionality in a layer of agent messaging.

2.3.2.3 Benefits of Open MAS Architectures

Earlier agent systems consisted of a single set of agents with explicitly defined and linked inter-agent communication and intra-agent operation by the system designer. These systems had closed architectures [14]. A closed architecture restricts the origin of agents operating in the system, and there is no separation of an agent's communication and internal operation. This architecture is not suitable to a MAS because intelligent agents are *autonomous* and are therefore separate from the *environment*; this means there needs to be a clear distinction between the agent's communication mechanism and its internal mechanism, an open architecture. The benefit of open architecture is that:

- There is no restriction on the programming language used to build up an agent.

- Agents from different time periods and origins can be added to the system so long as it adheres to the exact communication mechanism.
- There is no restriction on the creation of agents.

The Foundation for Intelligent Physical Agents, FIPA, has set standards for the open architecture operation. The FIPA Agent Management Reference Model covers the "framework within which FIPA agents exist," defining standards for creating, locating, removing, and communicating with agents. This is the *agent platform* and part of an agent's environment. One requirement of an open agent architecture is that some mechanism must be available for locating agents or agents offering services within the platform. Under the FIPA model, this is achieved through a separate agent called the Directory Facilitator (service agent): an agent which manages a searchable list of services offered by other agents within the platform [14].

2.3.2.4 A platform for Distributed Systems

An agent is separate from its environment, which means the agent's internal mechanisms will have the same operation regardless of the environment it is placed inside it. An agent must observe its surrounding environment and respond in which accordingly. Suppose you have an intelligent agent as a converter operating in an LV network. It is moved to a different feeder in the LV network; the converter should adjust its power flow in response to the power flowing in the feeder. For these reasons, agents are inherently distributable, meaning an agent platform must support the distribution of agents across a network.

2.3.3 Application of MAS in Power Engineering

The four broad fields of agent applications in power each use the property of flexible autonomy to bring a new set of techniques and abilities to bear on traditional issues and problems in power engineering.

Based on this, multi-agent systems should be considered for applications that display one or more of the following characteristics;

- There is a requirement for interaction between distinct conceptual entities, such as different control subsystems and plant items (like controlling a microgrid while taking account of thermal constraints, voltage control, and renewable energy sources.)
- Many entities must interact, where it would be impossible to model overall system behaviour explicitly (for example, the charging of EVs and ESSs in an LV network.)
- There is enough data/information available locally to undertake an analysis/decision without the need for communication with a central point (PV linked ESS charging and discharging, for example.)
- New functions need to be implemented within existing plant items and control systems (extending substation-based condition monitoring systems by adding data interpretation functions.)
- Over time, there is a requirement for functionality to be continually added or extended.

The specific benefits of MAS technology for the four fields of application are considered: Monitoring and Diagnostics, Distributed Control, Modeling and Simulation, and Protection.

Distributed control will be expanded on since it fits in line with the themes and the topic of the study.

2.3.3.1 Distributed Control in MAS

With the motivations detailed in section 1.1, the introduction of DGs, AD, decentralised market operation (trading of energy with non-grid sources) has made LV networks more complex. MAS, due to its benefits, has the means and potential to flexibly control more complex networks. Applications currently being investigated in this field include power system restoration, active distribution networks operation and microgrid control.

2.3.4 Technology Challenges of MAS

It is important to identify the critical technical challenges that are yet to be overcome to allow the most effective implementation of multi-agent systems within power engineering, these are:

- **Platforms**: several multi-agent system platforms exist. However, a reasonable selection is required to ensure long-term compatibility and the robustness needed for online applications.
- **Toolkits**: There is a role for toolkits that allow the reuse of existing agent behaviours and capabilities.
- **Intelligent agent design**: there needs to be guidance on how an agent should be designed or knowledge of the available options. These different implementation strategies will produce agents with differing degrees of reactivity, pro-activeness and social ability
- **Agent communication languages (ACLs) and ontologies**: ACLs are the enablers of the social abilities of agents. These define how agents exchange information, communicate and negotiate. Within the ACLs are protocols and content languages which allow meaningful messages to be composed and interpreted. International standards are set by the Foundation for Intelligent Physical Agents (FIPA). The community must agree on the adoption of appropriate agent communication language standards.
- **Data Standards**: the power engineering community has spent significant effort defining data standards for various application areas. For example, the Common Information Model (CIM) for data exchange between Energy Management Systems and related applications [14]. These standards cannot be directly applied for agent communication, as the conversational abilities of agents require a richer language than a data-passing standard. However, there is potential to use them as a foundation for an ontology.
- **Security**: due to the open architecture of agent systems, security is a key concern. If agents are to seamlessly join an agent community, there must be measures to determine the level of trust between agents and the security of messaging. Agents from a rival utility may be offered fewer services, for example, indicating the lower trust placed in them. Similarly, communication between two agents is open to attacks such as sender spoofing and message modification. But this is not an objective of this thesis, so it will not be considered in the design.

2.3.5 Standards and Interoperability

Due to the push for more integration of different systems, there need to be standards when designing MAS. FIPA is the accepted standard for MAS in general. FIPA aims to define specifications and standards that can support interoperability between agent-based systems developed by different actors such as companies and organizations (like other EV charging stations owned by different organizations, RESs plants owned by different organizations) [16]. FIPA acts as the basic architecture for MAS.

2.3.5.1 Multi-agent system architectures

Figure 2-3 shows the FIPA Agent Management Reference Model.

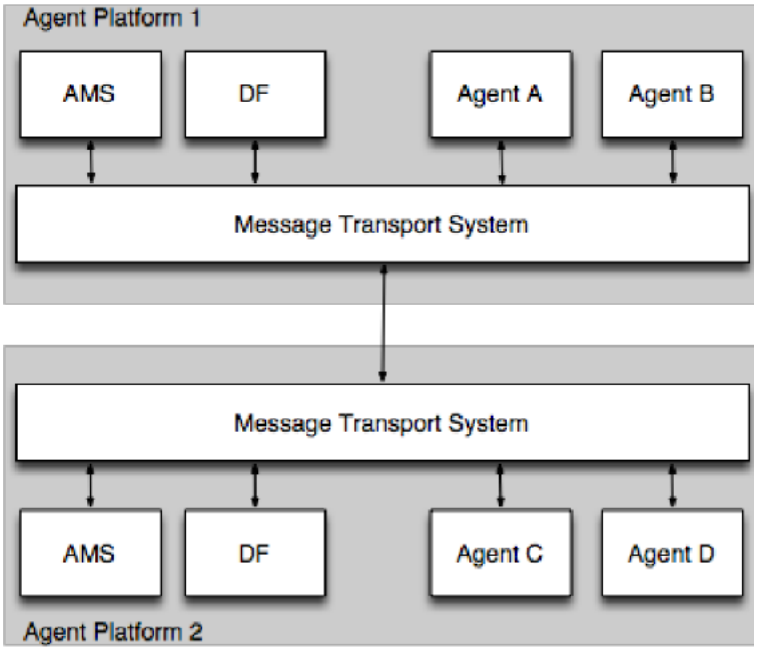

Figure 2-3: The FIPA Agent Management Reference model [16]

The FIPA Agent Management Reference model defines the standard framework within which FIPA agents exist and operate. It establishes the logical reference model for the creation, registration, location, communication, migration, and retirement of agents [16]. Figure 2-3 shows two agent platforms with each containing multiple agents (cognitive), a Directory Facilitator (DF) agent, Agent Management System (AMS) agent, and a message transport system by which the agents communicate with each other. The AMS contains a directory of agents registered with the platform and is a compulsory component, while the DF is optional and includes a guide of agents and the services they can offer other agents. The DF can be accessed by agents to find other agents that perform tasks to help meet their local goals (for

example, an EV looking for an ESS on the same feeder to charge its batteries). The DF and AMS are how MAS is an open architecture since new agents with possibly new functionality can be registered to the MAS at any time. This is good for a changing and expanding network like the active LV network.

2.3.6 Tools for the implementation of agents and MASs

When implementing a MAS, MAS development tools are required. The toolset must comply with the standards to which the developers wish to adhere. Agents implemented using the chosen toolset must display a level of robustness required for the application at hand. The Java Agent Development Framework (JADE) [17] is a favourite among researchers in power engineering. While JADE's support of FIPA standards and the robustness of the agents that can be implemented make it attractive, JADE also promotes a certain style of agent implementation that may not be optimal for exploiting autonomy. Regardless of the agent's internal structure, there is an opportunity to re-use agent designs and functionality for the benefit of the whole community.

2.4 Multi-agent organization overview

The mechanism to implement the decentralized system is the Multi Agent System (MAS), this is a system that consists of at least two autonomous and intelligent entities that work together to achieve a common goal [18].

Multi-agent organization describes how agents are organized to form a MAS. It describes the relationships and interactions among agents and the specific roles of each agent [19]. This section will discuss two organizational frameworks for the MAS: Hierarchal and Flat organization framework [19]. Each organizational framework is discussed, the various proposals (examples in literature) that exist for each of them are discussed, and a general framework is selected.

2.4.1 Hierarchical MAS

Hierarchical MAS are organized such that the agent's communication is governed by the hierarchal structure. This means the agents are not granted full/unrestricted autonomy and must work within a specific pattern to meet their objectives. The advantages of this structure are that

there is no need for a mechanism for agent location (or more specifically, no need for lower-level agents to waste resources and time looking for other agents by making use of the FIPA [17] structure and instead have a dedicated agent that saves it), agents can easily coordinate to meet both local and global objectives and the significant reduction in the amount of communication in the system. The disadvantage of this organization is the strict structure, which does not allow agents to dynamically re-organize themselves to best fit the needs of a specific task [19].

The inability to dynamically reorganize creates a dependency of lower-level agents to depend on higher-level agents and could result in the lower level agents being controlled by higher-level ones [19] (which could be quite similar to centralized control due to the agents being far more reactive, which has been established to be inadequate to meet the needs of an expanding and dynamic LV network), but this could also imply that higher agents might act as guides, and regulators to ensure that all the agent's act considerately (in harmony with) towards each other and their environment, sharing global information or even acting as intermediaries between lower-level agents.

2.4.2 Flat organization of a MAS

The flat organization of a MAS implies that lines of communication between agents are free and free to interact with each other. There is no fixed system structure (the designer's intent is vague). Still, agents can come together to create a new structure dynamically [19], meaning agents are more likely to be proactive and far more autonomous. What this further infers is that no agent has authority over any other agent and cannot be controlled or be regulated.

For such a system to function, it is required that the system be closed off to any additional agents. Each agent is aware of every agent in the system (making it rigid like a centralized system), or there has to be an agent location mechanism (an agent directory [17] and [20]) [19].

The advantages of a system that requires more proactive agents are that the self-interest of the agents is fully supported (like an EV user that wants a very specific charging sequence), a more open MAS system that allows for a more dynamic MAS [19] in the sense that the system can have varying objectives asynchronously (not in the sense of scalability or robustness). These advantages can become disadvantages because the unregulated communication architecture can result in more complex and cost-intensive communication hardware and software. The agents are more proactive and will require more overheads to function.

2.4.3 Framework Selection

Both structures have their advantages and disadvantages, but the hierarchal organization is more suited to meet the objectives of this thesis. The main reason is that the hierarchal organizational structure aligns with the themes of this study to regulate the LV network environment and allow it to handle new additions to the system while keeping the network's performance within regulations. The network has global objectives such as maintaining voltage and harmonic stability while individual (new) actors like EV users have local objectives such as battery charging. A hierarchal system is optimal because it allows for smaller actors (like EV users, IPPs) to pursue their desires (by dynamically setting their objectives) while ensuring they operate within a regulated body [21]. A fully decentralized system would be more complex and would give too much autonomy to induvial actors (which could make setting up a guide or regulations complex) and would require more work done on the part of these actors, which could stand as a barrier preventing them from engaging the MAS due to its complexity. The point of the MAS is to help ensure minimal interference in the network's operations and for other passive users in the network to expect the same service delivery regardless of changes to the network environment. A Hierarchy is preferred as it enables the easy introduction of new actors while ensuring they don't alter or impose their will on the network.

2.4.3.1 Proposal selection

To further reinforce the preference for a hierarchal organization (systems comprised of more reactive agents), ten different proposals were examined. Of these approaches, eight of them made use of the hierarchal multi-agent organization, while two ([22] and [23]) made use of the flat organization.

Four of the reviewed hierarchal models ([1], [10], [24] and [25]) made use of very similar principles. The Nash certainty equivalence (NCE) principle promotes a control scheme that seeks to achieve social optimality by establishing an EV and ESS charging/discharging profiles along with variable load (active demand, AD) optimization.
Implementation of the NCE-based MAS control is achieved through a charging negotiation procedure, which takes place at some time before the actual charging interval:

- A central authority (an agent or a utility) gives an estimation of the inelastic demand to all the lower agents with elastic demand.
- Each of the lower agents conducts optimization based on their own demands and constraints and proposes a new optimized demand profile,
- The central authority collects all the individual optimal strategies proposed and updates the aggregate elastic demand. This updated aggregate elastic demand is sent back to all the lower agents
- Steps 2 and 3 are repeated till there is minimal variation in the elastic profiles of the lower agents.

This approach has a straightforward and approachable structure that only requires basic information and very little communication. Other systems such as [11] and [21] require multiple agents for a single physical LV network entity (EV and ESS) that engage in peer to optimization, often with the selling and buying of energy from each participant. This added layer complicates regulation and adds an unnecessary control layer as the largest market participant is the LV network's inelastic demand.

2.5 MAS System Infrastructure

The MAS operating in the LV network describes the sinking and sourcing of current from the grid through coordination of multiple ESSs and EV which are represented as agents alongside a Master Agent (MA) to form the MAS. The real power to be transferred by all these agents is determined by an optimisation process. The MAS determines the optimal course of action through a weakly-coupled game (NCE) approach, which reaches its completion once the Nash equilibrium has been reached. A Nash equilibrium is when a system with independent participants is in a state where no changes can be made for one participant without affecting others. Figure 2-4 shows the flow diagram of the proposed algorithm.

In the model, each agent takes information to and from the MA, an aggregator that works as an advanced middleman between the DSO and the set of agents [1]. In contrast, the lower agents represent the behaviour of the DER ESS and EV installed in the network. Each agent characterizes the behaviour of the element it represents. For instance, the EV agent represents the behaviour of an EV charging station, considering not only the technical characteristic of the EV (battery size, nominal power) but also the needs of its owner (desired state of charge and time of the end of charging). The ESS represents the behaviour of the ESS itself, which helps manage the voltage level of the network by preventing voltage surges (taking excess solar power by charging) and voltage sags (by injecting stored energy via discharging).

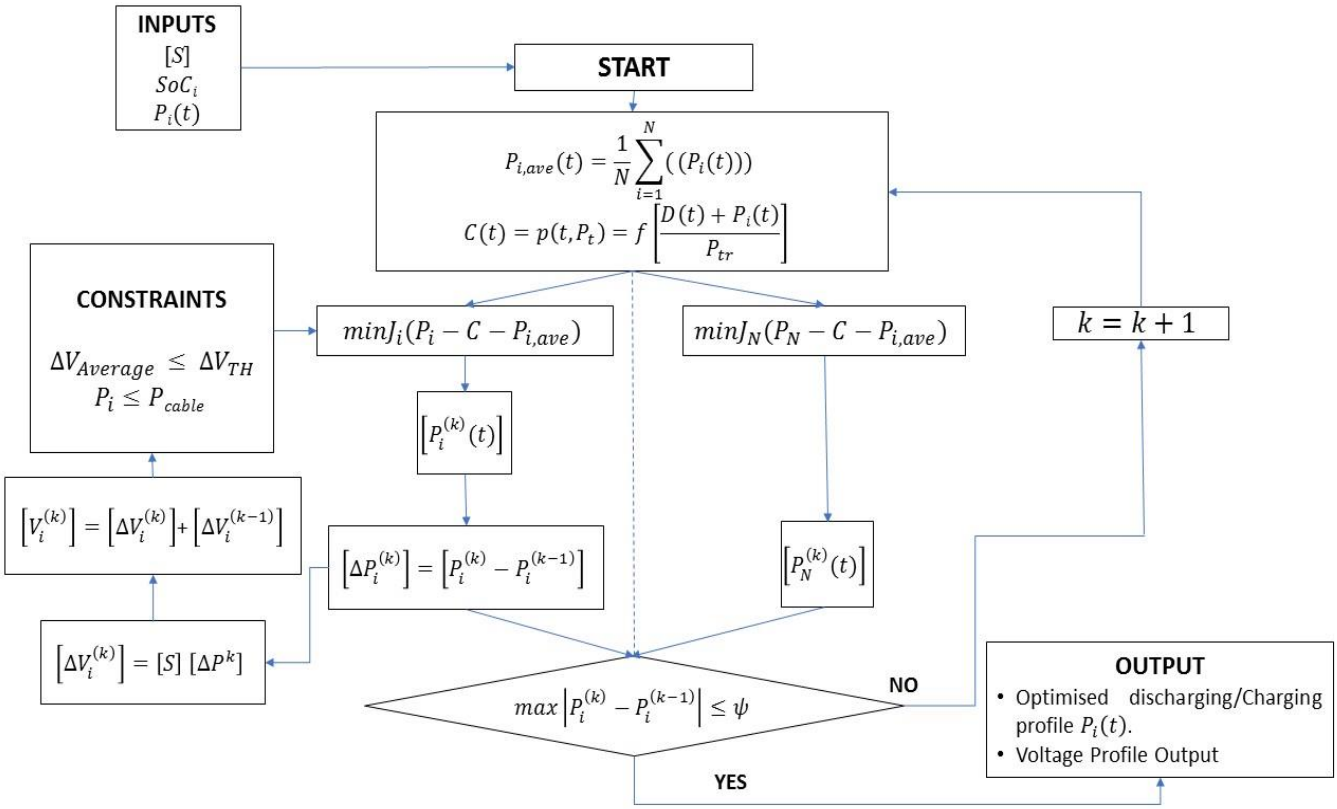

Figure 2-4: The flow diagram of the algorithm proposed in [1], [10], [24] and [25]

The algorithm begins with the ESS and EV agents (agents with elastic demand) sending their initial demand profile ($P_i(t)$ in equation (2-1)) to the MA and the MA using this to determine the virtual cost $p(t,P_t)$ and the average agent demand ($avg(P_t)$ in equation (2-2)) for the ESS and EV agents:

$$p(t,P_t) = f\left(\frac{D(t) + \sum_{i=1}^{N} P_i(t) + D_{PV}(t)}{P_{tr}}\right) \quad (2\text{-}1)$$

$$avg(P_t) = \frac{1}{N}\sum_{i=1}^{N} P_{EV,i}(t) + P_{ESS,i}(t) \quad (2\text{-}2)$$

Where:

- N is the total no. of EV and ESS agents;
- P_{tr} is the nominal power of the MV/LV transformer [kW];

- $D(t)$ is the load demand at time t [kW], this is the sum of demand from all 3 phases in the network;
- $D_{PV}(t)$ is the load demand at time t [kW];

The MA now sends back $avg(P_t)$ and $p(t, P_t)$ to the ESS and EV agents. Each ESS and EV agent performs a mono constrained optimization shown in equation (2-4) with δ (in equation (2-3)) being the tracking parameter [1]:

$$\frac{1}{2c}\max\left(\frac{\mathrm{dp(r)}}{dr}\right) \leq \delta \leq \frac{\mathrm{a}}{\mathrm{c}}\min\left(\frac{\mathrm{dp(r)}}{dr}\right) \quad (2\text{-}3)$$

$$min\, J_i(P_i, P_{-i}) = \sum_{t=0}^{T-1}\{p(t, P_t)\cdot \boldsymbol{P_i(t)} + \delta\cdot[\boldsymbol{P_i(t)} - avg(P_t)]^2\} \quad (2\text{-}4)$$

Where:

- $r = \frac{D(t)+\sum_{i=1}^{N} P_i(t)+D_{PV}(t)}{P_{tr}}$ (2-5)
- δ is the tracking parameter with a nonnegative constant value crucial for Nash's equilibrium;
- c is the capacity of the MV/LV transformer [kW];
- a is a parameter in the range $[\frac{1}{2} - 1]$;
- P_i is the demand of the ith agent [kW];
- P_{-i} is the power of the other agents minus the ith agent [kW];
- T is the final time of the period [24:00];

The optimisation performed in equation (2-4) is done for each phase of the agent i and is subject to voltage and power technical constraints, which are represented by equation (2-6):

$$\frac{\sum_{m=1}^{n} V_m^{(k-1)} + \sum_{m=1}^{n}\frac{\delta V_m}{\delta P_i}\left(P_i^k - P_i^{(k-1)}\right)\cdot KC}{n} \geq (1 - \Delta V_{TH})\cdot V_n \quad (2\text{-}6)$$

Where:

- n is the no. of ESS and EV agents in the same feeder as agent i;

- m is the internal iteration index ($m = 1,2, \dots, n$), considering the voltage variation of other EV and ESS agents in the same feeder;
- k is the external iteration index managed by the MA;
- V_m^{k-1} is the voltage at the agent buses at each of the respective phases in the previous iteration, all in the same feeder as agent i [V];
- KC is a coefficient greater than 1;
- P_i^k is the ith agent contribution at iteration k for each phase[kW];
- V_n is the network voltage base of 230V [V];
- ΔV_{TH} the average variation of the voltage, 0.3 [p.u];
- $\frac{\partial V_m}{\partial P_i}$ Is the coefficient of sensitivity from the Jacobian matrix for agent i for each phase of that agent[V/kW].

While the power constraints is bound by equation (2-7):

$$P_i^k(t) \leq (P_{Z,feeder} - D_{feeder}(t) - D_{PV,feeder}(t)) \cdot \frac{P_{i,rating}}{\sum_n^{m=1} P_{m,rating}}$$

(2-7)

Where:

- $P_{z,feeder}$ is the dynamic line rating of the feeder;
- $D_{feeder}(t)$ is the passive demand on the feeder at the respective phase.
- $D_{PV,feeder}(t)$ is the PV supply on each feeder.
- $P_{i,rating}$ Is the maximum charge rating of agent i.

2.5.1 Battery optimization and constraints

Finally, the MAS needs to ensure that EVs can meet individual customer needs by ensuring that each EV reach a user-defined state of charge ($SOC_i(T_{chag} - 1)$). This is translated in this constraint (equation (2-8)):

$$\sum_{t=0}^{T_{chag}-1} P_i(t) = (SOC_i(T_{chag} - 1) - SOC_i(t = 0)) \cdot \frac{C_{bat}}{C_{eff}}$$

(2-8)

$$|P_i(t)| \leq P_{plug}$$

(2-9)

- Where: T_{chag} is the charging period of the EV [h]
- C_{bat} is the charging capacity of the battery [kWh]
- C_{eff} is the charging/discharging efficiency of the agent
- $SOC_i(t = 0)$ is the initial state of charge
- P_{plug} Is the maximum charging power.

The optimal usage of storage depends not only on instantaneous data but also on the previous and future operational decisions. For this reason, the energy stored until the time t and the charging (or discharging) strategy proposed by the Agent are considered in the optimization process shown in (2-10) [1]:

$$SOC_i(t) = SOC_i(t = 0) + \sum_{t'=t_{in}}^{t} P(t')$$

(2-10)

To avoid overcharging or undercharge, (2-10) is subject to the following technical constraints:

$$SOC_i(t) \leq SOC_{i,max} = k_{max,i} \cdot E_{i,nom}$$

(2-11)

$$SOC_i(t) \geq SOC_{i,min} = k_{min,i} \cdot E_{i,nom}$$

(2-12)

- Where $SOC_{i,min}$and $SOC_{i,max}$ are the i^{th} battery state of charge suggested to avoid battery degradation respectively
- $E_{i,nom}$ is the nominal energy of the i-th battery
- $k_{max,i}$ with $k_{min,i}$are coefficients [0.0 ÷1.0].

Once each agent has completed the optimisation asynchronously, it sends back the new optimized $P_i(t)$ (this will be a sum of the optimised profiles for each phase of the agent) to the MA that checks if the global proposed behaviour satisfies the DSO request. The algorithm converges if the maximum

difference between two iterations is lower than a threshold ψ for every agent. Shown in equation (2-13):

$$max\left|P_i^k - P_i^{k-1}\right| \leq \psi$$

(2-13)

When the Nash equilibrium has been reached the optimal $P_i(t)$ is used in the LV network model and compared to the uncontrolled results.

2.6 Unbalanced Power Systems

There are various scenarios that would cause LV networks to operate under unbalanced conditions. This thesis will focus on network unbalance due to uneven loading/generation and transmission lines (as discussed in constraints).

2.6.1 Unbalance Indices and Limits

The IEEE definition of unbalance uses phase voltages. IEEE Std 112 uses another index to quantify voltage unbalance. The phase voltage unbalance rate (PVUR) is defined in [26] shown in the equation in (2-14):

$$\%PVUR = \frac{\Delta V_{phase-max}}{\overline{V_{phase}}}$$

(2-14)

Where $\Delta V_{phase-max}$ is the maximum phase voltage deviation from the average phase voltage magnitude ($\overline{V_{phase}}$), which is expressed in equation (2-15):

$$\Delta V_{phase-max} = \mathrm{V_{max}} - \overline{V_{phase}}$$

(2-15)

$$\overline{V_{phase}} = \frac{V_a + V_b + V_c}{3}$$

(2-16)

2.6.2 Balanced and Unbalanced network overview

A balanced 3-phase system (a,b,c) is when the voltage and current are all equal in magnitude and have a displacement of 120^o With phase a leading [7]. Unbalance can be caused by unequal loading, unequal mutual coupling between transmission lines [7], uneven transmission lines and uneven geometry of transmission lines on the towers (this means each phase might have a different position to the ground, guard line and other phases comparing with the lines of other phases which would result in a difference between the electrical parameters of the lines in the same network [27].

2.6.3 Voltage unbalance impact

Voltage unbalance has negative impacts on the power system equipment. A minor unbalance in voltage can result in a larger current unbalance [27]. Power system equipment such as three-phase rectifiers, transformers, protection devices and inverters [27] and [28] are affected by the unbalance. The excessive current unbalance causes the temperature of the rectifier's diodes to increase, decrease induction motor efficiency, transmission losses and increased core losses in power transformers indicating that network unbalance can cause severe economic loss [27].

2.7 Thevenin Equivalent Circuit overview

The ESSs and EVs discussed earlier are DC Battery storages and cannot be connected to the AC grid directly to sync excess power or source needed power from, so a device that consists

of an inverter (required to source power) and a rectifier (with a dc-dc converter to sync power that charges the ESS and EV). The device would be the converter shown in Figure 2-5.

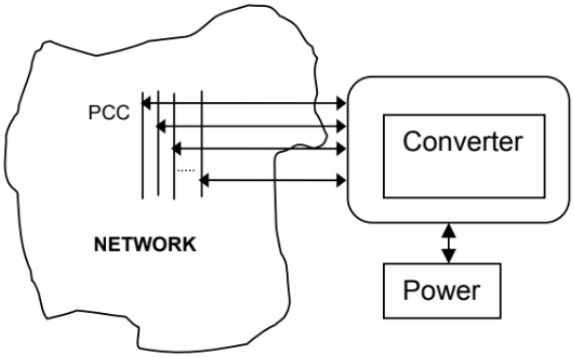

Figure 2-5: Converter connected to a PCC of a network [4]

The converter is the bridge between the battery and the network. It will inject or tap power from it, but due to the non-ideal nature of the wires between the load and the Point of Common Coupling (PCC), resulting in them having impedances, reactance, and resistance, that need to be considered when injecting or taping power. To do this, a Thevenin Equivalent circuit of Figure 2-5 will need to be determined to ensure optimal power injections and sourcing.

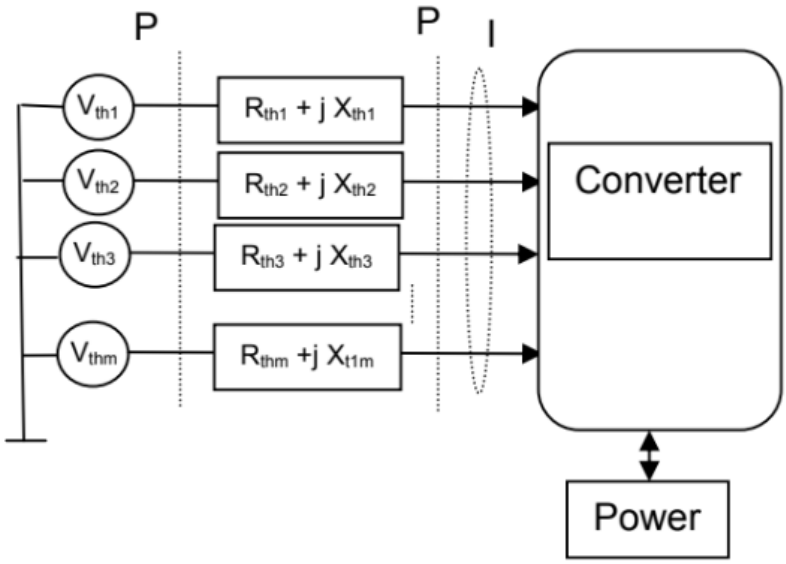

Figure 2-6: Thevenin Equivalent circuit of the network at a PCC with converter [4]

The equivalent circuit of Figure 2-5 can be represented by Figure 2-6. Using Thevenin, it can be shown that the entire network concerning the converter can be represented by m (usually m=3 per converter) equivalent Thevenin circuits (with different Thevenin equivalent

impedances) where the correct "null voltage" reference can be calculated [4]. The Thevenin voltage (V_{th}) is the Voltage being exposed to the users.

2.7.1 Justification for a localized Thevenin analysis

This thesis requires to be able to determine if the Thevenin parameters for an active and dynamic network, the traditional Thevenin equivalent method using open-circuit and short circuit tests are not practical [29]. The motivation to understand the Thevenin expression of a network from a certain point of view (the controllable charge/discharge profile ESS and EVs for this thesis) is to be able to manage voltage stability, and voltage stability is usually assessed using continuous power flow (CPF) a model-based statistic method [30]. The challenge with CPF is the need for accurate modelling of other entities (generators, transmission lines, and transformers) in the network (globalised data) and a significant amount of computational power [30]. These requirements prevent CPF from being a robust and flexible solution and go against the theme of the thesis. A control scheme that uses local data is a far more scalable solution and is also far more attractive to an active LV network with many independent entities with their own objectives [31].

There are various methods used to determine the local Thevenin equivalent circuit. The following section will discuss a variety of them.

2.7.2 Active TEI determination methods

This section will cover four methods: Least Squares (LS) method, a technique based on Tellegen's Theorem (TT), the Adaptive method (AD) and a method based on Coupled Single-Port Circuit (CP).

2.7.2.1 General On-line identification procedure

A 2-bus electric circuit in Figure 2-7 has a load bus k with a load of $\overline{S_k} = P_L + iQ_L$ with a voltage of $\overline{V_k}$ connected to a generator bus of voltage $\bar{E}_{th}$ via a Thevenin impedance of $\bar{Z}_{th}$.

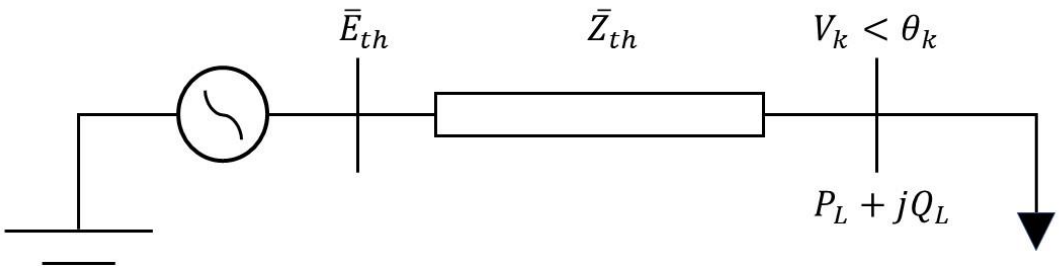

Figure 2-7: Simple 2-bus electric system [30]

The equations (2-17) and (2-18) holds:

$$\bar{I}_k = \frac{\bar{S}_k}{\bar{V}_k} = \frac{(\bar{E}_{th} - \bar{V}_k)}{\bar{Z}_{th}}$$

(2-17)

$$V_k^2 - \bar{E}_{th} \cdot \bar{V}_k + \bar{S}_k \cdot \bar{Z}_{th} = 0$$

(2-18)

The maximum power is transferred to the load when $|Z_k| = |Z_{th}|$ as seen from the load bus k where the voltage collapse will occur. The solution for when the maximum power will occur is when:

$$V_k = \frac{\bar{E}_{th}}{2}$$

(2-19)

$$\bar{Z}_{thev} = \bar{Z}_k = \frac{V_k^2}{\bar{S}_k}$$

(2-20)

2.7.2.2 Least Squares (LS) method

Another way to express $\bar{E}_{th}$ as shown in equation (2-21):

$$\bar{E}_{thev} = \bar{V}_k + \bar{Z}_{th}\,\bar{I}_k$$

(2-21)

With the rectangular expression of each being broken down into $\bar{E}_{th} = E_r + jE_j$, $\bar{V}_k = u + jw$, $\bar{I}_k = g + jh$ and $\bar{Z}_{th} = R_{th} + jX_{th}$. Re-arranging equation (2-21) to $\bar{E}_{th} - \bar{Z}_{th}\,\bar{I}_k = \bar{V}_k$ the following basic state estimation problem is below:

$$\begin{bmatrix} 1 & 0 & -g & h \\ 0 & 1 & -h & -g \end{bmatrix} \times \begin{bmatrix} E_r \\ E_j \\ R_{th} \\ X_{th} \end{bmatrix} = \begin{bmatrix} u \\ w \end{bmatrix}$$

(2-22)

In equation (2-22), g, h, u and w are real and imaginary components of $\bar{V}_k$ and $\bar{I}_k$ which means they are measurable at bus k and are known variables. E_r, E_j, R_{th} and X_{th} (the real and imaginary components of $\bar{E}_{th}$ and $\bar{Z}_{th}$) are unknowns representing the Thevenin equivalent parameters. This state estimation problem usually is unsolvable since there are only two equations to determine four unknowns. This is circumvented by assuming that the TE parameters remain constant for a period of time (time window, W) even with a changing $\bar{V}_k$ and $\bar{I}_k$ to get two extra equations to solve the problem.

2.7.2.3 Tellegen's Theorem (TT)

Tellegen's theorem depends only on the network topology and Kirchhoff's voltage and current laws. It works in all networks that obey Kirchoff's laws and is not hindered by network dynamics like linearity or time variance [32]. The general expression of TT is shown in equation (2-23):

$$\hat{I}^T \Delta U - \hat{U}^T \Delta I = 0$$

(2-23)

Where ΔU and ΔI represent the changes in voltage and current phasors of the buses of the incremented network (a network subject to power change at a certain bus, an example would

be a current injection pulse) while $\hat{I}$ and $\hat{U}$ are the voltage and current phasors of the buses of the adjoint network (a network without modification, base network). If the adjoint network is Figure 2-7, the maximum transfer limit of the network is reached when the Thevenin impedance is equal to the load impedance as shown in equation (2-24) which, using Ohm's law, result in equation (2-25).

$$\hat{Z}_{th} = \hat{Z}_k$$

(2-24)

$$\left|\frac{\Delta U_k}{\Delta I_k}\right| = \left|\frac{U_k}{I_k}\right|$$

(2-25)

2.7.2.4 Adaptive method (AD)

AD is proposed in [33], a fundamental assumption is that $R_{thev} \approx 0$ is made under the assumption that $X_{th} \gg R_{th}$ for high voltage level buses. The elimination of R_{th} results in $Z_{th} = X_{th}$. Resulting in equations (2-26) and (2-27):

$$E_{th}cos\beta = V_k cos\theta$$

(2-26)

$$E_{th}sin\beta = X_{th}I_k + V_k sin\theta$$

(2-27)

Similar to the LS method (equation (2-22)), we have an issue with more unknowns (3) than equations (2). The adaptive method works by first giving an early estimate for E_{th}, then it solves for X_{th} with that estimate then adaptively updates E_{th} depending on the difference between X_{th} for 2 sequential time periods.

2.7.2.5 Coupled Single-Port Circuit (CP) method

This is based on the concept proposed in [34]. In the CP method, the network is modelled as a multi-port network. The generator and load are extracted from the network while a branch and a tie bus (a bus with no current/power flowing through it) are inserted inside the network. The system can be described by equation (2-28):

$$\begin{bmatrix} -I_L \\ 0 \\ I_G \end{bmatrix} = [Y] \begin{bmatrix} V_L \\ V_T \\ V_G \end{bmatrix} = \begin{bmatrix} Y_{LL} & Y_{LT} & Y_{LG} \\ Y_{TL} & Y_{TT} & Y_{TG} \\ Y_{GL} & Y_{GT} & Y_{GG} \end{bmatrix} \begin{bmatrix} V_L \\ V_T \\ V_G \end{bmatrix}$$

(2-28)

The Y matrix is the system admittance matrix, V and I are vectors of voltage and current phasors, and the subscript L, T, and G represent load bus, tie bus, and generator bus.
Elimination of the voltage vectors of the tie busses can be found by equation (2-29).

$$V_L = KV_G - Z_{LL}I_L$$

$$Z_{LL} = (Y_{LL} - Y_{LT}Y_{TT}^{-1}Y_{TL})^{-1}$$

$$K = Z_{LL}(Y_{LT}Y_{TT}^{-1}Y_{TG} - Y_{LG})$$

(2-29)

For load bus k we can obtain equation (2-30);

$$V_{LK} = E_{eqk} - \left(Z_{eq_k} + Z_{couple-k}\right)I_{LK}$$

$$E_{eqk} = [KV_G]_k, Z_{eq_k} = Z_{LL_{kk}}, Z_{couple-k} = \sum_{i=1, i\neq k}^{n} Z_{LL_{ik}} \frac{I_{Li}}{I_{Lk}}$$

(2-30)

The TE parameters can be established by using equation (2-30), matrix K (equation (2-29)) is used to determine the Thevenin voltage (E_{th}) and Z_{th} is determined by the diagonal element $Z_{LL}$and the coupling of other loads through the network.

2.7.3 Algorithm Comparison

2.7.3.1 Time Complexity

All the estimation methods are more computationally effective than traditional methods. What distinguishes these methods is their time complexity and the number of measurements needed to generate a TEI estimate [35] and [30].

Of the four methods, LS stands out for its slower speed. Its model consists of four unknowns and two equations, making it unsolvable without two sets of measurements, requiring each TEI estimation by LS to operate in a specific time window, W [35]. The other methods do not require such operational conditions.

2.7.3.2 Qualitative analysis

LS is effective at detecting voltage instability as quickly as other methods but does this by making approximations of the TEI values (by assuming E_{thev} to be constant on a fixed time window (W), but this is unreliable in more practical networks (it lacks robustness), and to mitigate the inaccuracy would require more time (a longer W) [35] for more accurate TEI values, which would mitigate the advantage of localized TEI determination. TT (Tellegen) is unique for its speed, its ease of implementation and its robustness (it can be used on rapidly changing systems to better observe changes in TEI estimates). AD effectively works at a relatively small sampling time of about 20ms [35]. SP has the disadvantage of requiring more phasor measurement units (PMUs) at generator buses which results in more hardware complexity (increased financial cost and implementation complexity) and computational cost when compared to TT and AD. Still, the benefit of this model is that it mitigates any errors that could occur when estimating the TEI [35].

In [30], all four methods are tested on an NPCC 140 bus system; the system has 48 generators, a total load of 27.7 GW (4.3 GVar) and 223 transmission lines. LS and TT methods were able to indicate the system collapse (meaning the equation (2-20) held true for when the equation (2-19) occurred), while AD and CP methods failed to observe the system collapse.
TT and LS performed better in this test, and either option is viable based on the tests in [30]. TT (Tellegen's Theorem) will be further examined as it is the preferred option by the UCT team also.

2.7.4 Issues with Tellegen approach for determining TEI

It is essential to evaluate any possible issues that might come up when implementing TT TEI estimation. This is to re-enforce the quality of the method (and errors that might emerge developed in [4] not being out of the ordinary). Estimating TEI accurately is still a challenge as electrical networks are significant in scale, nonlinear in nature and varying in time [36], so there will still be issues with precision regardless of the approach to TEI determination.

Tellegen relies on a black-box model (the dynamics of the network are irrelevant to the method) and, as a result, is not able to consider the significance of some aspects on the TEI [36] (like the dynamics of a transformer and load power factor). The main idea behind local methods like TT is that, via PMUs (phasor measurement units, to observe phase current and voltage), there is enough information to observe the voltage stability margin [32], which TT shows to be an effective strategy as seen in [30] when compared to the adaptive method (AD) and coupled single-port method (CP).

The active method provides a usable estimation of TEI with the convenience of not having to model the network parameters; however, it is possible that the dynamics of the network loads can result in an error when determining the TEI [37] but this worse accuracy compared to a static/traditional Thevenin estimation method which takes a considerable amount of time to acquire the TEI parameters which is a precise cost, when observing other local TEI estimation methods, like LS, which increases in accuracy the more computational time it uses in determining the TEI values. This inaccuracy is compensated for by the TT method's robustness (being able to operate in different environments and changing environments like an active network) and its computational speed. The main appeal of TT is not only its accuracy but its speed and versatility so that accuracy issues will be expected in the TEI estimation; however, there is no literature discussing the standard of inaccuracy or what to expect specifically.

2.7.5 Implementation of Tellegen method

Each wire (between a Load and PCC) is represented by a Thevenin network that includes a Thevenin source having a voltage V_{th}, a Thevenin resistor having a resistance R_{th}, a Thevenin inductor having a reactance X_{th} and an inverter having a voltage V_{inv} [4] (voltage at PCC, V_{PCC}).

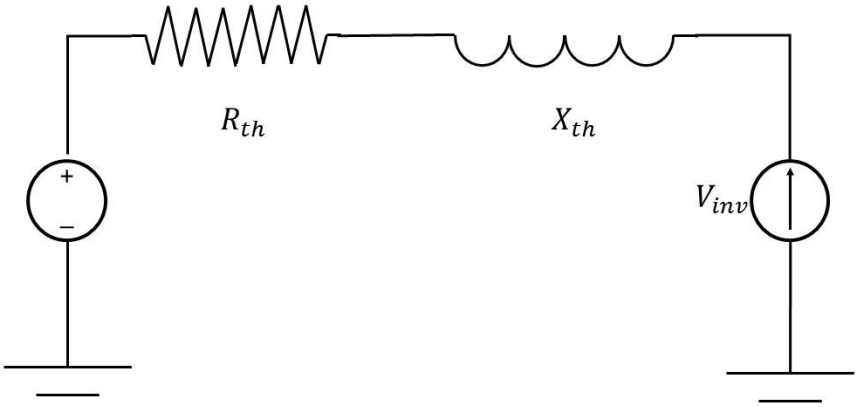

Figure 2-8: Wire model [4]

To determine R_{th} and X_{th} current I_{inv} will be injected at equal magnitudes and opposite phases that will isolate the inductor and resistor, as shown in (2-31) and (2-32). To determine R_{th} I_{inv} is injected in phase with $V_{inv+}$and anti-phase (180^o) with V_{inv-}(not necessarily the same magnitude as V_{inv+}) [4].

$$R_{th} = \frac{V_{inv+} - V_{inv-}}{2I_{inv}}$$

(2-31)

To determine X_{th} the same principle is used but instead, the magnitude of the phase of I_{inv} is 90^o relative to V_{inv} to result in the equation (2-32) [4].

$$X_{th} = \frac{V_{inv+90^o} - V_{inv-90^o}}{2I_{inv}}$$

(2-32)

To determine the optimal I_{inv} phase and magnitude, the R_{th} and X_{th} can be used.

2.8 Chapter Summary

The literature gives a broad view of what was discovered in each section of the review and used in later sections of the dissertation.

The first section in the review went over the use of distributed generation, the challenges and opportunities they posed and how to work around it. DG's would inject power to meet local demand, but an excess amount could result in voltage surges, hurting power quality, this can be mitigated through intelligent utilization of ESSs.

Section two discussed the difference between centralized and decentralized control schemes, and the two greatest factors were the engineering complexity and the computational cost. The research showed that a more decentralized approach was preferable due to its openness and flexibility.

Section three was an overview of MAS. It discussed the meaning of a multi-agent system, what it means to be an agent (emphasizing intelligent agents), the applications of MAS in power engineering and the tools for implementing a MAS (such as JADE and FIPA).

The Fourth section discussed multi-Agent organization. This entails how each agent is organized to form a MAS. The Hierarchal and Flat organizational frameworks were discussed, with the hierarchal model being the preferred choice as it was more suited to a system like a LV network. The method used in [1], [10], [24] and [25] was selected.

Section five describes the MAS framework used in [1], [10], [24] and [25]. It breaks down the algorithm used and details each relevant equation and constraint. The MAS determines the optimal course of action for each agent (the charging/discharging profile of each ESS/EV) through a weakly-coupled game (NCE) approach, which reaches its completion once the Nash equilibrium has been reached. A Nash equilibrium is when a system with independent participants is in a state where no changes can be made for one participant without affecting others, which means that there is minimal change in all the ESSs/EVs charging/discharging profiles.

The sixth section discusses unbalance in power systems, precisely due to loading/generation and transmission line unbalance. The causes and impact of voltage unbalance are discussed, and the IEE definition of voltage unbalance, Phase Voltage Unbalance Rate ($\%PVUR$), is detailed.

The last section goes over Thevenin Equivalent Impedance (TEI) determination method. There are two approaches to determining TEI; the active (local) method and the passive (parametric) method. The active method is preferred because it requires only local information for a particular agent (ESS/EV) and is more scalable. There were four active methods analysed; Tellgens Theorem (TT), Least Squares method, Adaptive method and Coupled Sing-Port Circuit method. TT is a preferred option due to its speed in determining the TEI and its robustness.

3 Methodology

The hypothesis: "A Multi-Agent System (MAS) enabled by Thevenin parameter estimations is a feasible solution for the regulation/control of a distributed and unbalanced LV network to minimize losses in an unbalanced network with multiple independent entities".

3.1 Approach

From the existing research, a more decentralized approach using MAS was observed to be the most suitable for expanding and changing LV network. Moreover, it is further established in the literature that hierarchal organization for the MAS technique is the most appropriate framework for design implementation [1], [10], [24] and [25]. The concept of this framework has been elaborated in section 2.5, which is the stage 1 of implementation (*i.e.*, the proactive measure). The second stage of implementation is making use of Thevenin Equivalent values to introduce a reactive control measure into the design [38]. Stage 1 is a multi-agent platform which is implemented in a Java Agent Development Platform (JADE), and Stage 2 is the implementation of the TEI component in Simulink. Based on these two stages, a decentralized framework based on MAS approach was developed [38]. The framework developed under the stage 2 has been significantly altered due to validation issues with the power injection. This means the currents measured were out of range and were not the most logical course of action.

3.2 Constraints of study

The system that was operated in is a LV network, meaning the system is operating with a nominal voltage of 230V at an operating threshold of 5% [39], and a time frame of 24 hours with a 1 hr interval. The primary network entities of interest are the ESS and EVs; and as these components are increasingly added to a network, they yield elastic demand profiles. Moreover, the PV and load elements will be considered passive and inflexible entities, with each being modelled with single-phase connections to introduce possible unbalance. The ESSs and EVs will be modelled as 3-phase devices to help accommodate the TEI meter developed [4].

3.3 Framework

The system can be broken down into two stages: Stage 1 is the proactive control measure (which involves determining the optimal power transaction for each agent), and Stage 2 is the

reactive control measure (which determines how the power is distributed on each phase). The reactive control measure deals with the live implementation of the optimal path set in stage 1 and ensures that each agent follows the agreements made beforehand in the MAS but optimally through each phase. Not all phases are equally active on the LV network. Thus, it is difficult to predict/plan for the switching of single-phase and 3 phase components loads which can result in system unbalance and cause significant system losses [38]. As a result, the system must have a real-time reactive measure to deal with this issue or else power quality objectives will not be met due to the increased losses in transmission and distribution networks. Integration of both active and reactive processes creates a system that operates cyclically with two stages, as illustrated in Figure 3-1, with stage 1 being the MAS operation and stage two representing the real-time optimal power injection, enabled by TEI measurements [38].

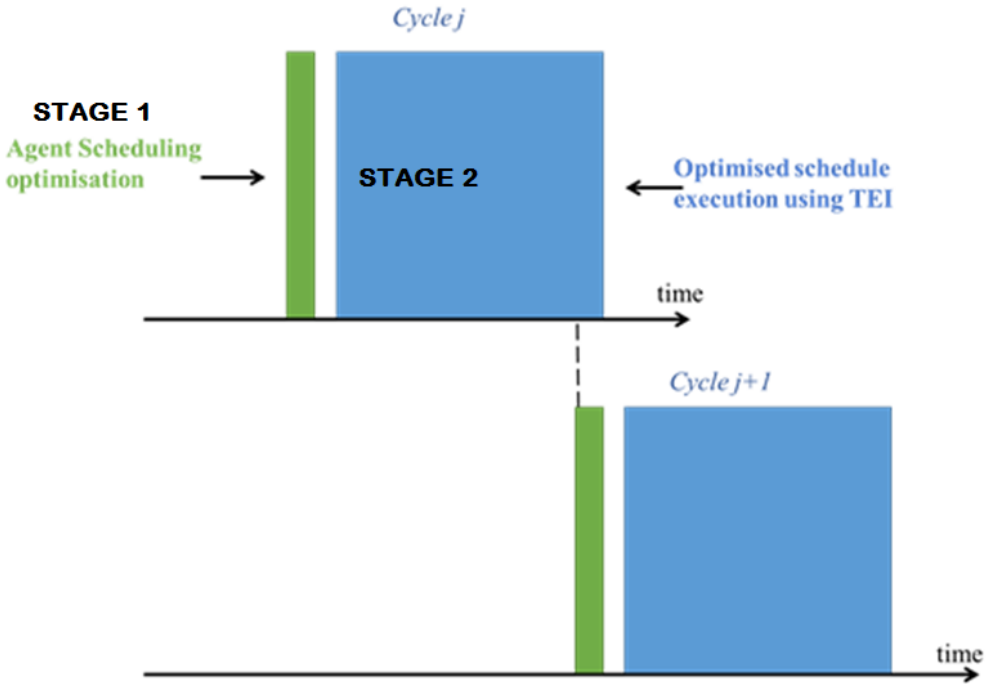

Figure 3-1: System Operation timing Diagram

The above figure shows the system operation diagram, the 1st stage is the planning Stage 1 and stage 2 is the implementation stage with TEI guided injection. Stage one has been elaborated on in section 2.5, while the stage 2 framework will be established here.

3.3.1 Stage 1

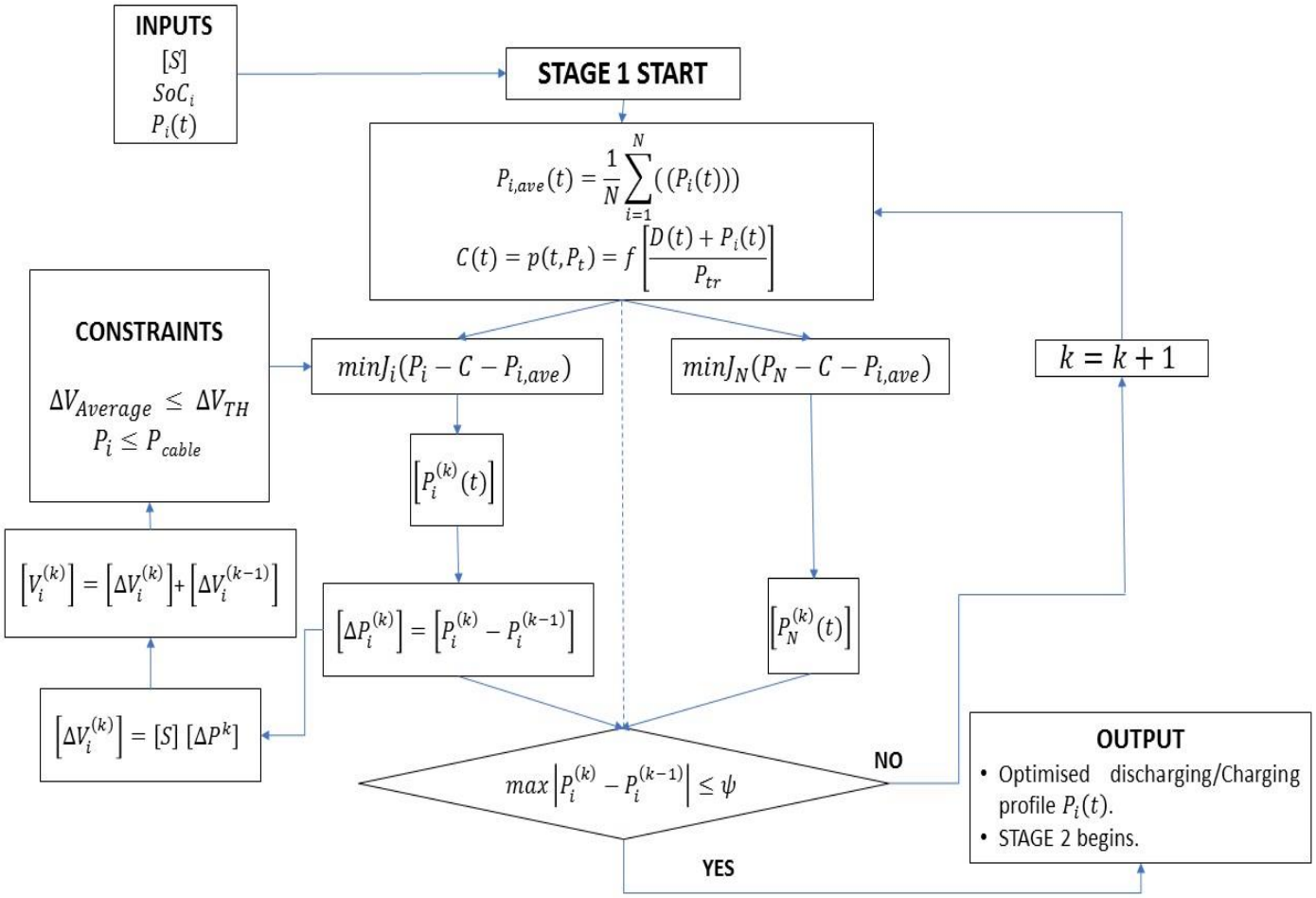

Figure 3-2: MAS algorithm [38]

This stage optimizes the charge/discharge profile of the ESS and EV to meet their local objectives while being mindful of global goals, which is to keep the voltage level within 5% [39]. The output of this stage is the input for stage 2.

3.3.2 Stage 2

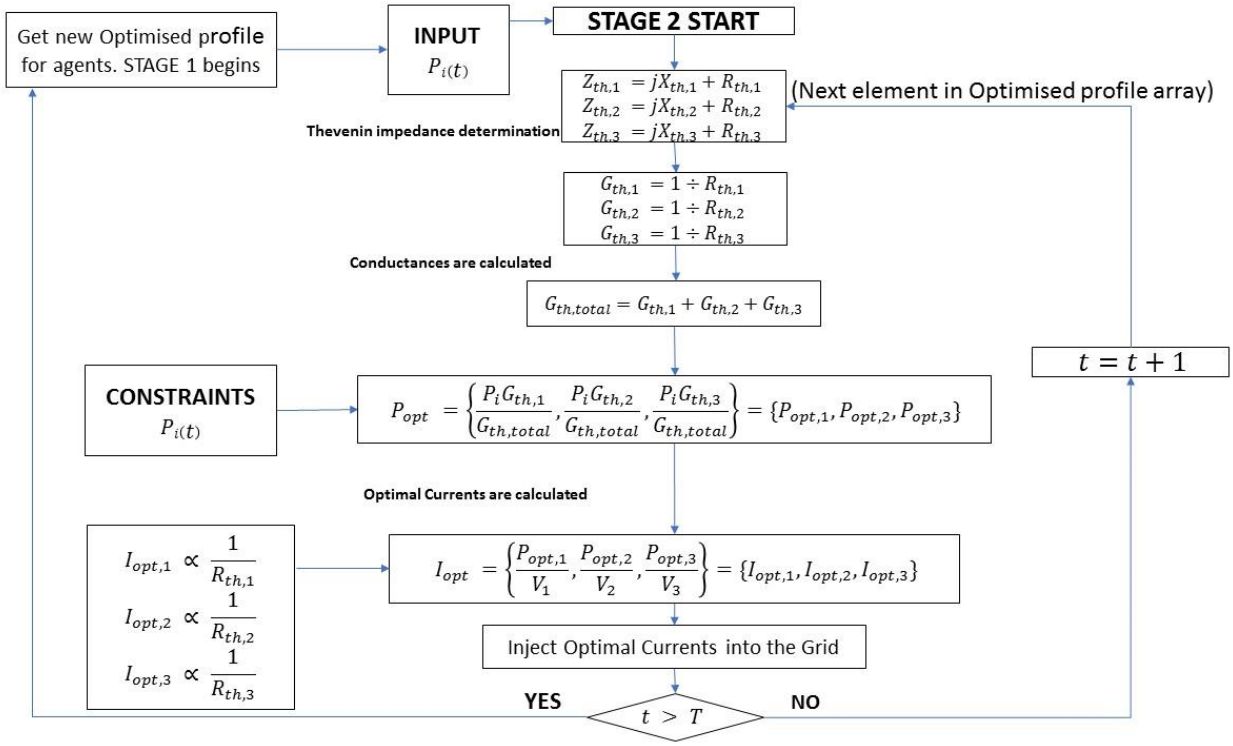

Figure 3-3: Flow chart of optimal currents determination

Stage 2 is the reactive control measure; it is about making sure that plan is executed regardless of any issues that might occur in the LV network, as stated in the introduction.

Stage 2 is a point of operation that is carried out by each agent (EV, ESS) independently. The operation will end once $P_i(t)$ has been fully executed. The algorithm for the detection of the TEI is noted in [40], where the network is modulated at a PCC to inject currents into the network. These are then used to calculate the impedance at the frequencies of interest, which is the fundamental frequency in this instance, and then calculate the fundamental frequency. This algorithm uses a modified frequency-based version of Tellegen's theory [41]. The method was proven accurate in the work where it was shown that the device was accurately able to detect changes of at least 20 mΩ [38] and [42].

Firstly, the Thévenin impedance ($Z_{th,n} = jX_{th,n} + R_{th,n}$) for n number of phases (three phases) is determined by each agent (EV, ESS). The divergence from the initial proposed framework (presented in [38]) starts here. Instead of making use of the methodology in [4] to determine I_{opt} , since it does not consider power actual power transfer but has more to do with balancing the network and will not ensure the ESSs and EVs charge/discharge adequately, the optimal current (I_{opt}) will be determined by coupling the Thevenin resistance values ($R_{th,n}$)

directly to the optimal power $P_i(t)$,The ESS and EV are 3-phase devices, and usually, power is transacted evenly through each phase. This is due to them not typically having a perception of the network unbalance. The 1st step is to take R_{th} and convert it to Thevenin conductance G_{th} as shown in equation (3-1):

$$G_{th,n} = \frac{1}{R_{th,n}} \ \Omega^{-1}$$

(3-1)

Where:

- n is the phase number

The total Thevenin conductance is then calculated as shown in equation (3-2):

$$G_{th,total} = G_{th,1} + G_{th,2} + G_{th,3} \ \Omega^{-1}$$

(3-2)

This total is then used to help determine the optimal power distribution P_{opt} as shown in equation (3-3):

$$P_{opt} = \left\{ \frac{P_i G_{th,1}}{G_{th,total}}, \frac{P_i G_{th,2}}{G_{th,total}}, \frac{P_i G_{th,3}}{G_{th,total}} \right\} = \{P_{opt,1}, P_{opt,2}, P_{opt,3}\}$$

(3-3)

Where:

- P_i is the power determined in Stage 1.

This is then used to determine the optimal current to be injected into each phase as shown in equation (3-4):

$$I_{opt} = \left\{ \frac{P_{opt,1}}{V_1}, \frac{P_{opt,2}}{V_2}, \frac{P_{opt,3}}{V_3} \right\} = \{I_{opt,1}, I_{opt,2}, I_{opt,3}\}$$

(3-4)

Where:

- V_n is the rms voltage per phase.
- $I_{opt,n}$ is the optimal rms current

$I_{opt,n}$ is the current that is injected into or sourced from the LV network environment. This process will be repeated until the array $P_i(t)$ is completed. Once this is done, stage 1 begins again and gets the next profile to be implemented in Stage 2.

3.4 Chapter Summary

The methodology used to meet research objectives consists of two stages. Stage 1 is making use of a MAS framework (discussed in 2.5) for the determination of the 24-hour optimal power transfer profile ($P_i(t)$) for each agent (ESS and EV) and Stage 2 is the distribution of each power per phase (for a 3 phase ESS and EV) by making use of the TEI sensor (discussed in 2.7) to determine the R_{th} for each agent. Then, the $R_{th}$is used to determine the G_{th} for each phase which is used to break down the $P_i(t)$ per phase in order to minimise losses due to network unbalance and to maintain voltage quality.

4 Network Modelling

This chapter discusses the modelling of the network used to test the methodology elaborated on in chapter 3. It shows the general model of all entities, what function they serve and why they were chosen.

4.1 Test Network

The LV network environment that was initially analyzed was a section of the five feeder Italian network used in [1] and [25]. It was initially modelled in Open DSS (which was used in [1], [10], [24] and [25]), but the software did not allow for the implementation of custom components such as the TEI device, so a platform switch was made to MATLAB Simulink. The next factor to affect the modelling of the test network was the computational cost of implementing the TEI device, with a single simulation lasting for at least 40 mins with just two TEI devices running in MATLAB. This section will discuss the test network, go into more details about the layout of the network and discuss how each component is modelled.

4.1.1 The test network

The test network is shown in Figure 4-1.

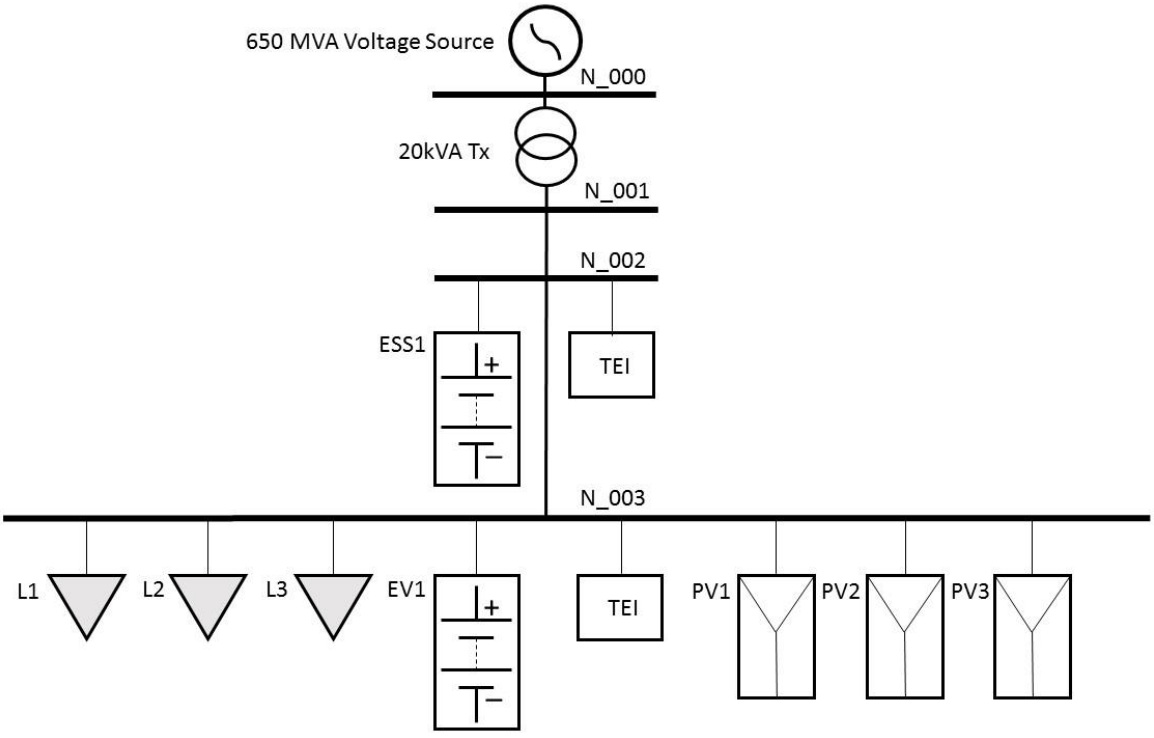

Figure 4-1: The test network

For expedience and to ensure a good understanding of the fundamentals of the TEI-OPI, a smaller network is modelled and experimented on. The separate entities on the network consist of a 3-phase source, a transformer, three single-phase variable loads, three single-phase PVs, two transmission lines, one EV and one ESS. The specification was acquired from [1] and [25]. There are two types of simulations conducted in this research that make use of this network model but with different simulation protocols and modifications.

4.1.2 TEI Meter

The TEI device determines the Thevenin impedance based on GPT [42] (making use of Tellegen's Theorem) and was elaborated on in chapter 2.7. Two TEI meters are operating in the network. Each one is connected in parallel to the ESS and EV shown in **Error! Reference source not found.**.

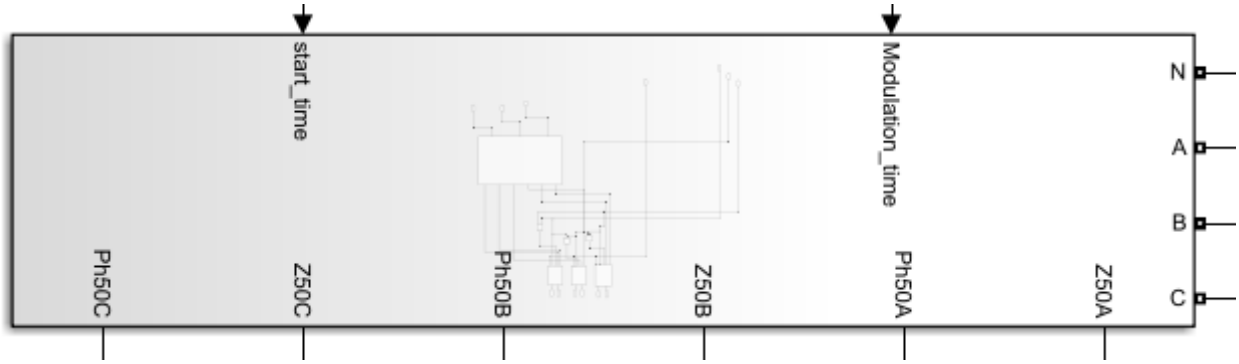

Figure 4-2: The custom TEI Simulink block [42]

The TEI meter has been built and tested [40] and has a different form of operation compared to the Simulink block. The block model cannot determine the Thevenin values as quickly as the prototype sensor and is subject to a modulation time. The modulation induces a significant overvoltage, but this is not a realistic feature of the MAS in operation. The output of the block is $Z_{th} = \overline{Z_{th}} \angle Z_{th,angle}$. This is later converted to $Z_{th,n} = jX_{th,n} + R_{th,n}$ for each phase and recorded and used to determine the optimal power distribution.

4.1.2.1 TEI Meter Block operation

The primary subsystems of the TEI meter are shown in Figure 4-3.

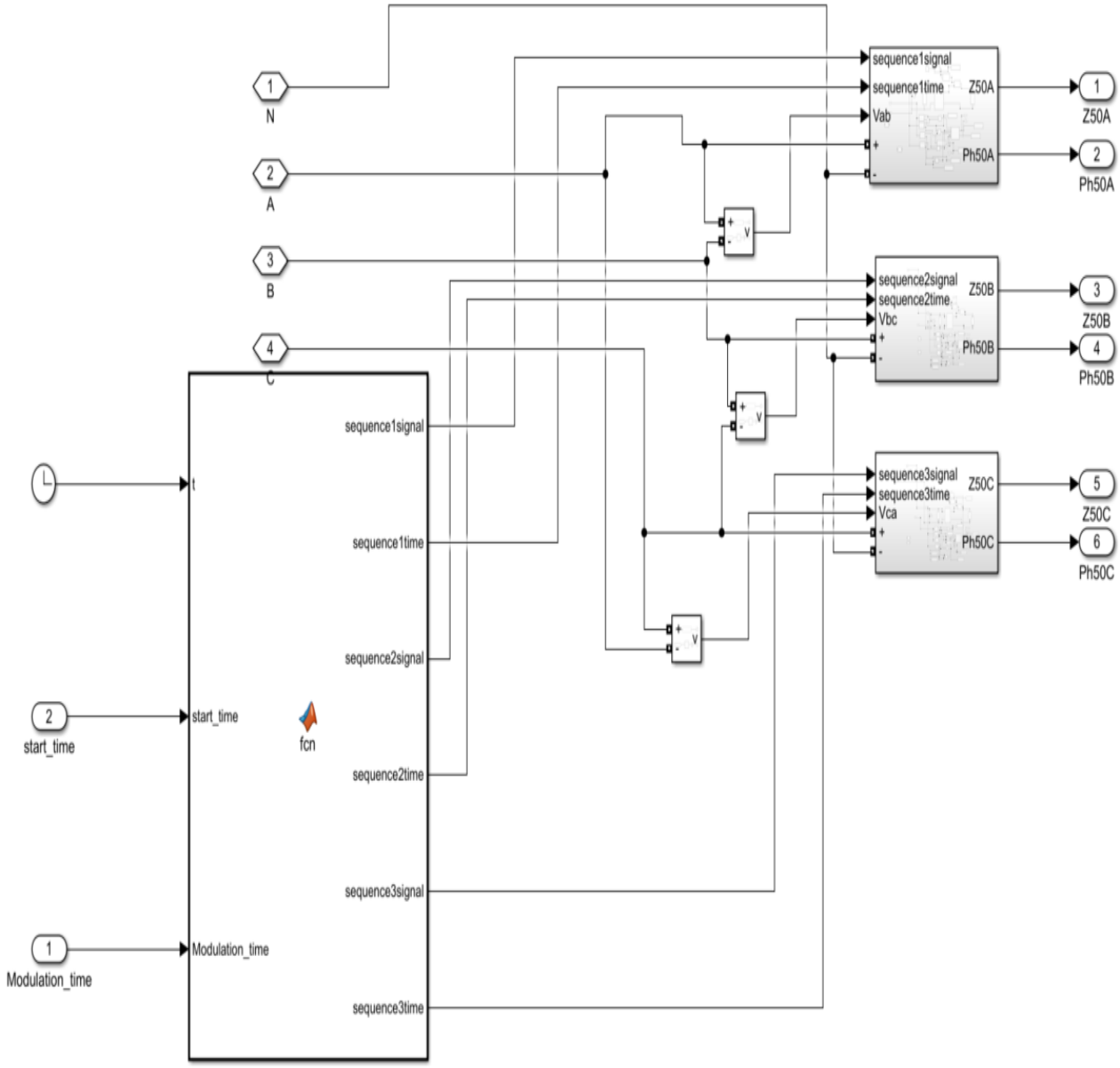

Figure 4-3: TEI Model primary subsystems

Two distinct components make up the TEI meter block (shown in **Error! Reference source not found.**): the timing block and a modulation block. The TEI block has six inputs, four of the inputs are physical connections to the PCC and Neutral while the other two inputs are user inputs to control the time at which modulation and TEI determination will begin (start_time) and the second user input (Modulation_time) is to determine how long the modulation lasts per phase (all the units are in seconds). There are three modulation blocks, with every block corresponding to each phase. The inputs are the time trigger signals from the timing block, a

physical connection to its corresponding phase, neutral connection and the corresponding line-line voltage signal.

4.1.2.1.1 Timing Block

The Timing block is a function block (MATLAB script), based on user inputs Modulation_time and start_time, triggers the modulation blocks by outputting a trigger signal and sequence time to indicate the operation time for a particular phase.

4.1.2.1.2 Modulation Block

The internal function of the modulation block is shown in Figure 4-4.

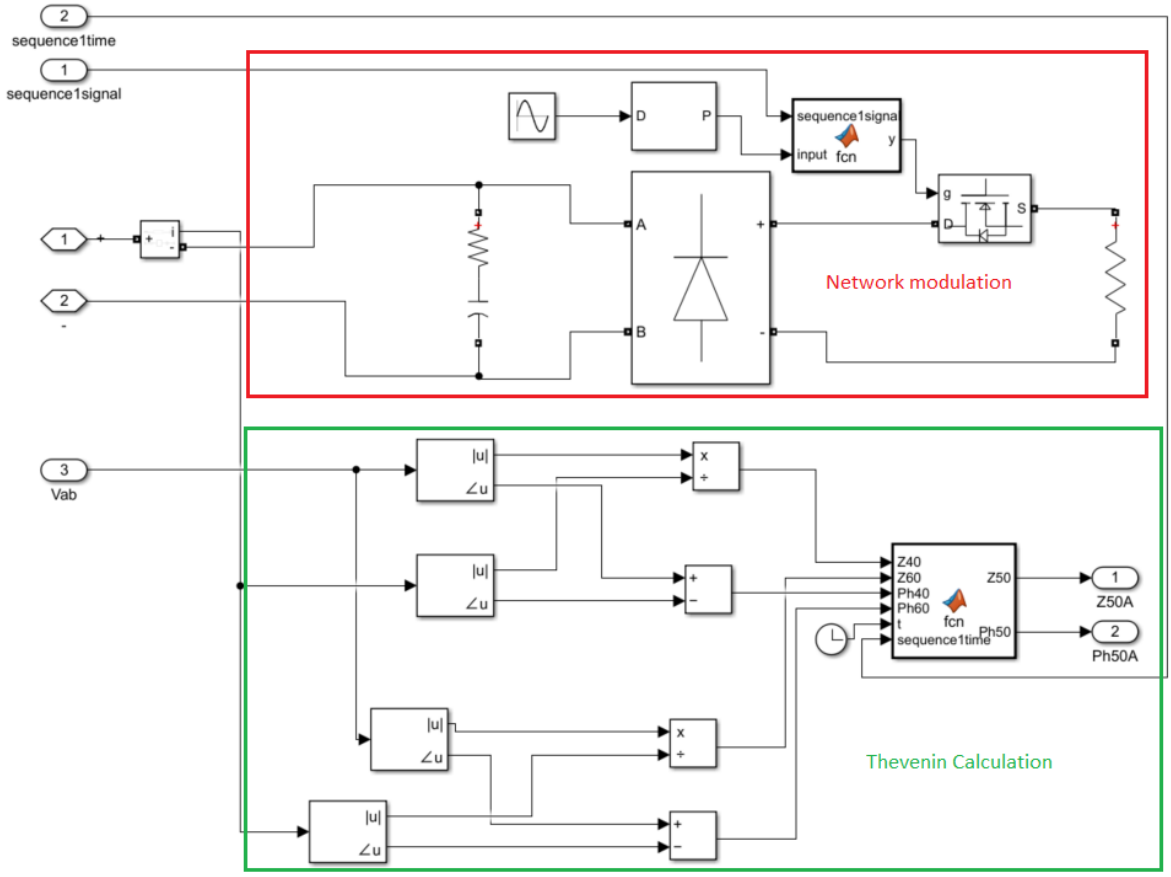

Figure 4-4: Modulation block

The modulation block has two components, the first component is the modulation circuit (Network modulation), and the second is the Thevenin estimation module (Thevenin calculation).

4.1.2.1.2.1 Modulation Circuit

This section of the modulation block is responsible for the current pulses injected into the network. The trigger is gotten from the sequence signal and sends a pulse signal which controls the MOSFET. There are three inputs into the circuit: the sequence signal and the two physical connections (phase and neutral).

4.1.2.1.2.2 Thevenin Calculation

This Thevenin calculator takes the measurement of the line-to-line voltage (the voltages of the lines experiencing polar modulation) and divides it by the phase current measured. This is used to determine the Thevenin impedance Z_{th} for that phase.

4.1.3 Voltage Source

The network has a 3-phase source with a 3-phase short-circuit level rating of 650MVA and a power generation of 10kW at 15kV phase-to-phase rms voltage, with a frequency of 50Hz, Y_g connection and a $\frac{X}{R} = 7$ (which is used to determine the internal impedances). These parameters are taken from the Italian network used in [1] and [25]. Figure 4-5 and Table 4-1 shows the Simulink block of the 3-phase source, the parameter and load flow settings.

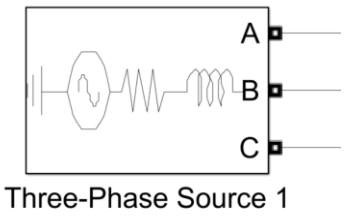

Figure 4-5: 3-phase source block

Table 4-1: Parameters for 3-phase source block

Parameters	Settings/values
Configuration	Wye ground (Y_g)
Phase-phase Voltage (V_{rms})	15kV
Phase angle of phase A	0^o
Frequency	50Hz
3-phase short circle level	650MVA
Base voltage	15kV
X/R ratio	7
Generator type	PV
Active power generation	10kW

Minimum reactive power	No limit
Maximum reactive power	No limit

4.1.4 Transformer

The transformer is a three single-phase transformer with a rating of 20kVA, a Y_g- Delta connection, it drops a phase-to-phase voltage of 15kV to 398.4V. The parameters for the 1st winding are $R_1 = 22.5\ \Omega$ and $L_1 = 2.8648\ H$, the 2nd winding has parameters $R_2 = 0.04761\ \Omega$ and $L_2 = 0.0060618\ H$ and the magnetization parameters of $R_m = 5.625\ M\Omega$ and $L_m = 17905\ H$.

The parameters are derived for the Italian network, but with the only change being the transformer rating, this was to make the network sensitive enough to experience voltage change (drop or surge). Some tests were conducted without the transformer. Figure 4-6 and Table 4-2 show the transformers Simulink block, parametric and configuration settings.

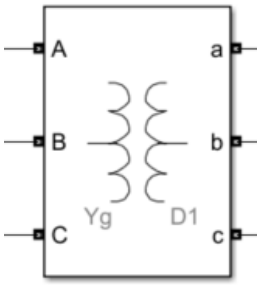

Figure 4-6: 3-phase transformer Simulink block

Table 4-2: Parameters for 3-phase transformer block

Parameters	Settings/values
Winding 1 Connection	Wye ground (Y_g)
Winding 2 Connection	Delta (D)
Core type	3 single-phase transformers
Measurement	None
Unit setting	pu
Nominal power	20kVA
Nominal frequency	50
Winding 1 V_{line}	15kV
Winding 1 R	0.002 pu
Winding 1 L	0.8 pu
Winding 2 V_{line}	398.37V
Winding 2 R	0.002 pu
Winding 2 L	0.8 pu

R_m	500 pu
L_m	500 pu

4.1.5 ESS and EV

The ESS and EV are modelled the same way in Simulink, but the expectations of their roles in the LV network vary and is taken into consideration on the MAS platform. However, for expedience and to focus more on their interaction with the LV network, the modelling for these two systems are simplified and are represented by current sources. The implication of this is the lack of model accuracy and not much consideration to the internal dynamics of energy storages. The three-phase ESS has a capacity of 48kWh with a rating of 24kW [43], and the three-phase EV with a capacity of 30kWh with a rating of 11kW [44].

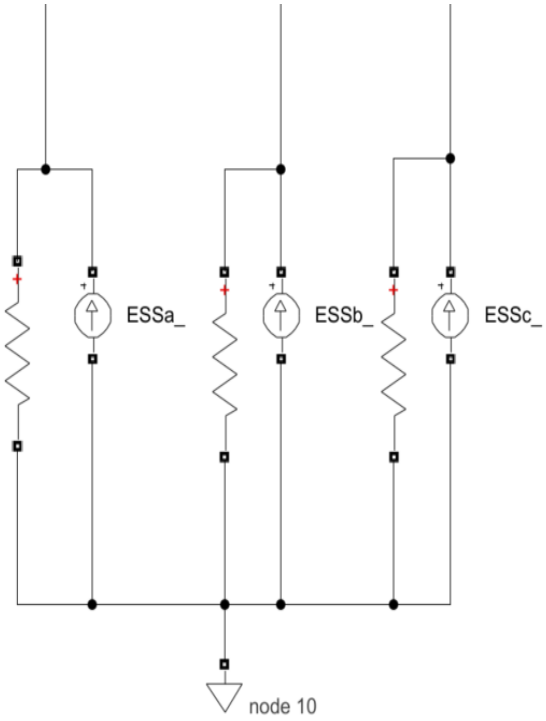

Figure 4-7: Constant amplitude current source

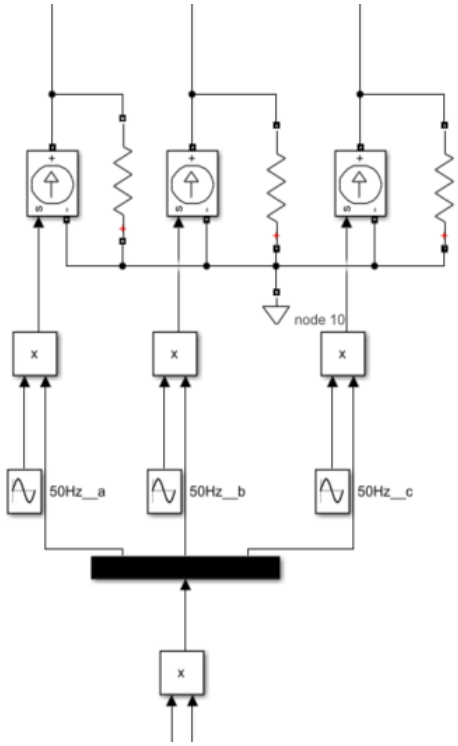

Figure 4-8: Variable amplitude current source

There are two different implementations for the 3-phase current source, version one (see Figure 4-7) is an AC Current Source block model that has the amplitude and angle parameters fixed before the simulation is run, while in version two (Figure 4-8), the AC/DC (Controlled) current source has a fixed angle. However, it is possible to dynamically change the amplitude during the simulation by combining it with a sine wave block and multiplying it by a variable. For simplicity, the AC source is modelled as an ideal source and the parameters are shown inTable 4-3.

Table 4-3: Parameters for constant-amplitude current source

Parameters	Settings/values
Peak amplitude	Dynamic variable
Phase (deg)	Dynamic variable
Frequency	50
Sample time	0s

The controlled current source is left mostly blank (refer to Figure 9-6), and its input signal is coupled to the sine wave block, which is the point of control. All the current sources are in parallel with a $1M\Omega$ resistor, this is due to current sources being modelled as extremely large (infinite) inductances that need a path of discharge.

Table 4-4: Parameters for Sine Wave block setup

Parameters	Settings/values
Peak amplitude	1
Sine type	Time based
Phase (deg)	Dynamic variable
Frequency	50
Sample time	0s

The input phase is usually aligned with the voltage at the PCC (to achieve a PF of 1). The rms current (the current going in/out of the device) and voltage at the PCC are recorded and used to determine PF, real power, apparent power, and reactive power as shown in Table 4-8.

4.1.6 Photo Voltaic (PV)

The PV is modelled just like the ESS and EV with the only distinction being that the demand is inelastic (meaning the demand cannot be altered and is a constraint that must be worked around similar to the passive demand) and only makes use of the model shown in Figure 4-7. The PV generation data was taken from the Italian model. The rms current and voltage are recorded and used to determine real and reactive power.

4.1.7 Load

The load model consists of three single phase loads, connected on separate phases. The load data is also derived from the Italian network. There are two RLC load models used, a model that takes in power (real and reactive) as inputs and the second model that takes in physical parameters (resistance, capacitance, and inductance). The power load model is used in the 24-hour test where the demand is changed 24 times, while the second model is used for the verification of the TEI meters accuracy. The parameters for both load models are shown Table 4-5 and Table 4-6.

Table 4-5: RLC Load parameters

Parameters	Settings/values
Nominal voltage	400
Nominal frequency	50
Active power	Dynamic variable (W)
Inductive reactive power	Dynamic variable (var)
Capacitive reactive power	Dynamic variable (var)

Table 4-6: RLC Branch parameters

Parameters	Settings/values
Branch type	RL
Resistance	Dynamic variable (Ω)
Inductance	Dynamic variable (H)

The rms current and voltage are recorded and used to determine the load power.

4.1.8 Transmission lines

There are two 3-phase transmission lines that connect bus1 to bus 2. The transmission lines are modelled based on data from the Italian network balanced lines with RL impedances. The Simulink block is shown in Figure 4-9, and the parameters are in Table 4-7.

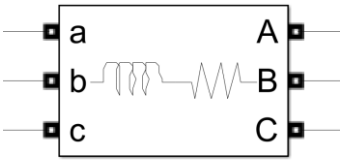

Figure 4-9: 3-phase series RLC Branch

Table 4-7: Transmission RLC branch parameters

Parameters	Settings/values
Branch type	RL
Resistance	Dynamic variable (Ω)
Inductance	Dynamic variable (H)

4.2 MAS Platform

This section discusses the MAS platform implemented with JADE. This section discusses the responsibility and role of each agent.. The JADE platform follows FIPA guidelines [17] and [20].

4.2.1 Agents and their roles

Table 4-8 below summarizes the role of each agent in the network.

Table 4-8: Responsibility table

Agent type	**Responsibilities**
Master agent	1. Collects data from agents. 2. Collects data (Sensitivity matrix) from the network aggregator. 3. Sends the average agent profile and sensitivity matrix to EV/ESS agents in the system 4. Initiates a new cycle of control action. 5. Decides when the Nash equilibrium is reached 6. Sends a global directive to each EV and ESS agent on how they should transfer power. 7. Equations (2-1) and (2-2) are used in this agent.
EV agent	1. Sends demand profile $P_i(t)$ to the master agent 2. Gets data from the master agent that concerns the EV. 3. Plans the activities of the EV throughout the day. 4. Observes the dynamics of the LV network. 5. Discharges or charges EV battery. 6. Takes in the preferences of the EV owner, such as charging or discharging requirements. 7. Equations (2-3), (2-4), (2-5), (2-6), (2-7), (2-8), (2-9), (2-10), (2-11), (2-12) and (2-13).
ESS agent	1. Sends demand/supply profile $P_i(t)$ to the master agent 2. Gets data from the master agent that concerns the ESS. 3. Plans the activities of the ESS throughout the day. 4. Observes the dynamics of the LV network. 5. Discharges or charges ESS. 6. Equations (2-3), (2-4), (2-5), (2-6), (2-7), (2-8), (2-9), (2-10), (2-11), (2-12) and (2-13).
RES agent	1. Sends inflexible supply data to the master agent.
Initialiser agent	1. Sets up the simulation

	2. Automatically creates other software agents.
DSO agent	1. Aggregates Load data for the network. 2. Aggregates voltage data for each feeder 3. Determines sensitivity matrices $[S]$ for the ESS and EV to be used in optimisation.

4.2.2 Agent Software algorithm

This section briefly summarizes the inner workings of all the agents. It describes the pseudo-code of the systems. Figure 4-10 shows the simulation structure of the MAS.

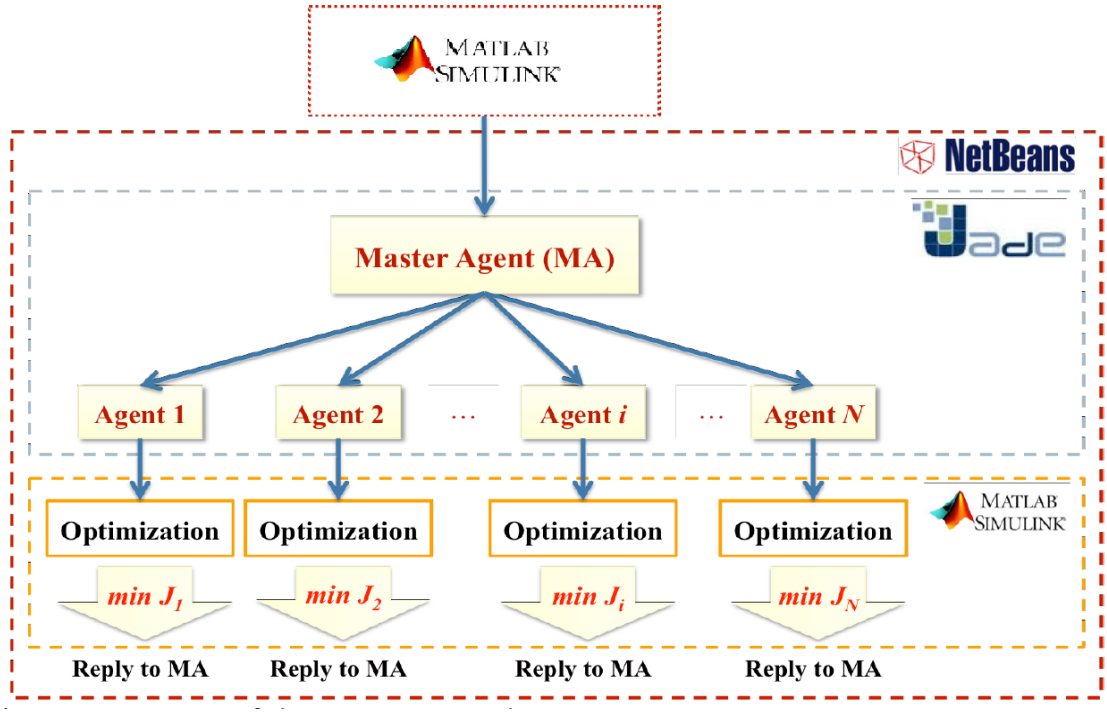

Figure 4-10: Structure of the MAS control [1]

4.2.2.1 DSO Agent

The DSO agent's sequence of operation works like this.

- Determine the sensitivity matrix $[S]$ for each ESS and EV
- State the number of feeders in the network
- List the number of EVs and ESSs (the number on each feeder)
- Take the 1.5kW power injection data (real power and voltage per phase) from the ESS and EV

- Take the 0.5kW power injection data from the ESS and EV.
- Find the difference between the real power and voltage for each phase from every EV and ESS, then divide the voltage difference by the power difference ($S = \frac{\Delta V}{\Delta P}\ V/kW$) (if there is a 3-phase ESS and a 3-phase EV on the same feeder, there will be a subtraction of the power and voltage of each of the ESS phases from the power and voltage of the EV and divide the voltage difference by the power difference to create a matrix of length 9, 3x 3).
- Output the sensitivity matrices as CSV files.
- Aggregate the load data and create a passive demand profile ($D(t)\ kW$) for the whole network and individual feeders then output it as a csv file.

4.2.2.2 Initializer Agent

This agent is responsible for creating all other agents in the JADE and is the first agent created (created manually).

- State the number of ESSs, EVs and PVs. (These are created Java classes)
- Create the no. ESS, EV and PV agents with the corresponding class names
- Record the number of agents and output the data as a text file
- Create the Master agent.

4.2.2.3 Master Agent

- Find the number of ESS, EV and PV agents from the initializer agent text file.
- Access the $D(t)$ determined by the DSO agent.
- Send the total number of ESS and EV agents (N and N_{feeder}) to all the ESS and EV agents.
- Send a signal to the ESSs, EVs and PVs to send their demand profiles $P_i(t)$.
- Wait for the agents to send their initial guesses for $P_i(t)kW$
- Determine the average agent (ESS and EV) power $P_{i,ave}(t)$
- Determine the virtual cost $C(t)$
- Send the $C(t)$ and $P_{i,ave}(t)$
- Wait for the ESSs and EVs to determine their optimal profiles (asynchronously) with the data.

- Check if the Nash Equilibrium is reached; if not, repeat the process till the equilibrium is reached. If reached, send a signal back to the agents to output the current $P_i(t)$ and terminate the platform.

4.2.2.4 EV/ESS Agent

- Start a MATLAB session (using the MATLAB engine).
- Get initial data from Master Agents such as N and the number of agents per feeder N_{feeder}
- Access the $[S]$ for the corresponding agent
- Get the $D(t)$.
- Generate an initial guess, this will vary for the EVs and ESSs.
- Input and operation time varies for the ESS and EV.
- Wait for the Master agent to give the go-ahead and send the initial $P_i(t)$.
- Receive the $C(t)$ and $P_{i,ave}(t)$
- Use $C(t)$ and $P_{i,ave}(t)$ to perform a mono-constrained optimisation $min\, J_i(P_i, P_{-i})$ in MATLAB.
- Send the new $P_i(t)$ to the Master agent.
- Wait for the Master agent to determine if the Nash Equilibrium is reached, if not, receive the new $C(t)$ and $P_{i,ave}(t)$ and repeat the optimisation process till equilibrium is reached.
- If the Master Agent determined the Nash Equilibrium is reached, then export the optimal $P_i(t)$

4.2.2.5 PV agent

- Import the PV generational profile.
- Wait for the go-ahead signal from the Master agent to send the PV generation curve
- Repeat this process till the last agent terminates the platform.

5 Simulation Protocol

There are two main batches of simulations, the 1st batch verifies the performance of the TEI in the 4-bus test network while the 2nd set of simulations runs a full day simulation of the 4 bus test network similar to the work done in [1] [10] [24] and [25]. The Simulink model is shown in Figure 5-1.

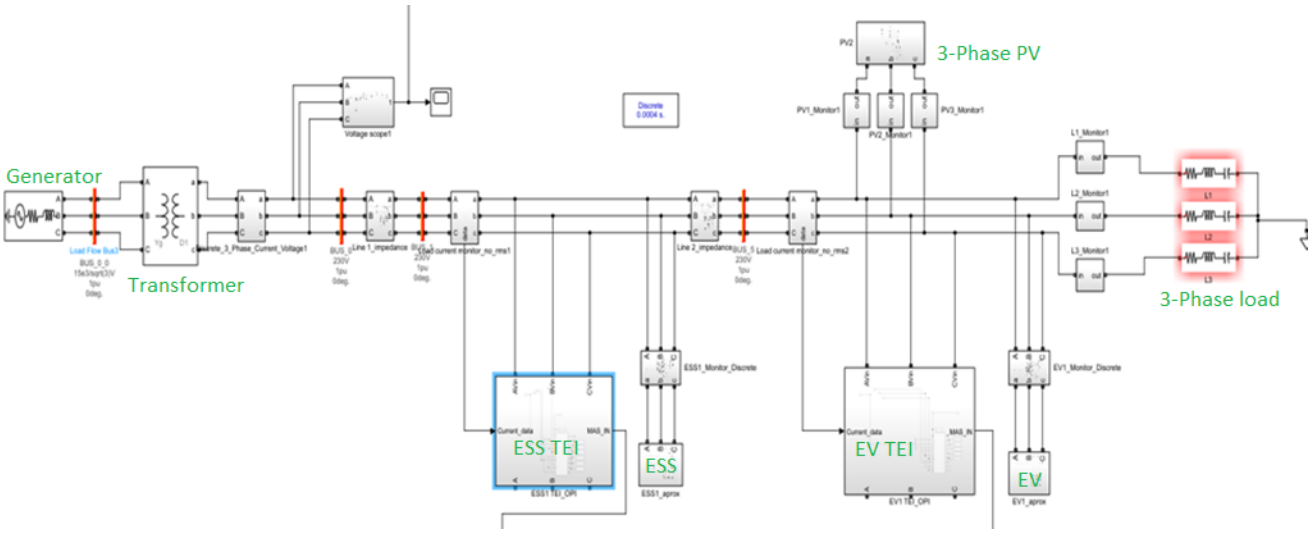

Figure 5-1: Simulink model of the test network

5.1 TEI Device verification and validation

This series of tests assess the performance of the TEI block model under a variety of test cases, TEI accuracy verification under various network conditions, and various test cases. The accuracy of the TEI is determined by comparing hand calculated Thevenin impedance values to the TEI determined Thevenin values.

5.1.1 TEI Accuracy tests

This section presents the results of the assessment of the accuracy of the TEI device at two different points in the network, the 1st point is at bus 2 (ESS position in the test network), and the 2nd point is at bus 3 (load and EV position). There will be two different sets of loads, loads of 0.9 pf and loads of 1 pf. The simulation is discrete with a sample time of 0.0004s and a

fundamental frequency of 50Hz. Figure 5-2 and Figure 5-3 shows the power gui parameters, it has been set to a discrete simulation type with a sample time of 0.0004 s.

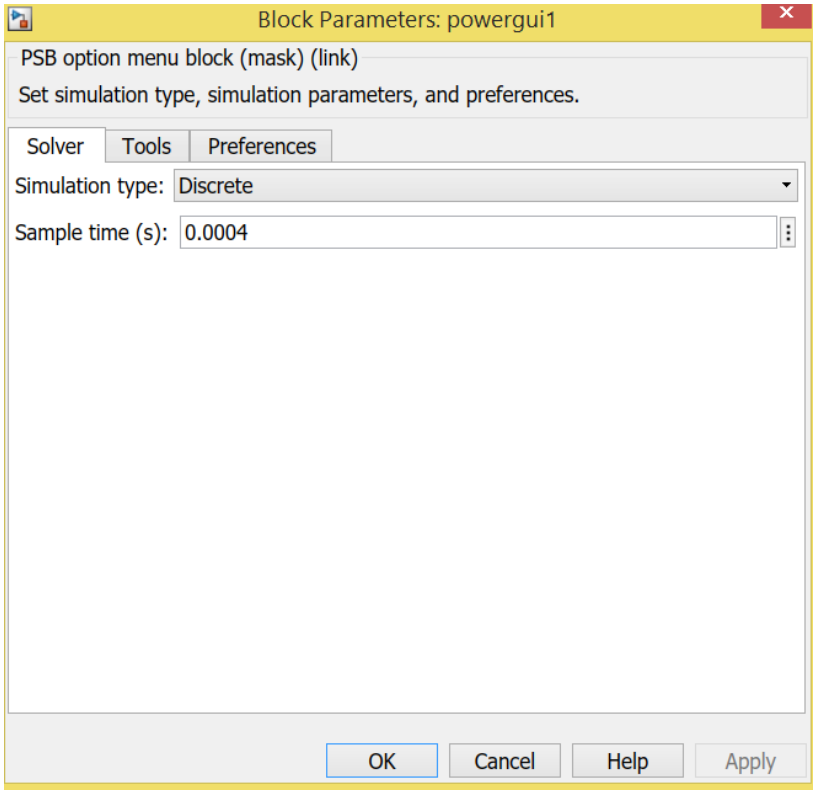

Figure 5-2: powergui parameters

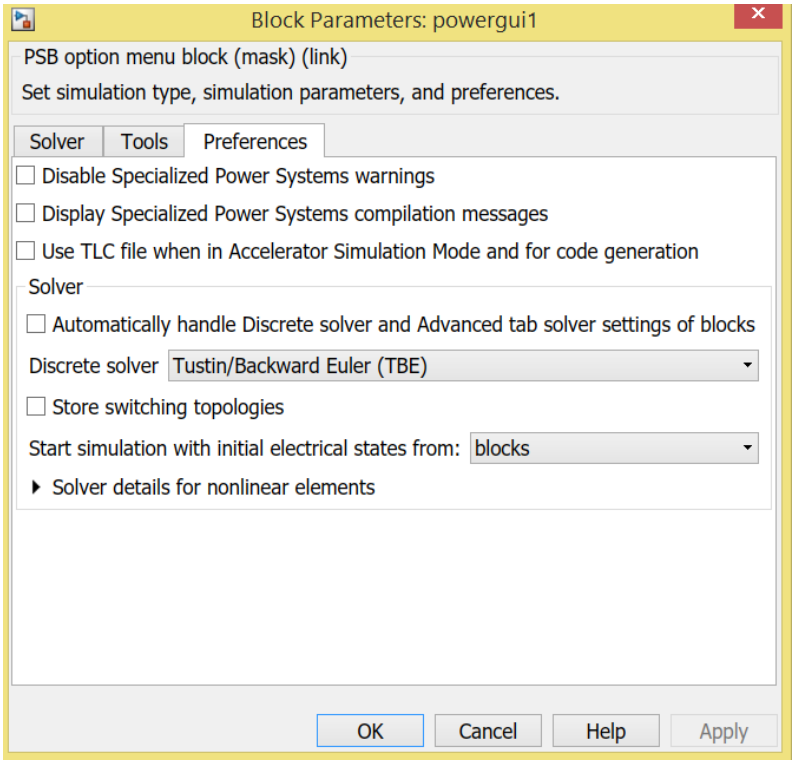

Figure 5-3: simulation preferences

5.1.1.1 Calculation formulation

To derive the Thevenin values, the Test network is simplified to a Thevenin equivalent network (current sources are disconnected and voltage sources are connected to ground) with the transformer reduced to its equivalent circuit ($R_m, X_m, R_1, X_1, R_2, X_2$) and the voltage source represented by its internal impedance. The second winding is the reference point.

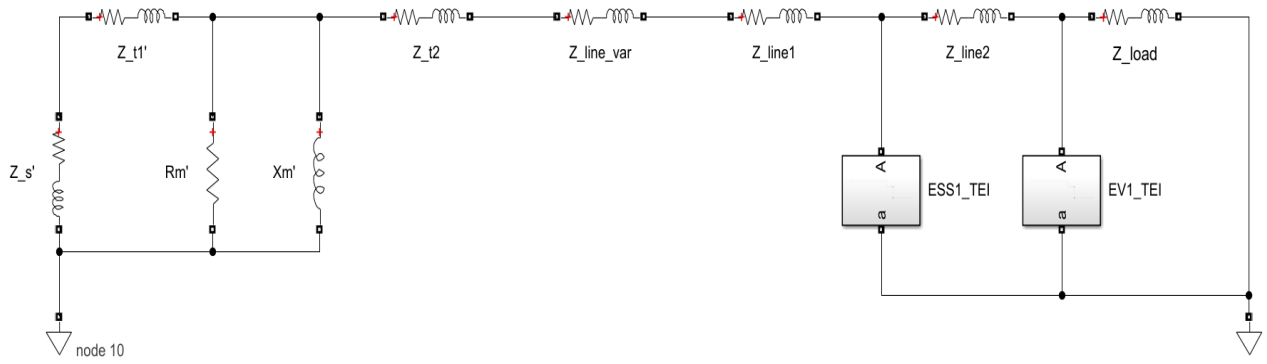

Figure 5-4: Thevenin equivalent network per phase.

Figure 5-4 is the simplified network model (with all the voltage sources shorted and the current sources open), this is replicated for each phase and is further simplified in Figure 5-5, with the voltage source and transformer impedance combined.

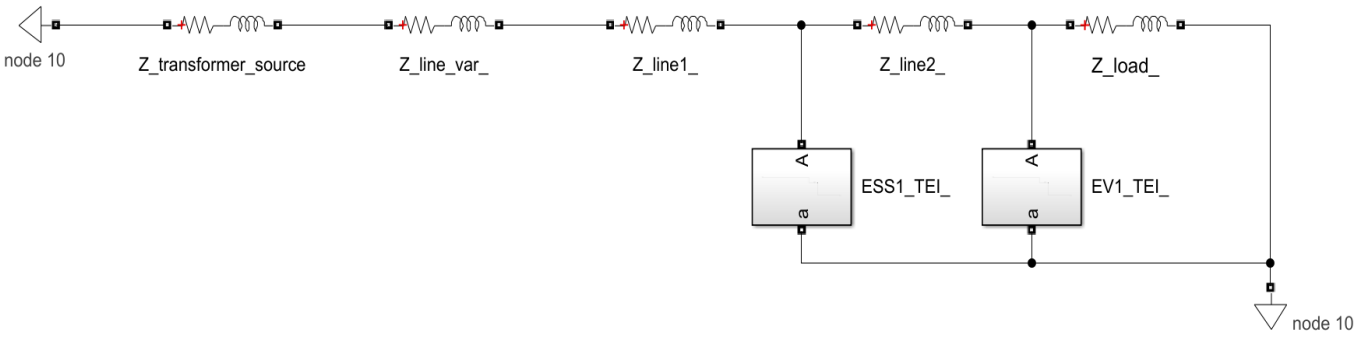

Figure 5-5: Thevenin equivalent network with reduced transformer and source model

The Thevenin impedance will be evaluated at two points (ESS and EV PCC). Their Thevenin impedances are expressed in equations (5-1), (5-2), (5-3), (5-4), (5-5), (5-6) and (5-7).

$$Z_{th,ESS} = \frac{1}{\frac{1}{Z_{t\_s} + Z_{line\_var} + Z_{line1}} + \frac{1}{Z_{line2} + Z_{load}}}\ \Omega$$

(5-1)

$$Z_{th,EV} = \frac{1}{\frac{1}{Z_{t\_s} + Z_{line\_var} + Z_{line1} + Z_{line2}} + \frac{1}{Z_{load}}}\ \Omega$$

(5-2)

$$Z_{t\_s} = Z_{t2}\ + \frac{1}{\frac{1}{Z_{t1}{}' + Z_s{}'} + \frac{1}{R_m{}'} + \frac{1}{X_m{}'}}\ \Omega$$

(5-3)

$$Z'_{t1} = \frac{Z'_{t1}}{a^2}\ \Omega$$

(5-4)

$$Z'_s = \frac{Z_s}{a^2}\ \Omega$$

(5-5)

$$R'_m = \frac{R_m}{a^2}\Omega$$

(5-6)

$$X'_m = \frac{X_m}{a^2}\ \Omega$$

(5-7)

Where:

- $Z_{th,ESS}$ is the Thevenin impedance as seen by the ESS at bus 2.
- $Z_{th,EV}$ is the Thevenin impedance as seen by the ESS at bus 3.
- Z_{t_s} is the combined impedance of the transformer and the 3-phase voltage source
- Z_{line_var} is the variable transmission impedance that will be static for this test.
- Z_{line1} is the impedance for transmission line 1
- Z_{line2} is the impedance for transmission line 2

- Z_{load} is the variable impedance of the RL load.
- $a = \frac{V_1}{V_2} = \frac{15000}{398}$
- $Z_s = R_s + iX_s$
- $V_{L-L} = \sqrt{3}V_{ph} = 15000V$
- $S_s = 65MVA$
- $\frac{X}{R} = 7$

Which can help solve equations (5-8), (5-9), (5-10) and (5-11):

$$\tan(\theta_s) = \frac{X}{R} \quad (5\text{-}8)$$

$$S_s = \frac{V_{ph}^2}{Z_S} \quad (5\text{-}9)$$

$$R_s = Z_s Cos\left(\tan^{-1}\left(\frac{X}{R}\right)\right) = \frac{V_{ph}^2}{Z_S} Cos\left(\tan^{-1}\left(\frac{X}{R}\right)\right) \quad (5\text{-}10)$$

$$X_s = Z_s Sin\left(\tan^{-1}\left(\frac{X}{R}\right)\right) = \frac{V_{ph}^2}{Z_S} Sin\left(\tan^{-1}\left(\frac{X}{R}\right)\right) \quad (5\text{-}11)$$

Equation (5-1) for bus 2 and Equation (5-2) for bus 3 are used to determine the Thevenin impedance per phase. There are 24 different tests done with 24 different 3-phase RL loads.

5.1.1.2 Load of 0.9 PF and 1.0 PF

There are 24 different balanced 3-phase loads that will be examined, varying from 10 Ω to 240 Ω per phase. The loads are modelled with RLC branch parameters like in **Error! Reference source not found.** to ensure simplicity with modelling.

5.1.1.3 Impact of Transformer

This is the same model in Figure 5-1 but without the transformer and a scaled-down voltage source. This will replicate the test in 5.1.1.2 (but only for a 1 pf) and compare the results of the two simulations.

5.1.1.4 Unbalanced system response

For this dissertation, impedance value accuracy is not necessarily critical, this is because the specific state of the network is irrelevant to the ESS and EV as their role is to charge and discharge most efficiently. Observing the quality of transmission (how large/small R_{th}) of each phase compared to the other for example, it would be more beneficial for the ESS to know phase A has a smaller R_{th} than phase B to divert more power to it, it is irrelevant to know the specific impedance value. This section presents the results of the analyses into how accurate the TEI is at recognizing unbalance in the network. A 5 Ω 3-phase impedance is used to introduce unbalance in the network. The transmission line undergoes a line impedance unbalance that goes from 5%, 10%, 15%, 20%, 25%, 30%, 35% and 40%. This unbalance is done for each phase, as shown in Table 5-1. The label 5**a** means an unbalance of **5**%, with phase **a** being the average impedance ($R_a = 5\Omega$), while Bus 2 (ESS PCC) is the point of analysis.

Table 5-1: The set resistance of the transmission line

R_a (Ω)	R_b(Ω)	R_c (Ω)	%unbalance (phase)
5	5.25	4.75	5a
4.75	5	5.25	5b
5.25	4.75	5	5c
5	5.5	4.5	10a
4.5	5	5.5	10b
5.5	4.5	5	10c
5	5.75	4.25	15a
4.25	5	5.75	15b
5.75	4.25	5	15c
5	6	4	20a
4	5	6	20b
6	4	5	20c
5	6.25	3.75	25a
3.75	5	6.25	25b
6.25	3.75	5	25c
5	6.5	3.5	30a

3.5	5	6.5	30b
6.5	3.5	5	30c
5	6.75	3.25	35a
3.25	5	6.75	35b
6.75	3.25	5	35c
5	7	3	40a
3	5	7	40b
7	3	5	40c

5.1.1.5 Simultaneous Modulation

Since the operation of the LV network will have multiple ESSs and EVs with TEI meters, it is worth examining the impact of multiple TEI meters operating simultaneously. The tests carried out in section 5.1.1.2 will be replicated but with the ESS (bus 2) and EV (bus 3) TEI operating simultaneously.

5.1.2 Case Studies

These case studies give a standalone analysis of the TEI device and the network's response to changes in loading and unbalance. These tests show the real-time performance of TEI and how it reacts to changes in a network. Each simulation lasts over 160 seconds with four segments (40 seconds each) and a sampling rate of 0.2s. The case studies are:

- Line Impedance fixed, and Load impedance at 0.9 PF are constant (the load and line impedance are balanced).
- Line Impedance fixed and Load impedance changes in magnitude three times (the load and line impedance are balanced): Increase demand by 0, 1.5, 2, and 2.5 times the base load of 1kW.
- Line Impedance fixed, and Load impedance changes %unbalance three times: %Unbalance changes from 0%, 10%, 15% and 20%.
- Line Impedance changes magnitude three times (balanced) and Load impedance fixed: Increase impedance by 0, 1.5, 2, and 2.5 times.

- Line Impedance changes %unbalance three times and Load impedance fixed: %Unbalance changes from 0%, 10%, 15% and 20%.

5.2 24 Hour simulation

The objective of these simulations is to observe the impact of the integration of MAS regulation and TEI guided optimal charging on a network. Its performance under unbalanced and balanced conditions was assessed with a focus on the voltage profile. The simulation process is illustrated in Figure 5-6.

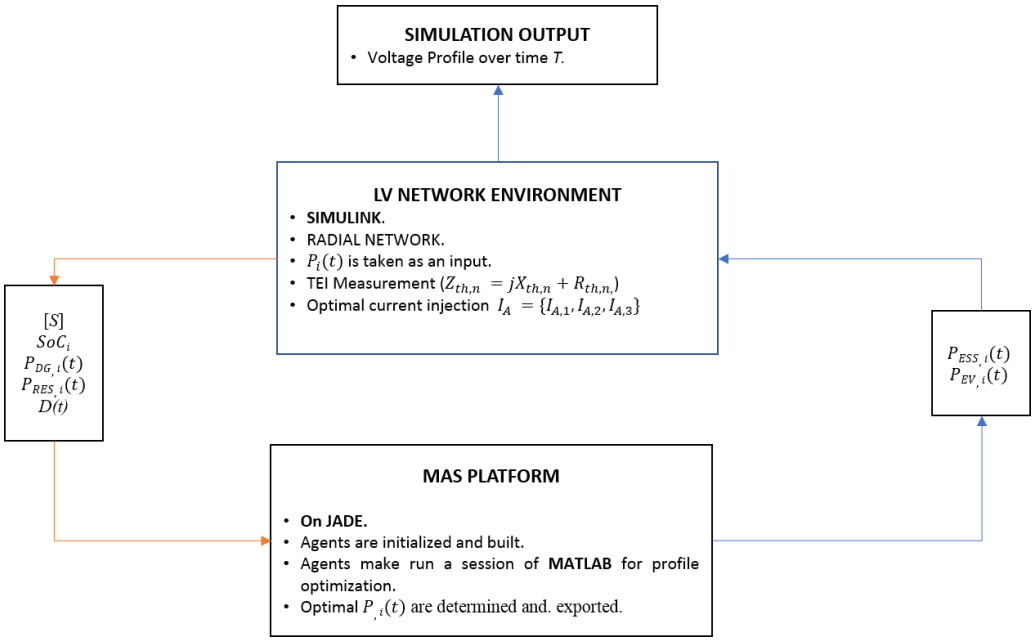

Figure 5-6: Flow diagram of the simulation

5.2.1 Summary of operation

The simulation begins with the loading of data (acquired from Open DSS simulations conducted on the Italian network model provided). There are two separate 24-hour simulations: the first simulation considered the guidance of the TEI data and uses this to determine the injections of the ESS and EV. The second simulation has the ESS and EV inject the power evenly across the three phases. It is to be noted that the ESS serves two functions: it acts as a loading mechanism to absorb the excess energy from the PV and it supports the network by supplying the absorbed energy for the EV when it is charging.

5.2.1.1 Basic System assessment

The basic system assessment shows network operation without any power transaction in the ESS or EV. It highlights the real power of the load and PV and their impact on the LV network voltage.

5.2.1.2 MAS System assessment

This section presents the results of a test conducted with all entities present in the network. There is a test done with uncoordinated charging, and coordinated (MAS) charging, the voltage profiles of both systems are compared and discussed.

5.2.1.3 ESS assessment

The ESS assessment test consists of the ESS and a single transmission line (the line between bus 1 and bus 2) loading the voltage source and the transformer. There is no 3-phase PV, EV or 3-phase load present, the impact of the ESS is analyzed, and the shape of the curve is discussed. The impact of the TEI on the system is analyzed.

5.2.1.4 ESS and EV assessment

The ESS and EV assessment are exclusively for the EV and ESS and is accompanied by the two transmission lines in the network. The impact of the ESS and EV are examined.

5.2.1.5 ESS, EV and 3-phase Load assessment

A test with the exclusion of the 3-phase PV.

5.2.1.6 ESS, EV and 3-phase PV assessment

A test with the exclusion of the 3-phase load.

5.2.1.7 Full Test network assessment

All entities are present, and the performance of the whole system is analyzed

5.2.1.8 Unbalanced system analysis

The tests carried out here is an extension of the tests carried out in 5.1.1.4 but examines the losses incurred by the ESS and EV (the 3 phase RL load and the 3-phase PV are absent), injecting power optimally, the voltage unbalance and a full system test with a 50% transmission unbalance.

6 Simulation results and Discussion

The results of the simulation protocol discussed in chapter 5 are presented and analyzed in this chapter.

6.1 TEI block assessment results and accuracy validation

6.1.1 TEI accuracy validation

This section analyses the accuracy of the TEI device (issues in accuracy are to be expected as discussed in section 2.7.4, where the constraints with Tellegen's Theorem and active TEI measurement are discussed).

6.1.1.1 Traditionally (passive) determined TEI values

This section presents the results of the traditional TEI determination.

6.1.1.1.1 Constant parameters

The constant impedances used to hand calculate Thevenin impedance values are:

- $Z_{t\_s} = 0.064 + 2.542i\ \Omega$ the combined impedance of the transformer and the voltage source per phase.
- $Z_{line\_var} = 1 + 0.0314i\ \Omega$
- $Z_{line1} = 0.25 + \ 0.182i\ \Omega$
- $Z_{line2} = \ 0.16 + \ 0.082i\ \Omega$

6.1.1.1.2 3-phase RL load at 1 PF

The calculations for a system with a purely resistive load at bus 2 (ESS PCC) and bus 3 (EV PCC) are shown in Figure 6-1 and Figure 6-2.

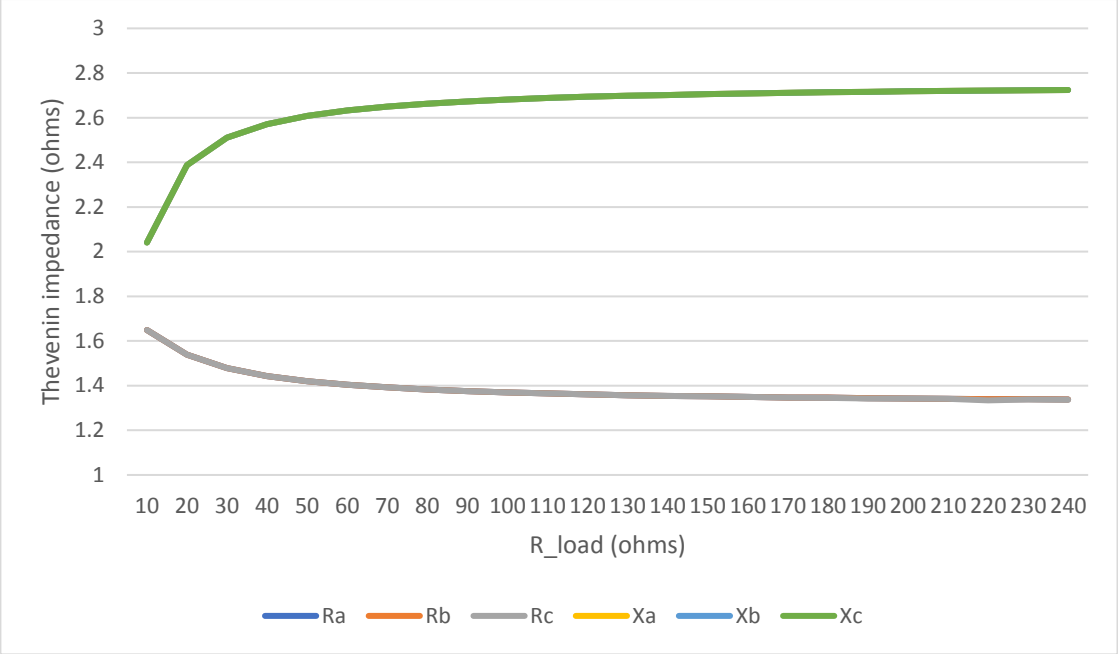

Figure 6-1:Traditionally determined Thevenin impedance at Bus 2 for a variable 3-phase load with a 1 pf

Figure 6-1 and Figure 6-2 have an independent variable of R_{load}, as R_{load} increases R_{th} decreases and X_{th} increases.

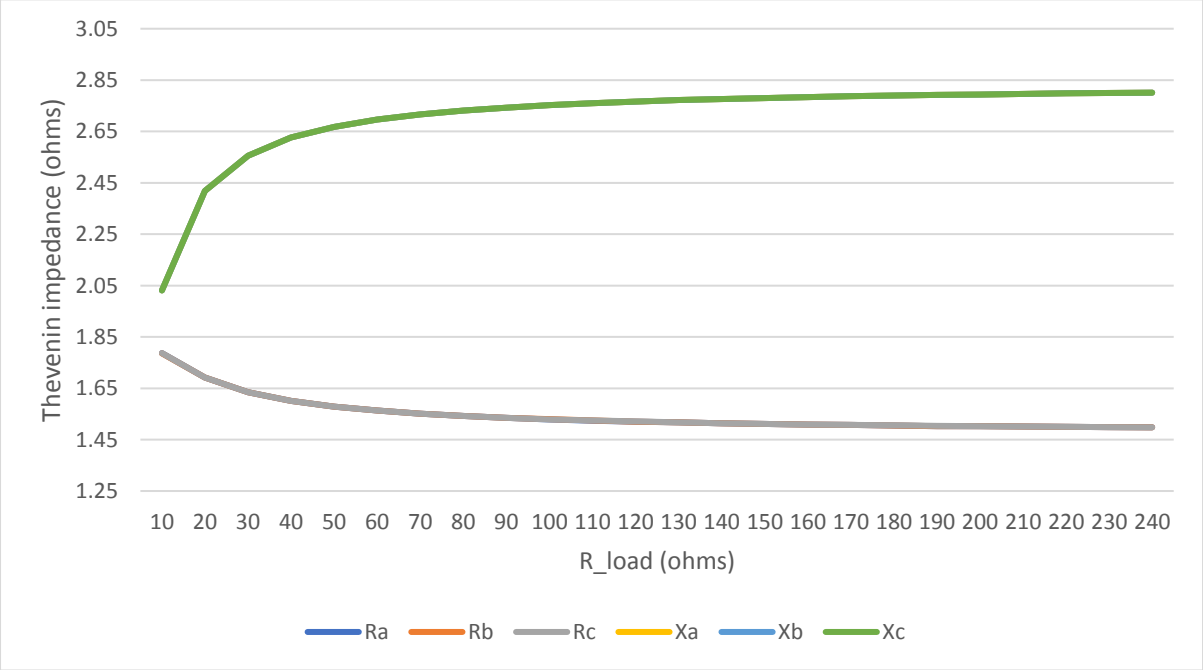

Figure 6-2: Traditionally determined Thevenin impedance at Bus 3 for a variable 3-phase load with a 1 pf

6.1.1.1.3 3-phase RL load at 0.9 PF

The calculations for a system with a 3-phase RL load of 0.9 PF at bus 2 (ESS PCC) and bus 3 (EV PCC) are presented in Figure 6-3 and Figure 6-4.

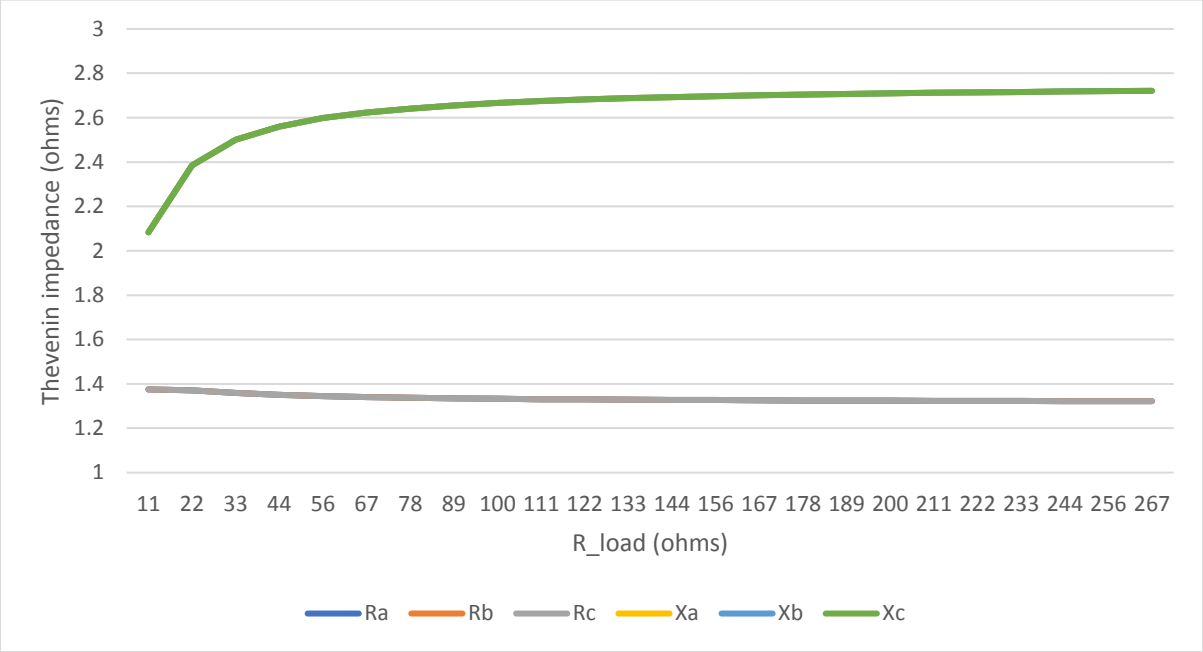

Figure 6-3: Traditionally determined Thevenin impedance at Bus 2 for a variable 3-phase load with a 0.9 pf

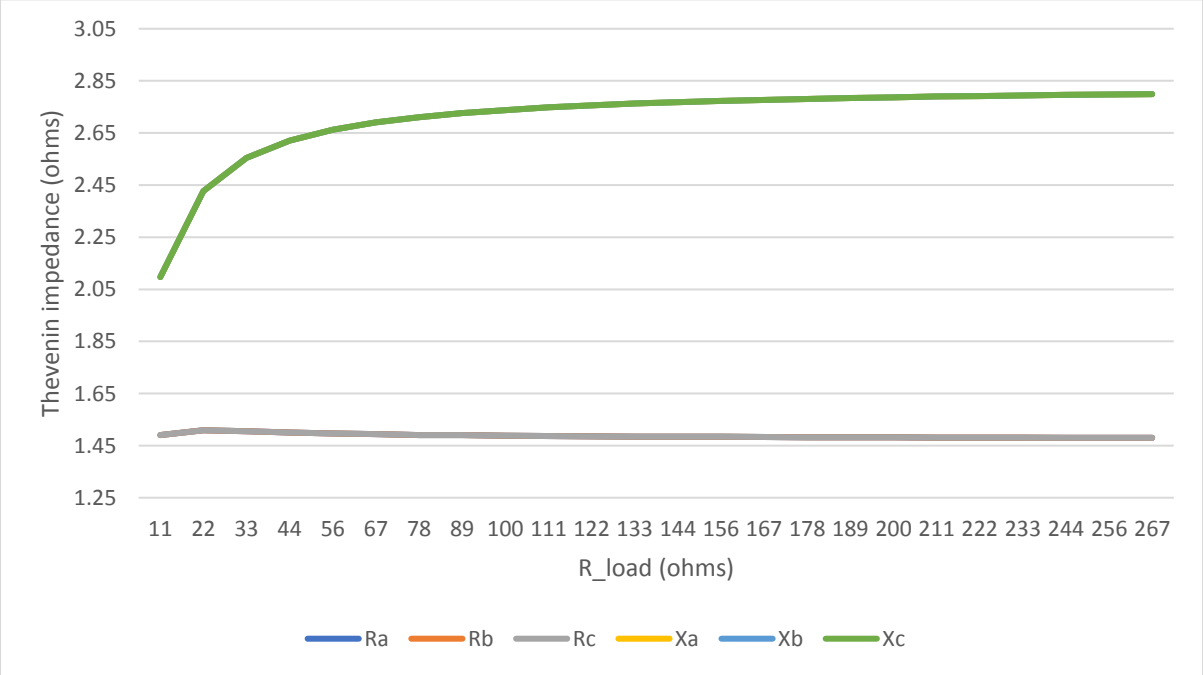

Figure 6-4: Traditionally determined Thevenin impedance at Bus 3 for a variable 3-phase load with a 0.9 pf

The results for X_{th} and R_{th} follow the same pattern discussed in section 6.1.1.1.2.

6.1.1.2 TEI Simulation results

6.1.1.2.1 3-phase RL load at 1 PF

Here are the measurements for the TEI sensor for a load resistive load that varies from $10\ \Omega - 240\ \Omega$ (24 different loads) are shown in Figure 6-5 and Figure 6-6.

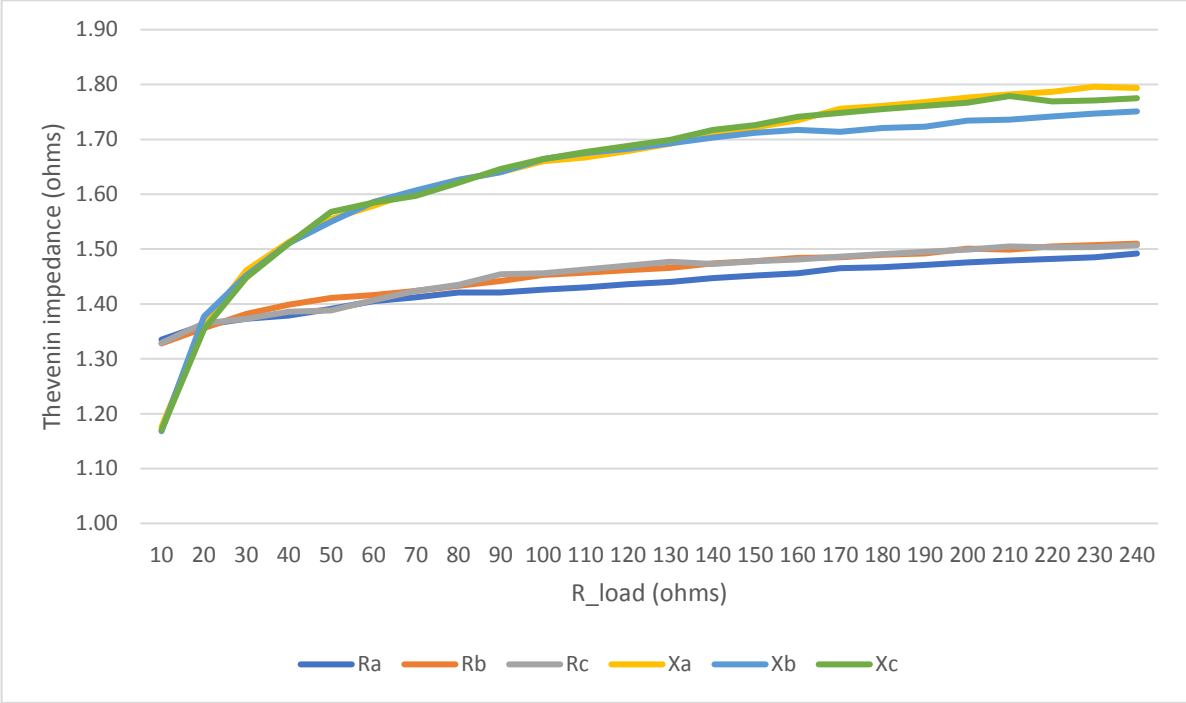

Figure 6-5:Measured Thevenin impedance at Bus 2 for a variable 3-phase load with a 1 pf

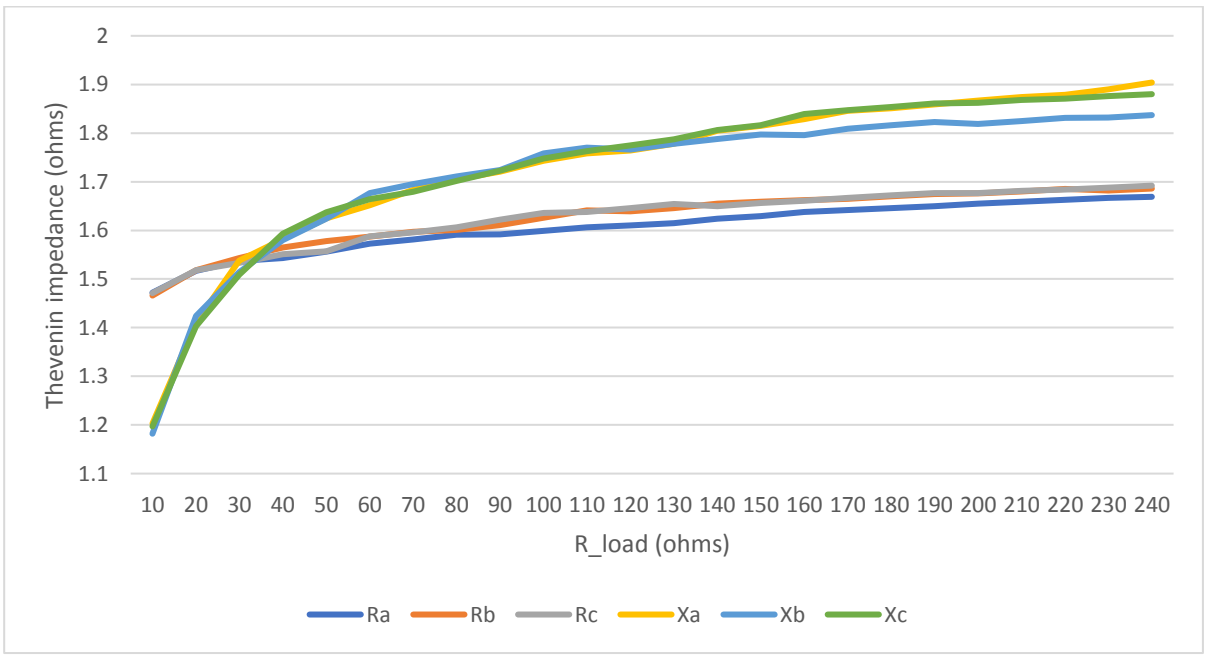

Figure 6-6: Measured Thevenin impedance at Bus 3 for a variable 3-phase load with a 1 pf

Figure 6-5 and Figure 6-6 have an increasing R_{th} and X_{th} on an increasing R_{load}.

6.1.1.2.2 3-phase RL load at 0.9 PF

The measurements for the TEI sensor for a RL load (Z_{load}) that varies from $11.1\ \Omega - 267\ \Omega$ (24 different loads) are presented in Figure 6-7 and Figure 6-8.

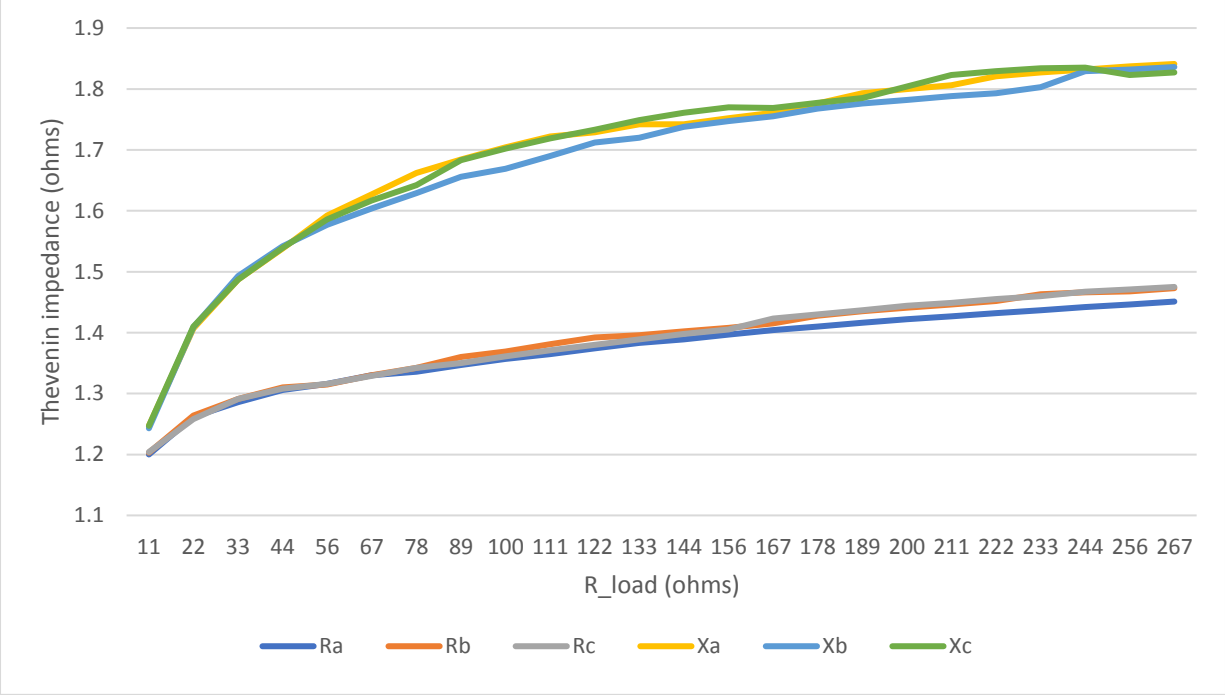

Figure 6-7: Measured Thevenin impedance at Bus 2 for a variable 3-phase load with a 0.9 pf

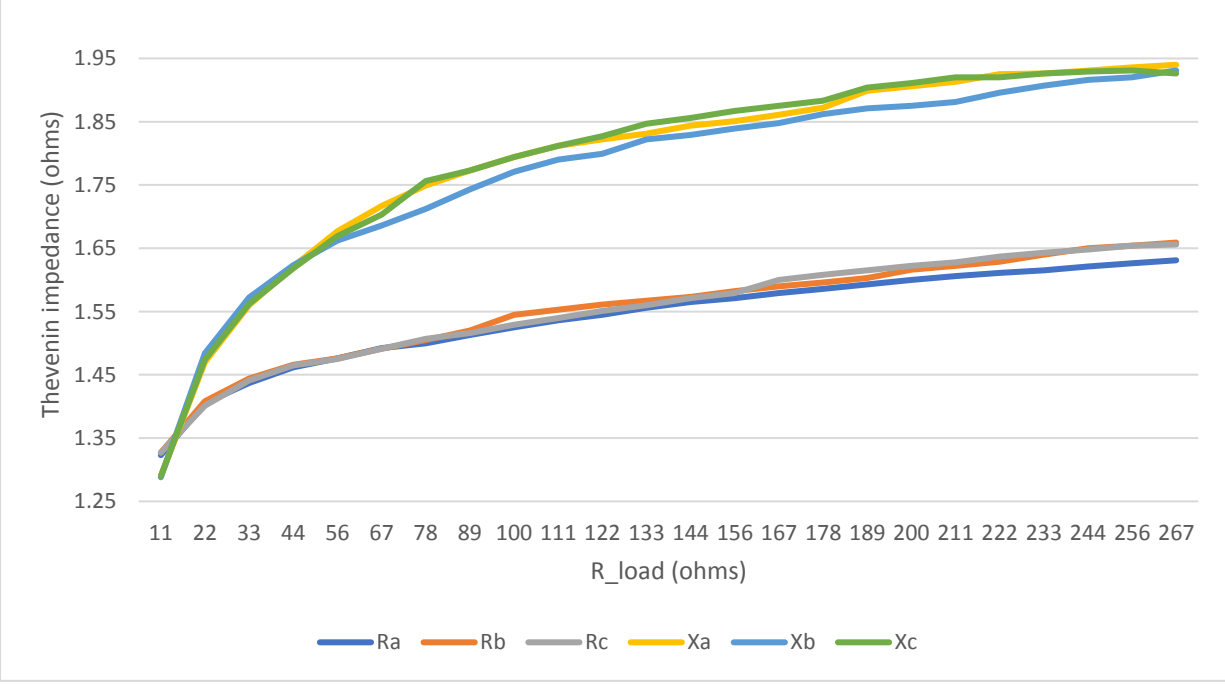

Figure 6-8: Measured Thevenin impedance at Bus 3 for a variable 3-phase load with a 0.9 pf

The results of Figure 6-7 and Figure 6-8 are similar to the results of Figure 6-5 and Figure 6-6 with an increasing Z_{th} on an increasing R_{load}. The behavior of the Thevenin output is independent of the power factor of the load.

6.1.1.3 Analysis and Discussion of the comparison of Passive TEI with the results of the Active TEI sensor model

This section compares the results presented in sections **Error! Reference source not found.** and 6.1.1.2 by determining the % difference between the hand calculated Thevenin impedances (the accurate results) and the measured impedances. This % difference is determined by equation (6-1):

$$\%Difference = (1 - \frac{Z_{th,hand}}{Z_{th,measured}}) \cdot 100 \quad (6\text{-}1)$$

Where:

- $Z_{th,hand}$ is the hand calculated Thevenin Equivalent Impedance or TEI (and is treated as the accurate value).
- $Z_{th,measured}$ is the TEI determined by the TEI sensor discussed in sections 2.7.4, 2.7.5 and 4.1.2.

The results of the difference between the hand calculated TEI and measured TEI are presented in Figure 6-9, Figure 6-10, Figure 6-11 and Figure 6-12.

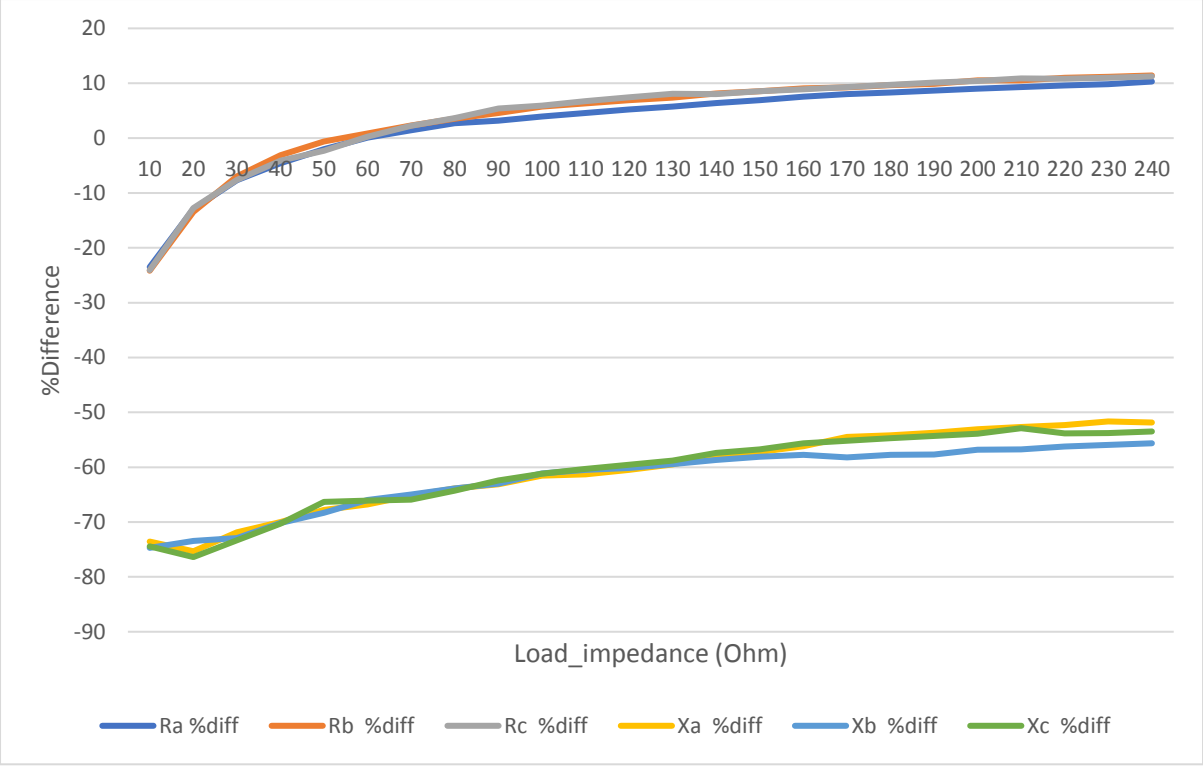

Figure 6-9: Percentage difference between the hand calculated Thevenin values and TEI determined Thevenin values for bus2 for a variable load at 1 pf

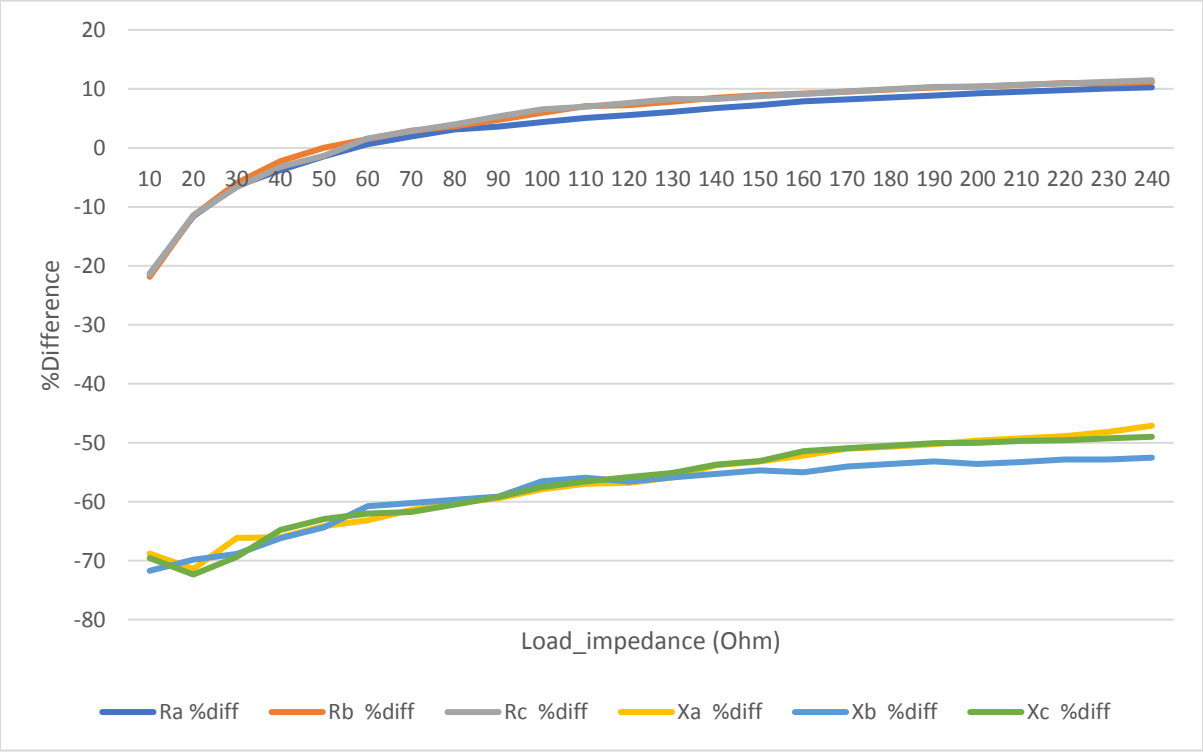

Figure 6-10: Percentage difference between the hand calculated Thevenin values and TEI determined Thevenin values at bus3 for a variable load at 1 pf

Figure 6-9 and Figure 6-10 shows that the value of hand calculated Thevenin resistance is much closer to that of the measured resistance and shows poor accuracy between the measured and hand calculated values of the reactance. The accuracy (when compared to normal means of determining Thevenin impedance) of the reactance ranges from -50% to -70% while the resistance varies from -20% – 12%. The absolute minimum difference ($|\%Difference_{minimum}|$) for both the Thevenin resistance and reactance is 0.073% (bus 2) and 0.6% (bus 3) at $Z_{load} = 60\ \Omega$. At lower Z_{load} the TEI sensor determines Z_{th} to be smaller than the hand calculated values with the $\%Difference$ flattening to around 12%. This flattening is due to decreased effect of the load change, as the earlier load changes were more significant and would result in a more pronounced change in load current flowing through the network (like changing R_{load} from 10Ω to 20Ω is reducing the current demand by 50% while changing from 230Ω to 240 Ω results in a change of 4%).

The results show that there is a relationship between loading (the amount of current flowing through the network) and the level of accuracy (when compared to hand calculated Thevenin values) of the TEI sensor, it appears that higher currents might cause an underestimation of the Z_{th} values (small load resistance of 10Ω) and an overestimation at lower loading (240Ω). Higher current means a lower Voltage (this is dependent on the VA rating of the MV/LV transformer, and a weaker transformer, changing the specified 650 kVA transformer to a smaller 20kVA transformer, was purposefully selected for these reasons). This can be observed in the equations (2-31) and (2-32) discussed in chapter 2.7 of the literature review, which shows the voltage is proportional to the difference in voltage measured at the PCC of the TEI sensor. The inaccuracy of the TEI estimation (when compared to the hand/analytical method derived in section 5.1.1.1) was to be expected as discussed in section 2.7.4 and stated in [34] and [36]. The TEI device makes use of the convenient active parametric estimation method (Tellegen's Theorem) which took on a black-box approach to get Z_{th} and did not need model specific data of the network. This convenience came at the cost of accuracy [34].

Figure 6-11 and Figure 6-12 are the replication of the results just discussed for an Z_{load} with a 0.9 pf.

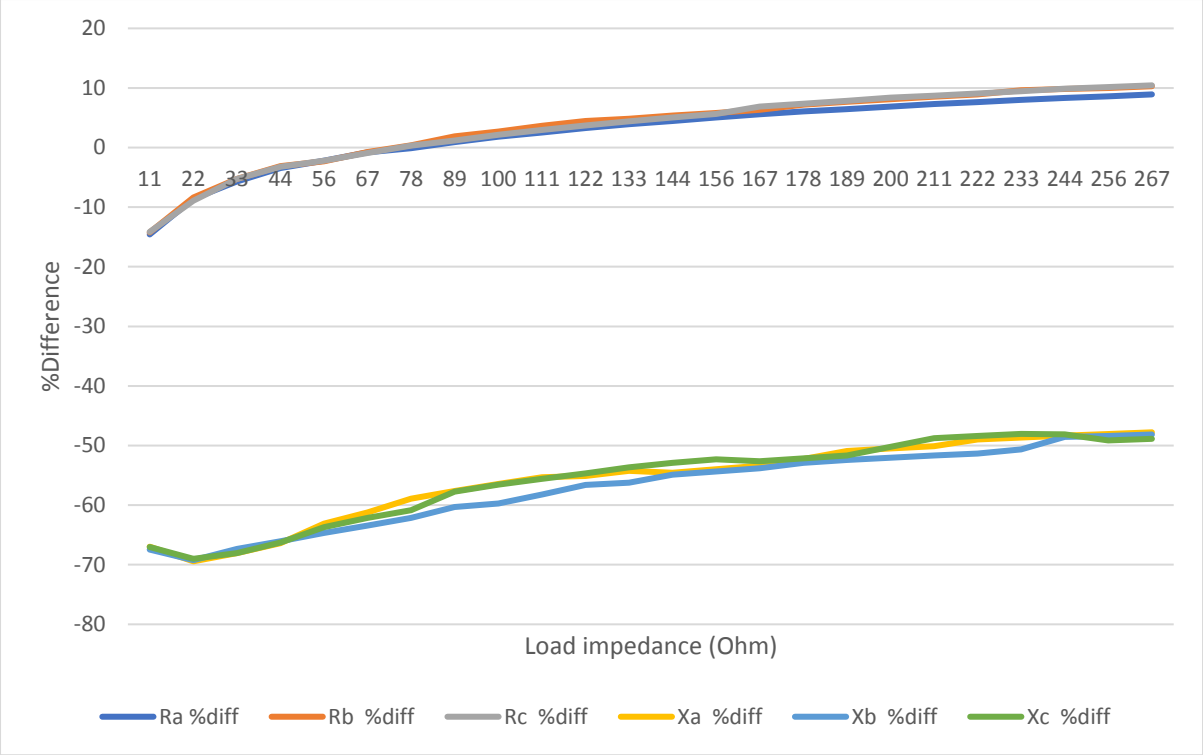

Figure 6-11: Percentage difference between the hand calculated Thevenin values and TEI determined Thevenin values for bus2 for a variable load at 0.9 pf

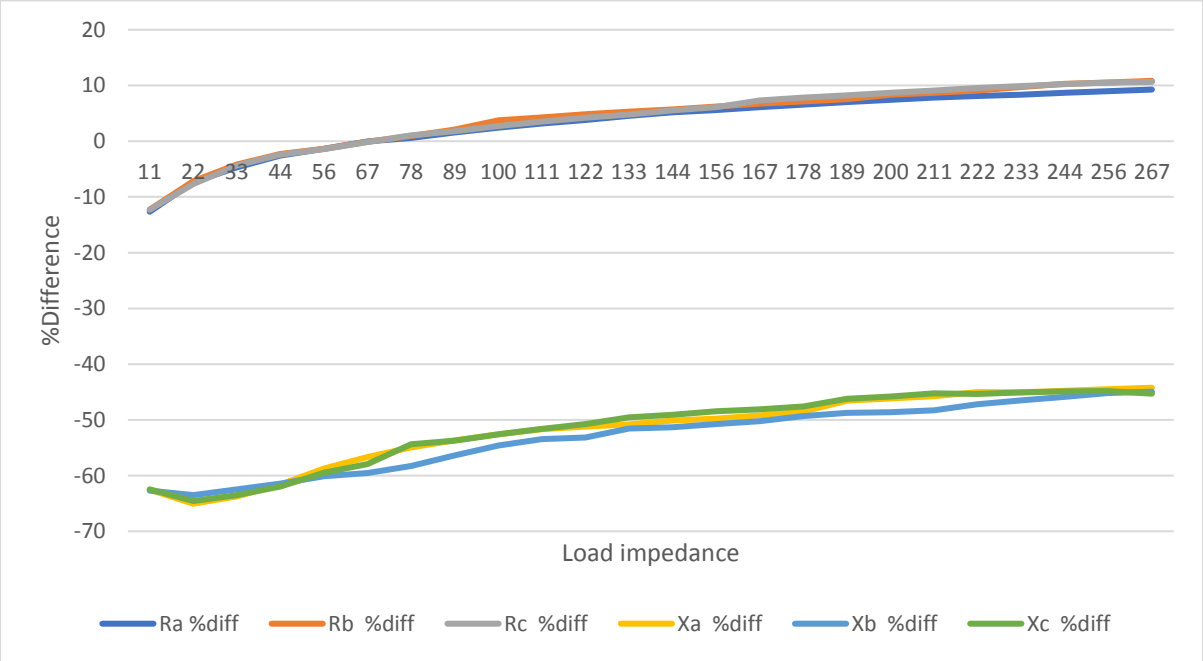

Figure 6-12: Percentage difference between the hand calculated Thevenin values and TEI determined Thevenin values at bus3 for a variable load at 0.9 pf

The observations in Figure 6-11 and Figure 6-12 appear to be the same as that of a completely resistive load. The only significant deviation between the test with a load of 0.9 pf and 1 pf is the alignment of the reactive impedance $\%difference$ at higher impedance for the system with a 0.9 pf load. This is likely due to the increased presence of reactive elements than for a purely resistive load.

The massive deviation in the $\%Difference$ for X_{th} is not clear from the results as seen in Figure 6-9, Figure 6-10, Figure 6-11 and Figure 6-12. Thus, it has been observed (in [45]) that the Transformer has an impact on the TEI sensors accuracy.

6.1.2 Impact of Transformer

These are the results (Figure 6-13, Figure 6-14, Figure 6-15 and Figure 6-16) of TEI estimation conducted without a transformer present in the LV test network (with every other component directly coupled with the 3-phase Voltage source). The results of this section are compared to the results in section 6.1.1 (the impact of the transformer) and highlight some of the constraints on the TEI sensor. The loading is purely resistive, so only the results of section 6.1.1.2.1 are of concern.

6.1.2.1 Traditionally determined TEI values

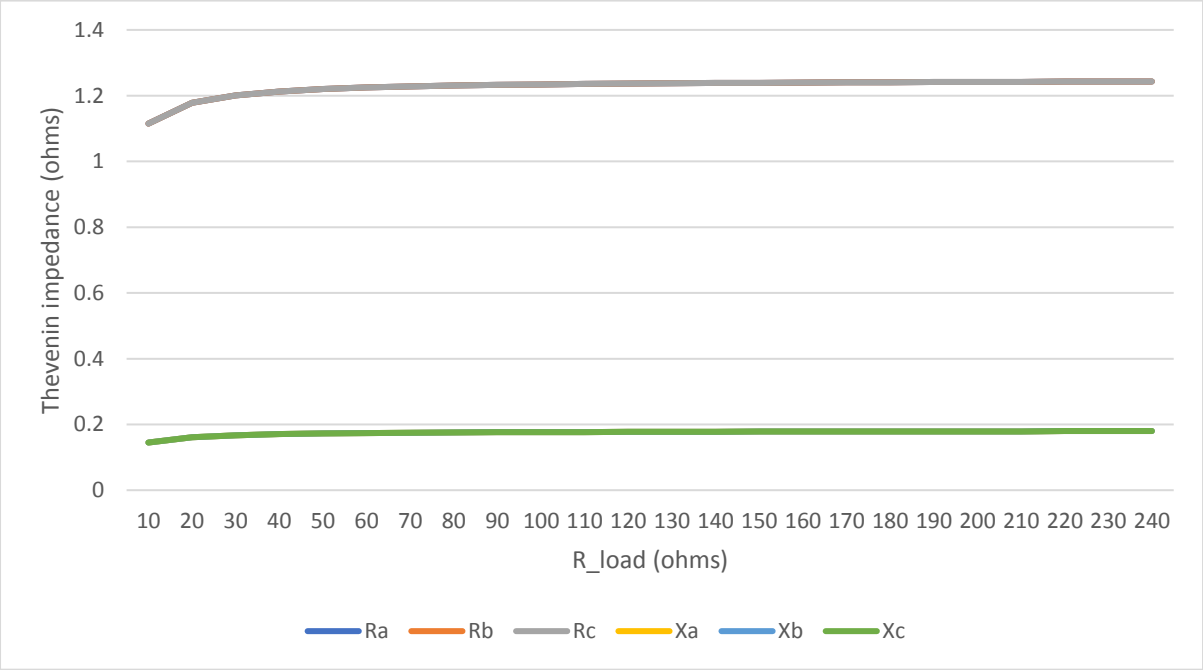

Figure 6-13: Traditionally determined Thevenin impedance at bus 2 for a variable 3-phase load with a 1 pf (no transformer)

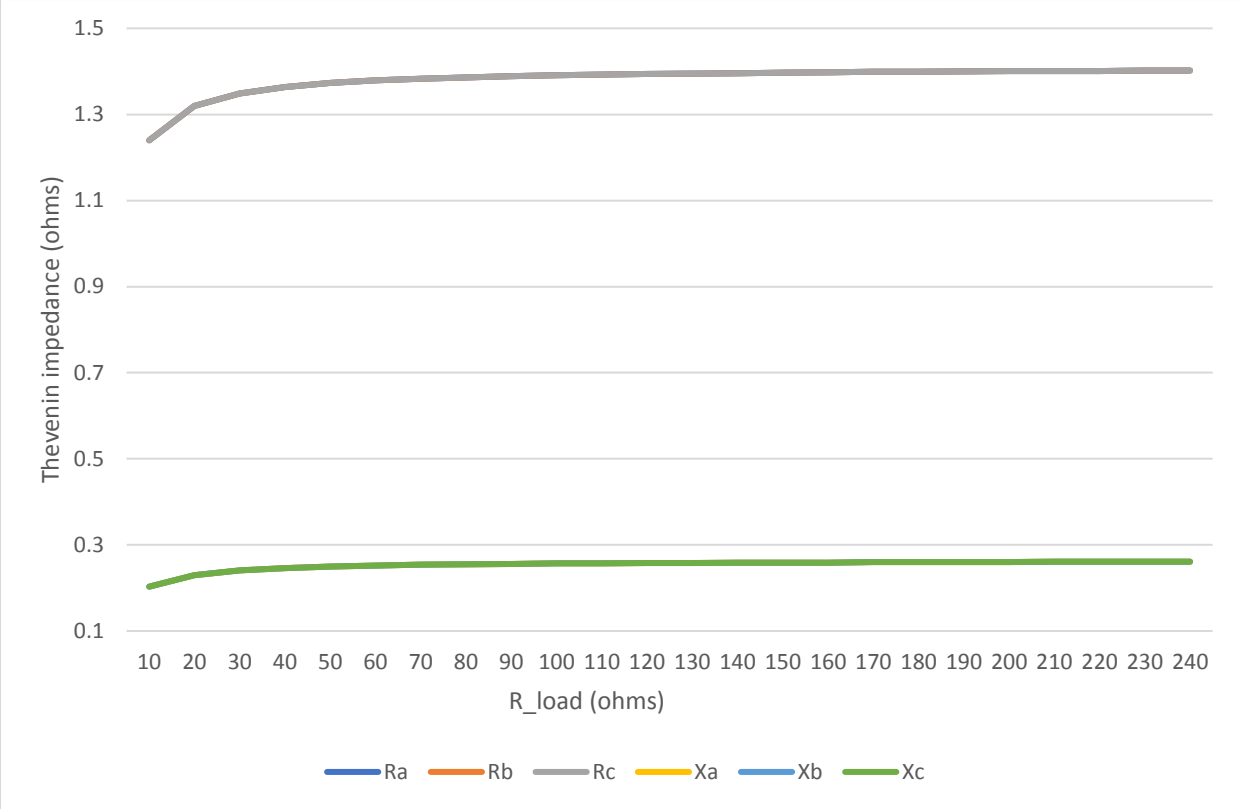

Figure 6-14: Traditionally determined Thevenin impedance at bus 3 for a variable 3-phase load with a 1 pf (no transformer)

The calculated R_{th} and X_{th}, in Figure 6-13 and Figure 6-14, increases with an increasing R_{load}.

6.1.2.2 Measured values

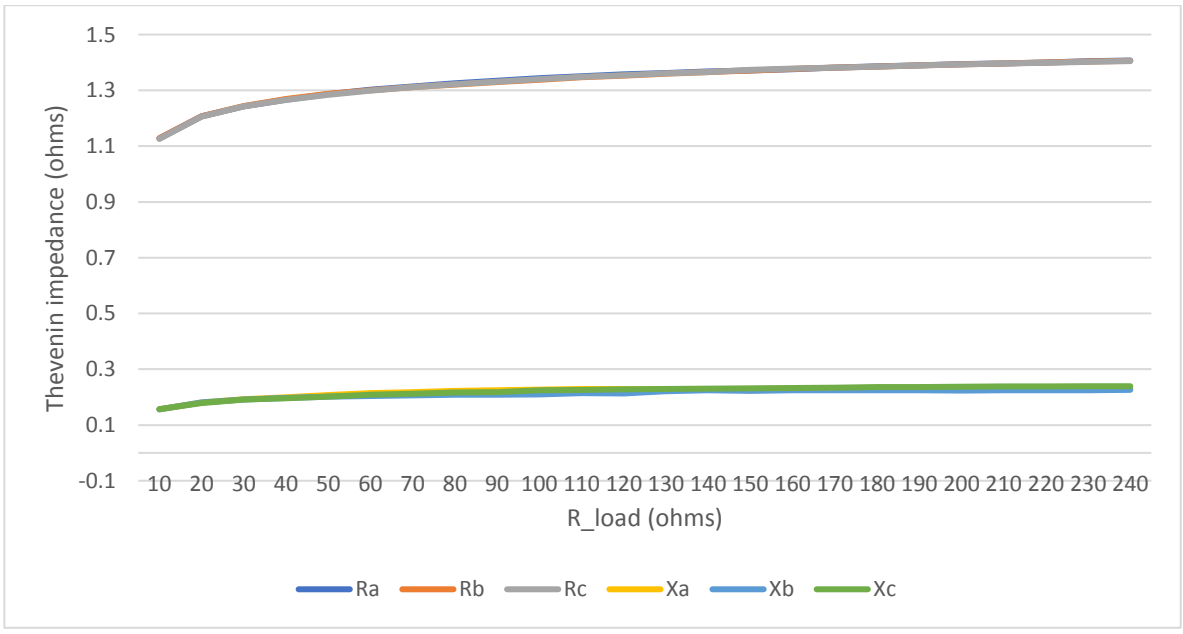

Figure 6-15: TEI measured Thevenin impedance at bus 2 for a variable 3-phase load with a 1 pf (no Transformer)

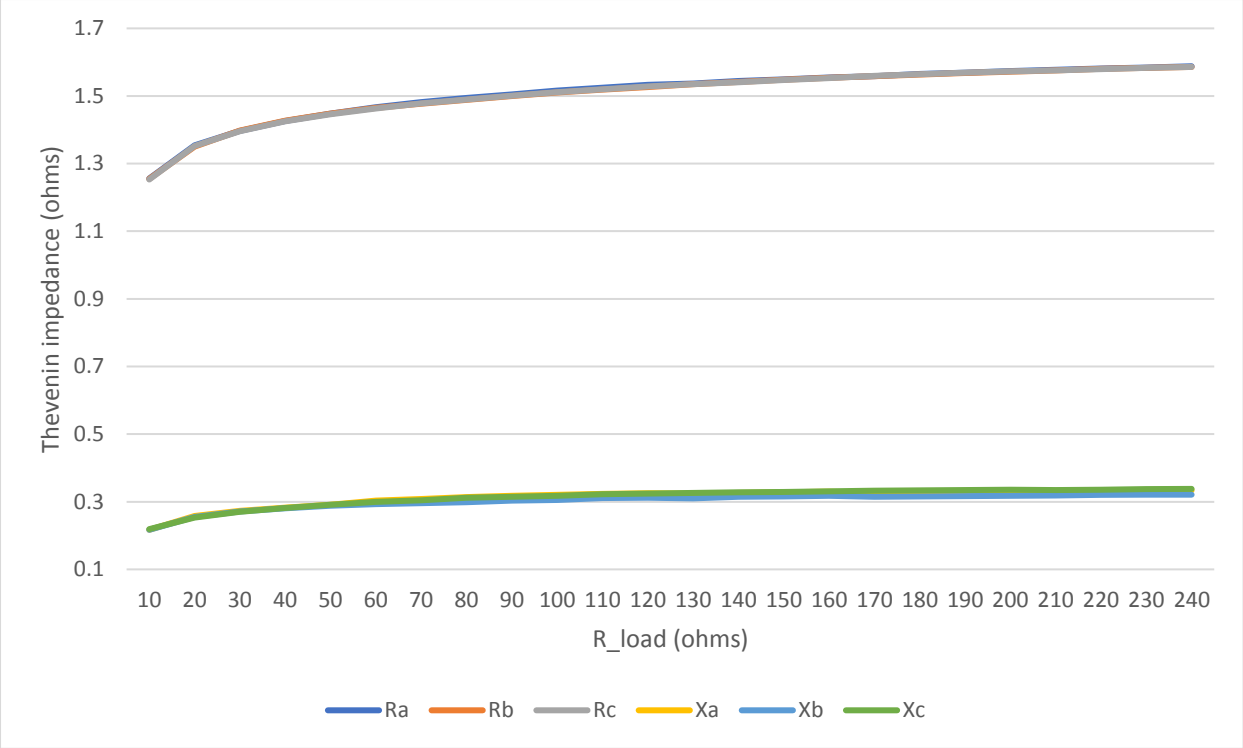

Figure 6-16: TEI measured Thevenin impedance at bus 3 for a variable 3-phase load with a 1 pf (no Transformer)

The measured R_{th} and X_{th}, in Figure 6-15 and Figure 6-16, increases with an increasing R_{load}.

6.1.2.3 Analysis and discussion

This section discusses the results presented in sections 6.1.2.1 and 6.1.2.2 and compare them to the results in sections **Error! Reference source not found.** and 6.1.1.2.

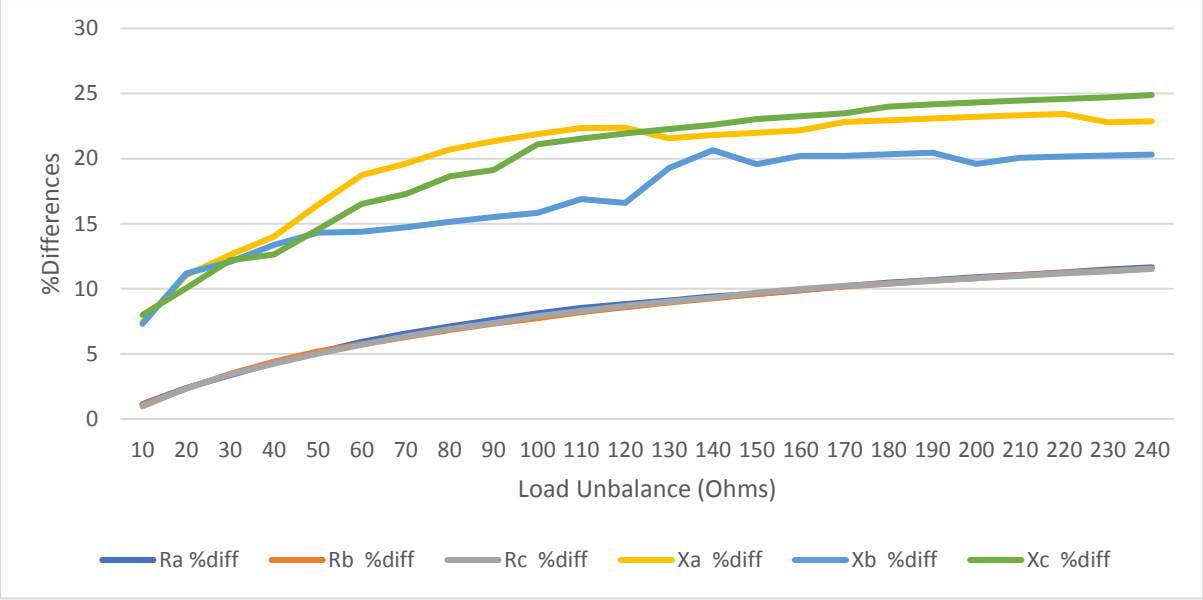

Figure 6-17: Percentage difference between the hand calculated Thevenin values and measured Thevenin values at bus 2 for a variable load at 1 pf (Transformer)

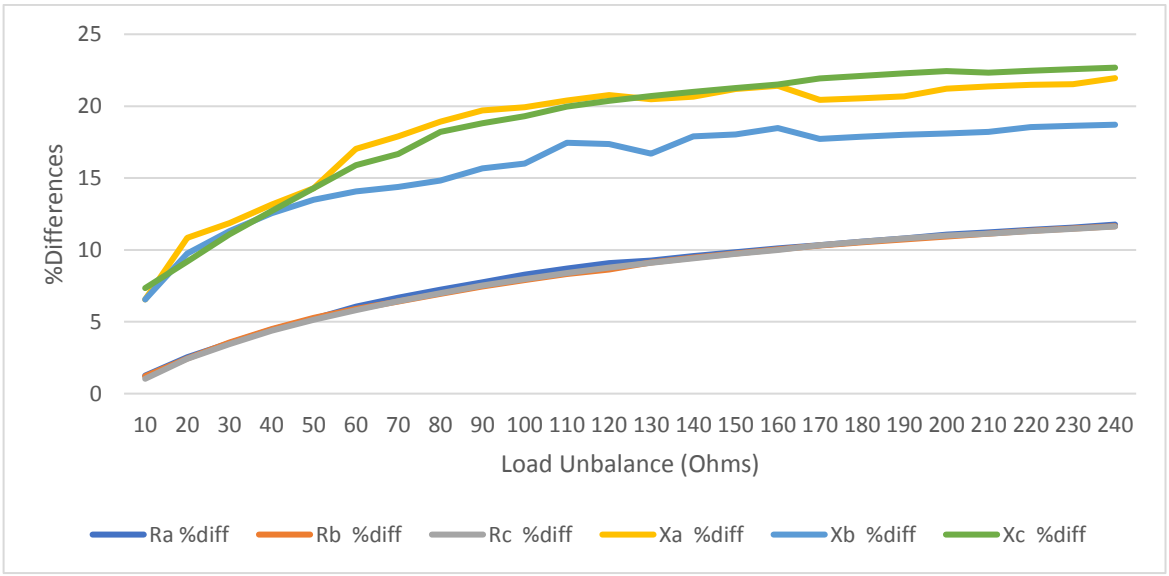

Figure 6-18: Percentage difference between the hand calculated Thevenin values and measured Thevenin values at bus 3 for a variable load at 1 pf (Transformer)

Figure 6-17 and Figure 6-18 show the $\%Difference$ (determined by the equation (6-1)) between the hand calculated TEI values and the measured TEI values. Both figures show there is a stronger correlation between hand calculated values for the resistance and a weaker correlation for the reactance (very similar to the results in section 6.1.1.2). With the $\%Difference$ of the Thevenin reactance (X_{th}) ranging from 7% – 25% while the resistance varies from 0.9% – 12% (the maximum $\%Difference$ is similar to the tests carried

out in section 6.1.1). The $|\%Difference_{minimum}|$ for both the Thevenin resistance and reactance is 0.9% (bus 2) and 1.03% (bus 3) at $Z_{load} = 10\ \Omega$ (the lowest Z_{load}).

Similar to findings in section 6.1.1, there is an inverse relationship between loading and the accuracy (the proximity between the hand calculated values and the TEI measured values) of the TEI sensor, meaning the stronger the loading, the less accurate the TEI determined Thevenin values. However, this means that on a network with a more suitable transformer and heavy loading, the TEI sensor will accurately and conveniently estimate TEI and will result in optimal performance when needed most (under heavy system operation). Figure 6-19 and Figure 6-20 highlight the average $\%Differences$ (the average of the phases for each bus) for operation with and without the transformer for the respective buses.

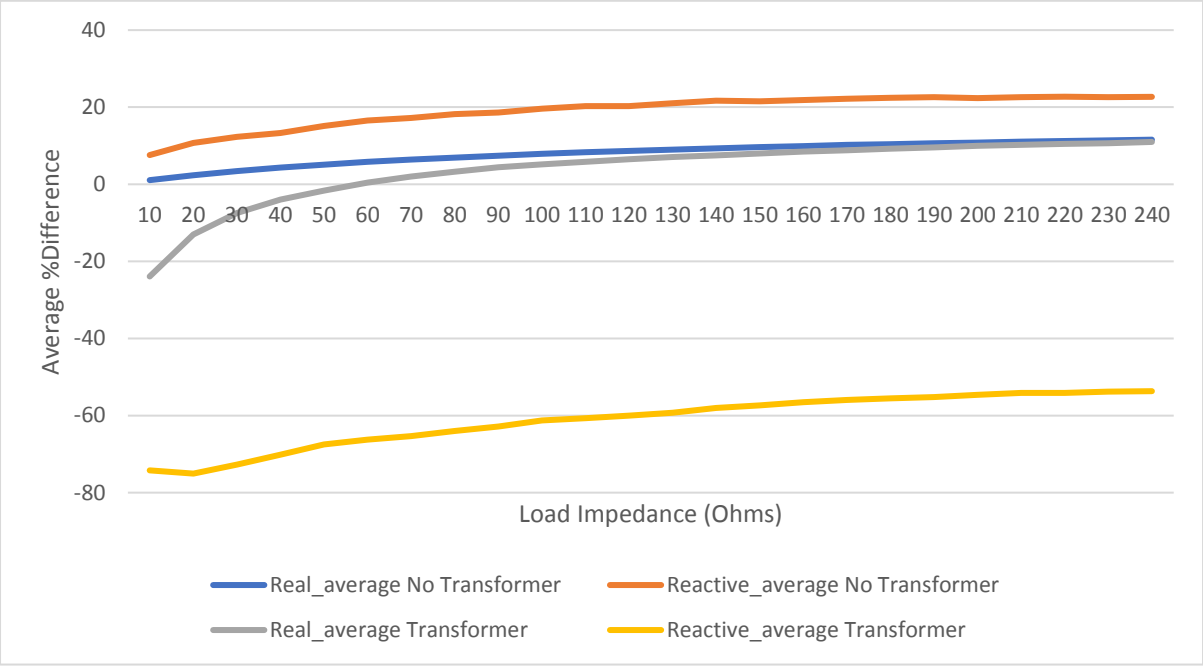

Figure 6-19: The average percentage difference in Thevenin impedances (measured and calculated) for bus 2

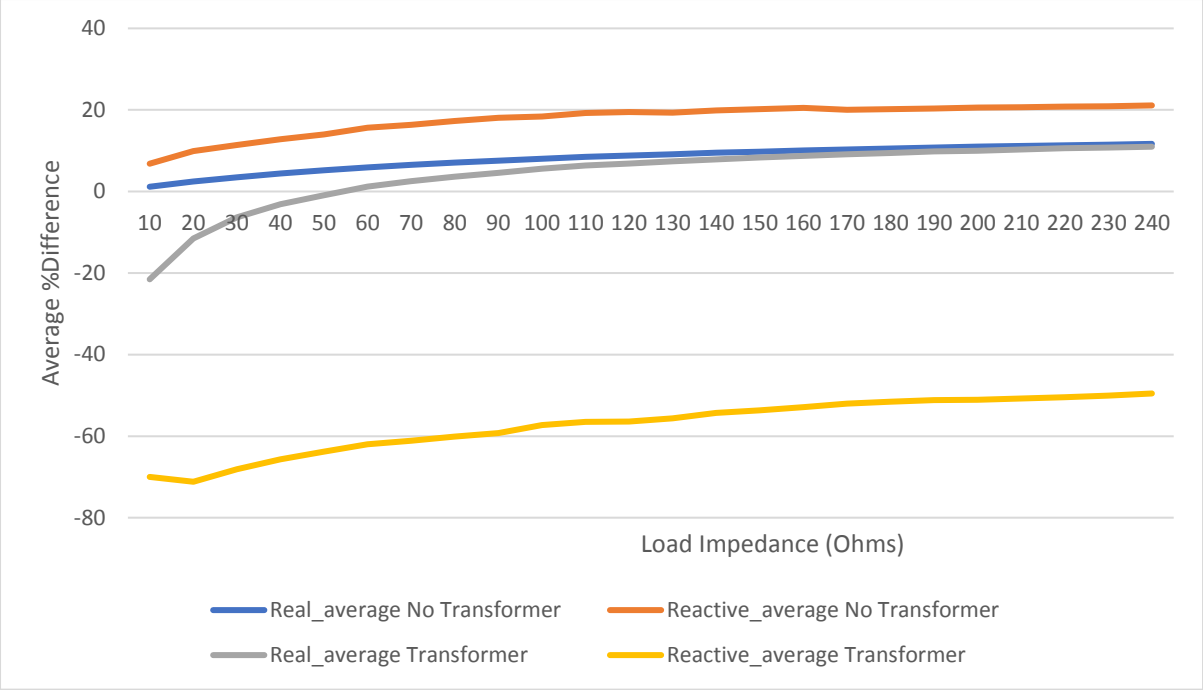

Figure 6-20: The average percentage difference in Thevenin impedances (measured and calculated) for bus 3

The most significant discrepancy between the tests presented in section 6.1.1 and in this section is the absence of smaller measured Thevenin impedances than hand calculated impedances (This is observed from all the $\%Differences$ being positive for the non-Transformer test). This is because the network was directly coupled to the voltage source (the $V_{L-L}$was adjusted from 15kV to 0.4kV) that possessed a much larger rating than the much smaller 20kVA transformer, the result of which is small/no voltage drop (a weaker modulating effect) observed. This result shows thatthe impact of higher loading ($Z_{load} = 10\Omega$) is minimal; hence, this is the reason why the values of impedance measured were never smaller than the hand calculated Thevenin values.

The results also show that there is a closer correlation for hand calculated TEI and measured Thevenin resistive values than there are for reactive values regardless of if there is a transformer present. The Transformer presence (not it's quality or rating) has a significant impact on the measurement of X_{th} regardless, the discrepancy is a tradeoff for using robust and quick local TEI estimation methods, and this tradeoff is in line with the themes (robustness, scalability) of this thesis. The results from sections 6.1.1 and 6.1.1.2 show that while the value of Z_{th} measured is not always accurate, which is expected ([34] and [36]). The TEI sensor will operate well (0.9% - 1.03% difference) in a system with a well-conditioned transformer and under heavy loading conditions (which is when optimal performance is most critical).

6.1.3 Unbalanced system response

This section presents the analyses of the TEI sensor's ability to recognize network unbalance. A $Z_{line\_var} = 5\ \Omega$ is used instead of the value used in section 6.1.1. Z_{line_var} undergoes an unbalance of 5%, 10%, 15%, 20%, 25%, 30%, 35% and 40%. This unbalance is done along each phase, meaning there will be three tests (for 3 phases) for each unbalance level. The results are shown in Table 6-1.

Table 6-1: A table showing the measured values

$R_{thh,ess,a}$ (Ω)	$R_{thh,ess,b}$ (Ω)	$R_{thh,ess,c}$ (Ω)	$X_{thh,ess,a}$ (Ω)	$X_{thh,ess,b}$ (Ω)	$X_{thh,ess,c}$ (Ω)	%INCREASE TEI	%DECREASE TEI	%unbalance (phase)
7.494	7.522	7.145	2.236	2.223	2.224	0.378	4.656	5a
7.132	7.501	7.524	2.228	2.242	2.205	0.297	4.929	5b
7.515	7.139	7.511	2.217	2.233	2.232	0.056	4.9473	5c
7.607	7.657	6.896	2.245	2.213	2.225	0.650	9.3447	10a
6.883	7.615	7.654	2.229	2.251	2.197	0.517	9.6119	10b
7.649	6.890	7.624	2.208	2.234	2.240	0.331	9.6227	10c
7.720	7.791	6.643	2.253	2.203	2.241	0.915	13.954	15a
6.635	7.728	7.787	2.230	2.259	2.197	0.760	14.153	15b
7.784	6.642	7.737	2.198	2.235	2.249	0.602	14.157	15c
7.833	7.925	6.395	2.262	2.193	2.241	1.175	18.354	20a
6.386	7.841	7.921	2.231	2.268	2.187	1.019	18.559	20b
7.918	6.393	7.850	2.188	2.236	2.257	0.865	18.561	20c
7.945	8.059	6.147	2.270	2.183	2.242	1.427	22.639	25a
6.137	7.954	8.055	2.231	2.277	2.177	1.270	22.839	25b
8.052	6.145	7.963	2.179	2.237	2.266	1.121	22.835	25c
8.058	8.193	5.898	2.279	2.174	2.242	1.674	26.803	30a
5.889	8.067	8.189	2.232	2.285	2.168	1.515	26.997	30b
8.186	5.896	8.075	2.169	2.237	2.274	1.373	26.987	30c
8.170	8.326	5.649	2.287	2.164	2.243	1.916	30.847	35a
5.640	8.179	8.323	2.233	2.294	2.158	1.758	31.036	35b
8.320	5.647	8.188	2.159	2.238	2.282	1.619	31.025	35c
8.281	8.460	5.401	2.295	2.154	2.244	2.154	34.782	40a
5.392	8.291	8.456	2.234	2.302	2.148	1.995	34.966	40b
8.454	5.399	8.300	2.149	2.239	2.290	1.860	34.950	40c

It is quite clear from the table that the unbalance measured diverges from the %DECREASE (the transmission line with an impedance lower than the median line impedance) and %INCREASE (the transmission line with an impedance higher than the median line impedance), with the TEI sensor being able to recognize the lower impedance transmission line but being unable to differentiate from the transmission lines with the upper and median

impedances. The phase allocation of the transmission unbalance is irrelevant to the TEI's sensor's ability to recognize line unbalance.

6.1.3.1 Discussion and analysis

Figure 6-21 shows three-line graphs, with the independent variable being the transmission line unbalance set in the Simulink model and the measured unbalance (with data from the TEI sensor). The grey line is the set unbalance meant to be used as a benchmark.

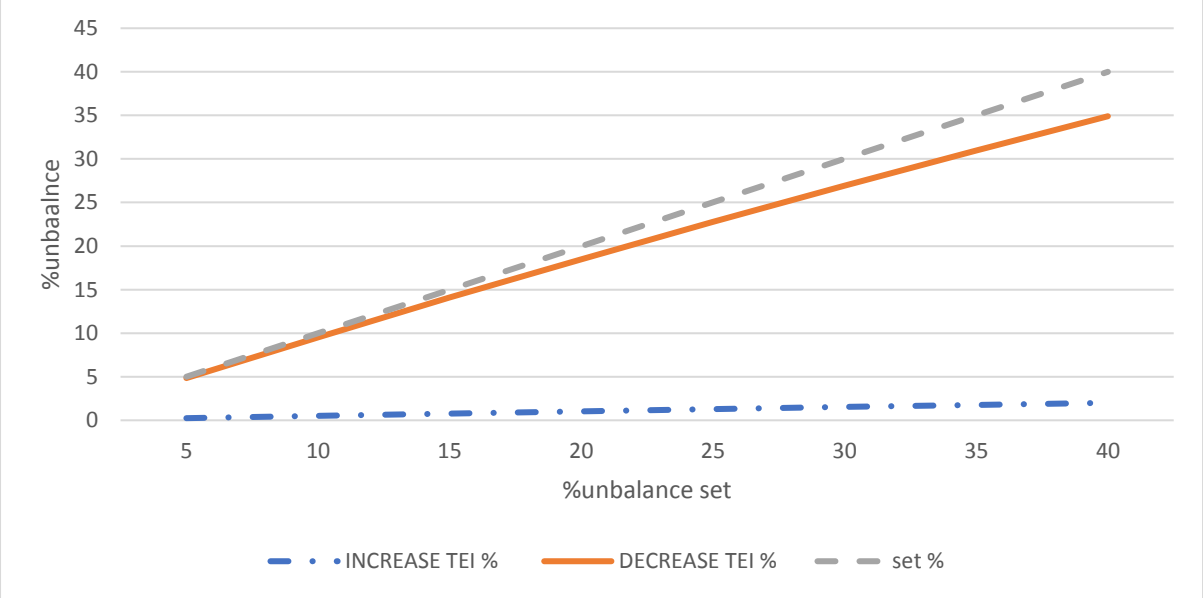

Figure 6-21: The TEI's ability to detect line unbalance

There are three lines in Figure 6-21, first-line (grey dashed line) indicates the unbalance set, the second line (orange solid line) indicates the negative unbalance measured (the line impedance - %unbalance), and the third line (blue) is the positive unbalance measured (the line impedance + %unbalance). The unbalance measured by the TEI is not accurate for a positive or negative unbalance. The TEI is better at detecting negative unbalances (lower impedances) than detecting a positive one (higher impedance), with the negative unbalance having a much stronger correlation. These tests indicate that the TEI sensor has limitations of operation which have been identified through these series of tests. The TEI's limited ability to recognize unbalance does not hamper the algorithm discussed in chapter 3.3, as it is an independent variable and can be replaced by an updated model.

6.1.4 Simultaneous Modulation

The system described in section 3.3 requires the use of multiple TEI sensors, and the impact of these sensors operating simultaneously has not been analyzed. The test is like the one conducted in 6.1.1.2.1 with a resistive load changing but with both TEI sensors (the sensor at bus 2 and bus 3) modulating simultaneously. The difference between both is analyzed by examining the $\%Change$ shown in equation (6-2):

$$\%Change = (\frac{Z_{th,simultaneous}}{Z_{th,sepreate}} - 1) * 100 \quad (6\text{-}2)$$

Figure 6-22 and Figure 6-23 presents the TEI values measured at bus 2 and bus 3 with a variable load at bus 3.

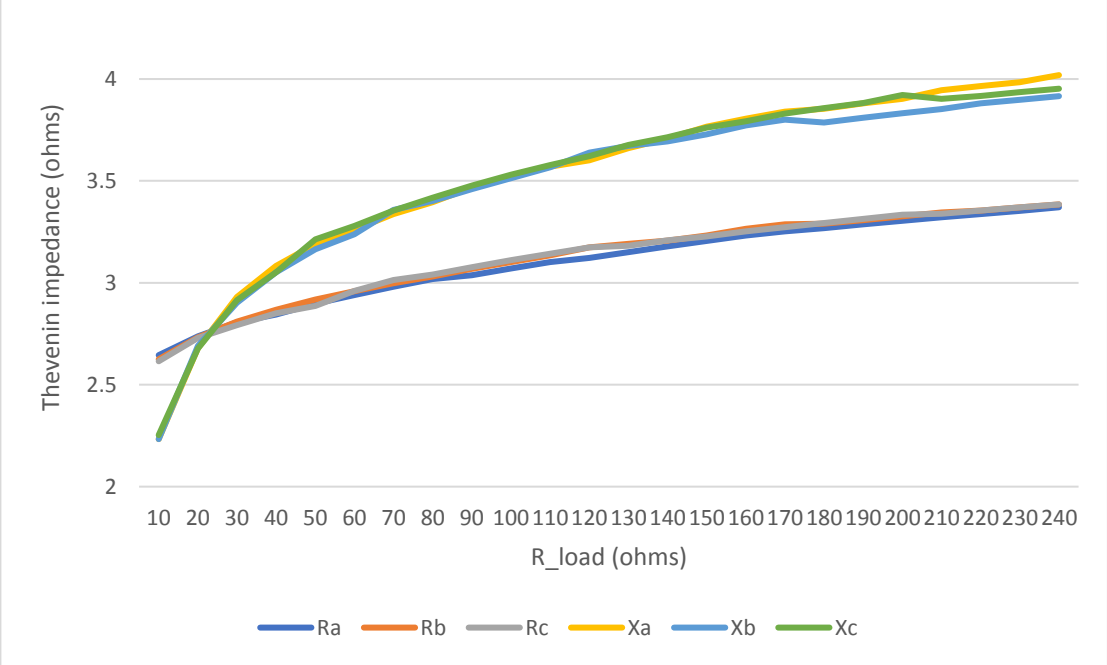

Figure 6-22: TEI measured Thevenin impedance at bus 2 for a variable 3-phase load with a 1 pf

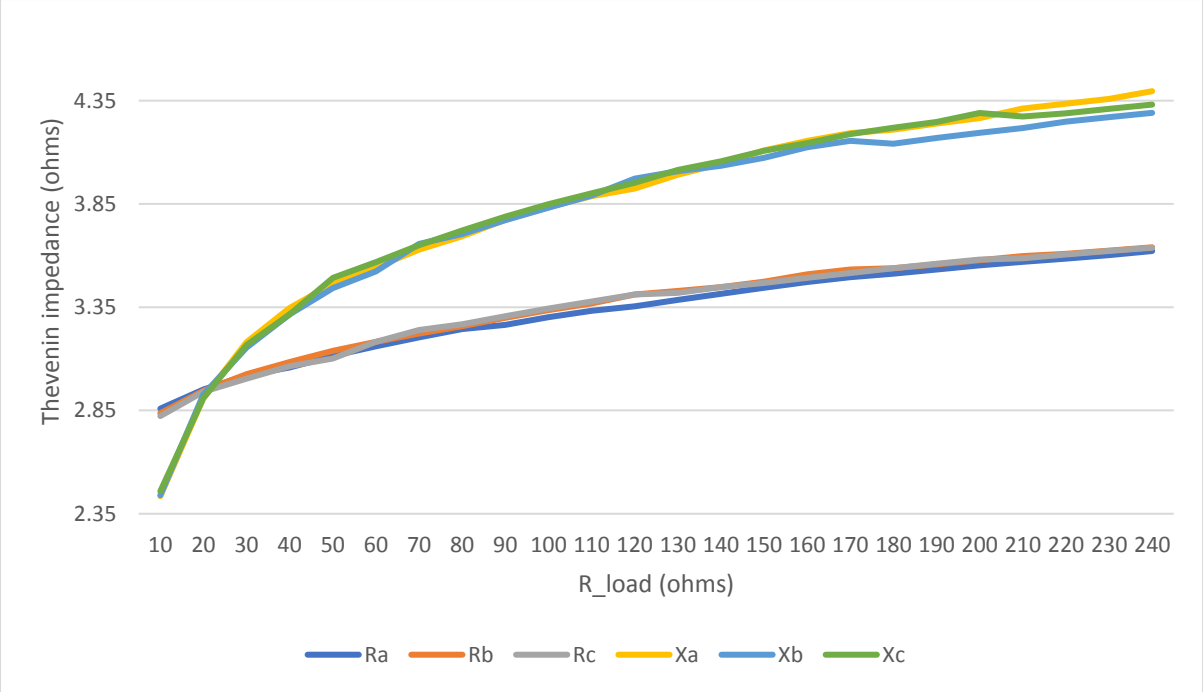

Figure 6-23: TEI measured Thevenin impedance at bus 3 for a variable 3-phase load with a 1 pf

6.1.4.1 Discussion and analysis

Early in the project, there was a question about whether simultaneous modulation to determine the Thevenin impedance was viable. This section compares the results of both implementations in Figure 6-24 and Figure 6-25.

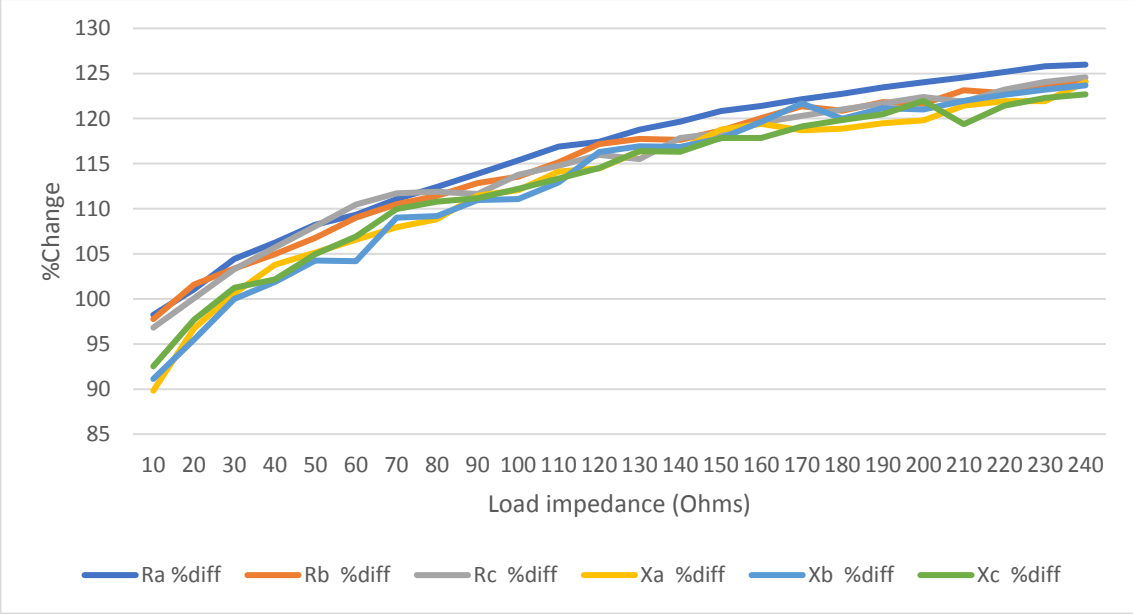

Figure 6-24: The percentage change in Thevenin impedance measured for Separate to Simultaneous modulation at bus 2

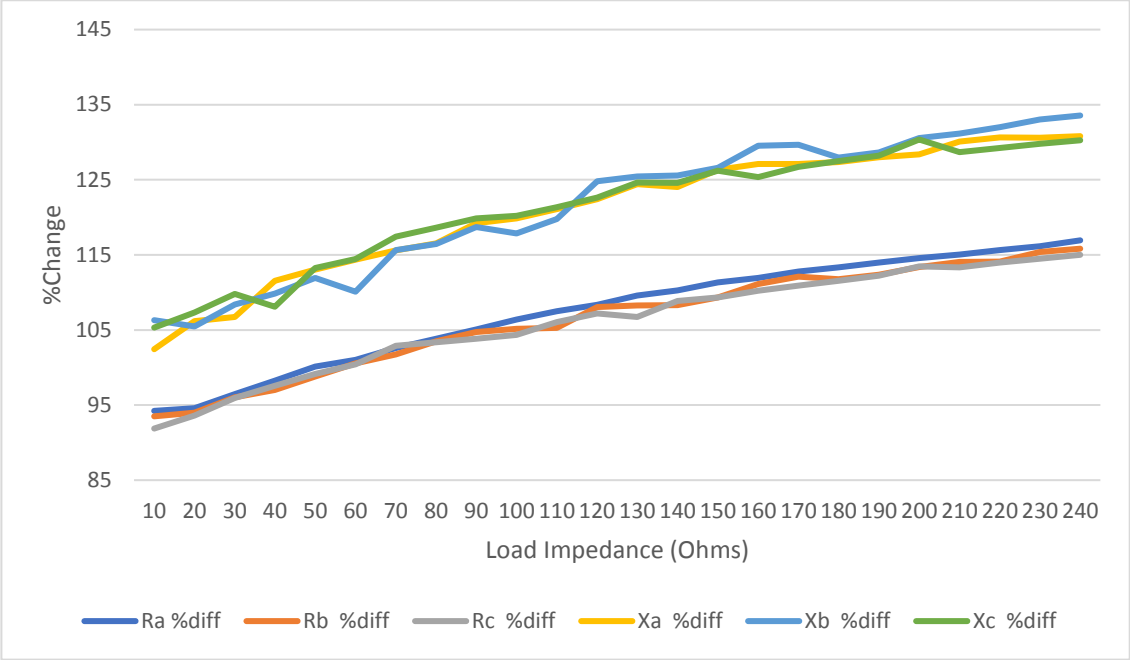

Figure 6-25: The percentage change in Thevenin impedance measured for Separate to Simultaneous modulation at bus 3

Figure 6-24 and Figure 6-25 shows that the $Z_{th,simultaneous}$ is at least double the size of $Z_{th,seperate}$. These results makes sense once equation (2-31) and (2-32) are analyzed and has more to do with those equations not accounting for the increase in current I_{inv} being pulsed (which is double the amount due to two TEI sensors operating). The actual I_{inv} flowing through the network is more than double and results in a V_{inv} doubling in value which results in Z_{th} being double (since I_{inv} doubling is not accounted for). This is not much of an issue for this project as the objective is to transfer power proportionally to the Thevenin impedance of the network from any point in the network. What is important is if the TEI meter can detect unbalance and how accurately it can detect them, which does not appear to be too well from the results shown in section 6.1.3.

6.2 Case Studies

This section presents the networks reaction to unbalance, loading and the impact of the TEI sensors modulation on the test network. Five case studies were conducted over 160s and had a sample time of 0.2s. The system consists of three loads (at 0.9 pf), an ESS and EV discharging power of 2kW, a transformer and a voltage source (230V nominal voltage). These tests analyzed the performance of the TEI in real-time.

6.2.1 Line Impedance fixed, and Load impedance at 0.9 PF are constant (the load and line impedance are balanced).

This is the test of a static system. The voltage of the network and the power across each relevant entity is shown in Figure 6-26.

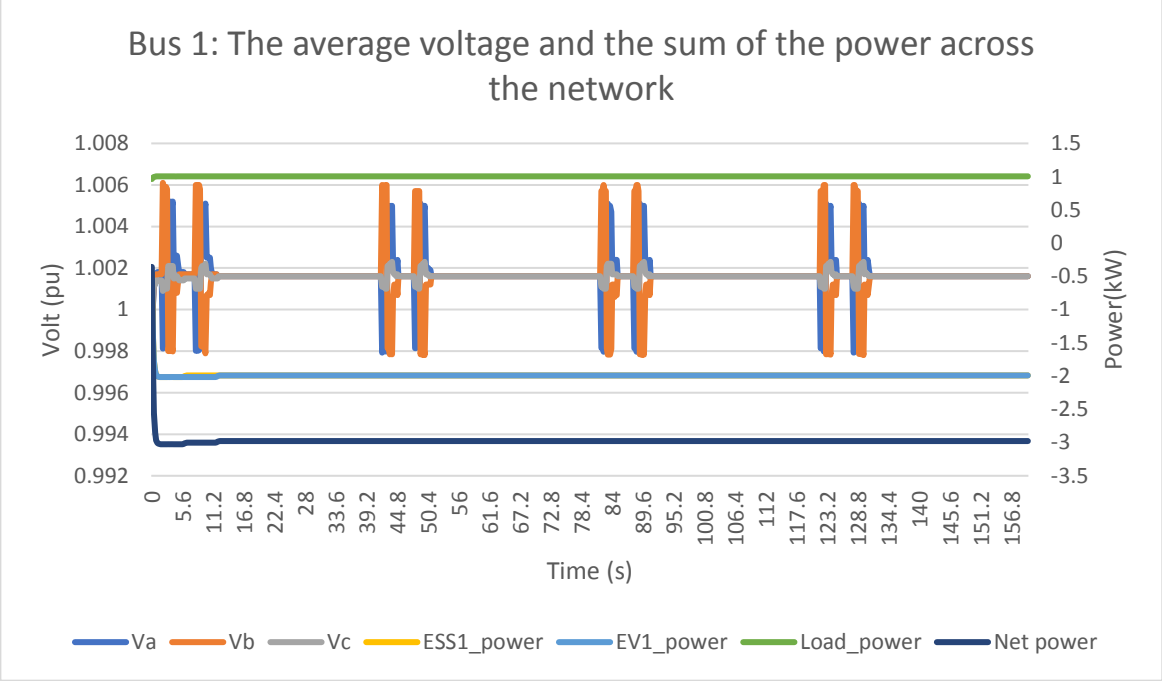

Figure 6-26: The Voltage and power of the test network (Case 1)

The results in Figure 6-26 are for a static system. There are four different sets of pulses on the voltage signal. These pulses are the TEI meter injecting current (modulating) into the network for each phase to help determine the Thevenin impedances, this was discussed in 2.7.2.3 and 2.7.5. There are two distinct pulses: the first pulse is for the ESS TEI (PCC bus 2) and the second pulse is the EV TEI (PCC bus 3).

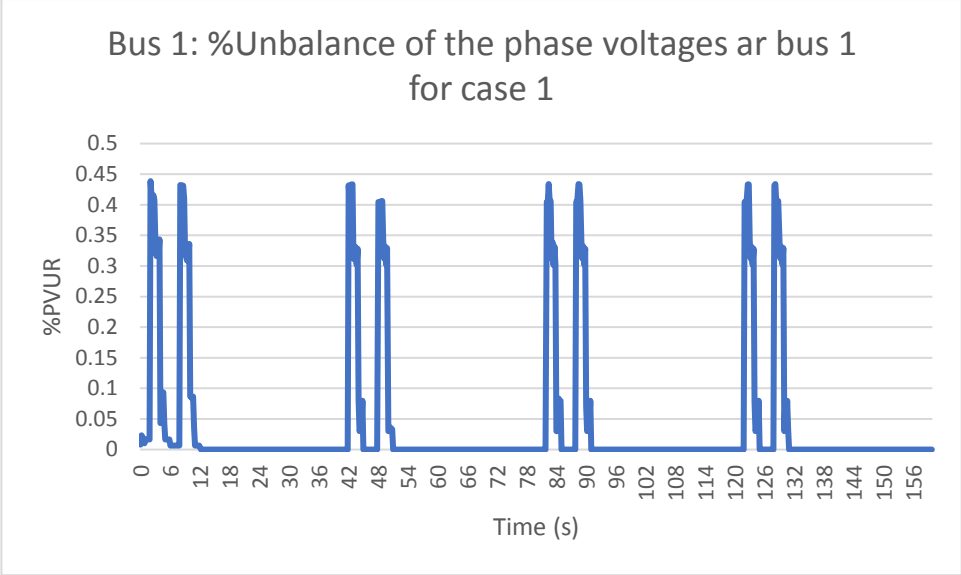

Figure 6-27: Case 1 %PVUR at bus 1.

Figure 6-27 shows the line representation of the voltage unbalance according to the IEE definition; this is based on the equation (2-16), %PVUR is phase voltage unbalance rate. These pulses impact the voltage unbalance (Figure 6-27) because the TEI modulates each phase separately, resulting in voltage unbalance. The TEI sensor has been implemented in real LV networks and does not have such an impact on the network voltage. The pulses can be ignored because they don't reflect real network operation.

6.2.2 Line Impedance fixed and Load impedance changes in magnitude three times (the load and line impedance are balanced)

This case study has a balanced 3-phase RLC load that will change demand from 1kW, 1.5kW, 2kW and 2.5kW. The results of the simulation are presented in Figure 6-28 (the average voltage and component power), Figure 6-29 (the current and voltage per phase) and Figure 6-30 (R_{th} measured at bus 2).

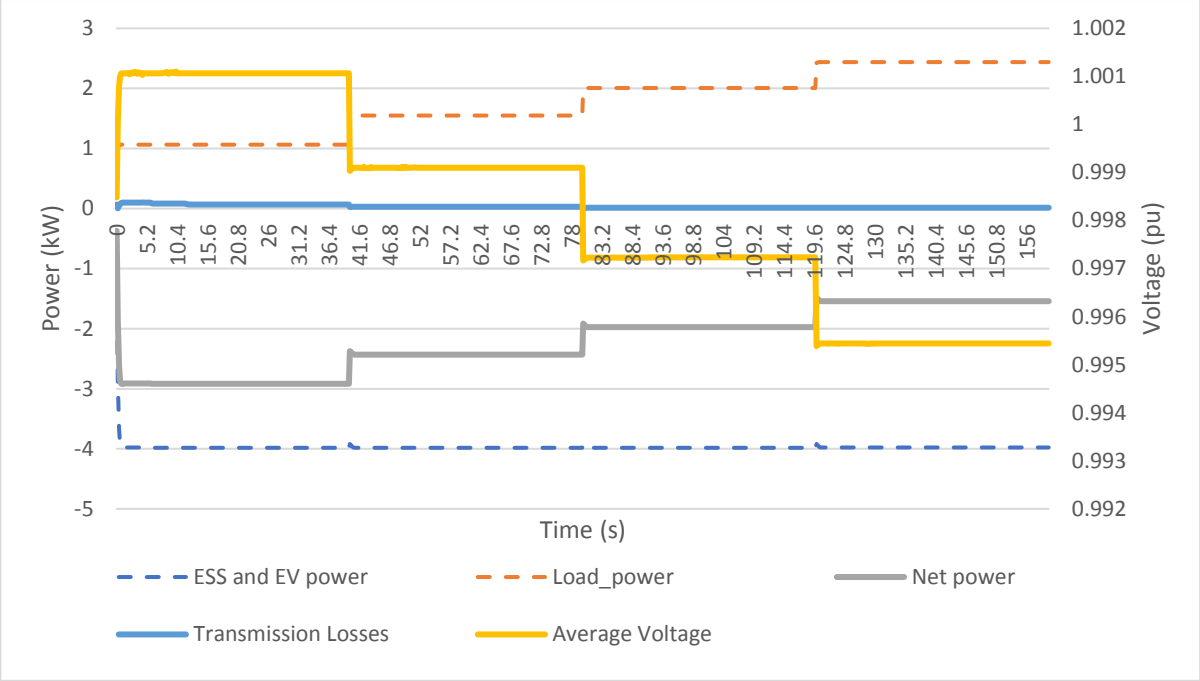

Figure 6-28: The average voltage at bus 1 and the power across each element in the network

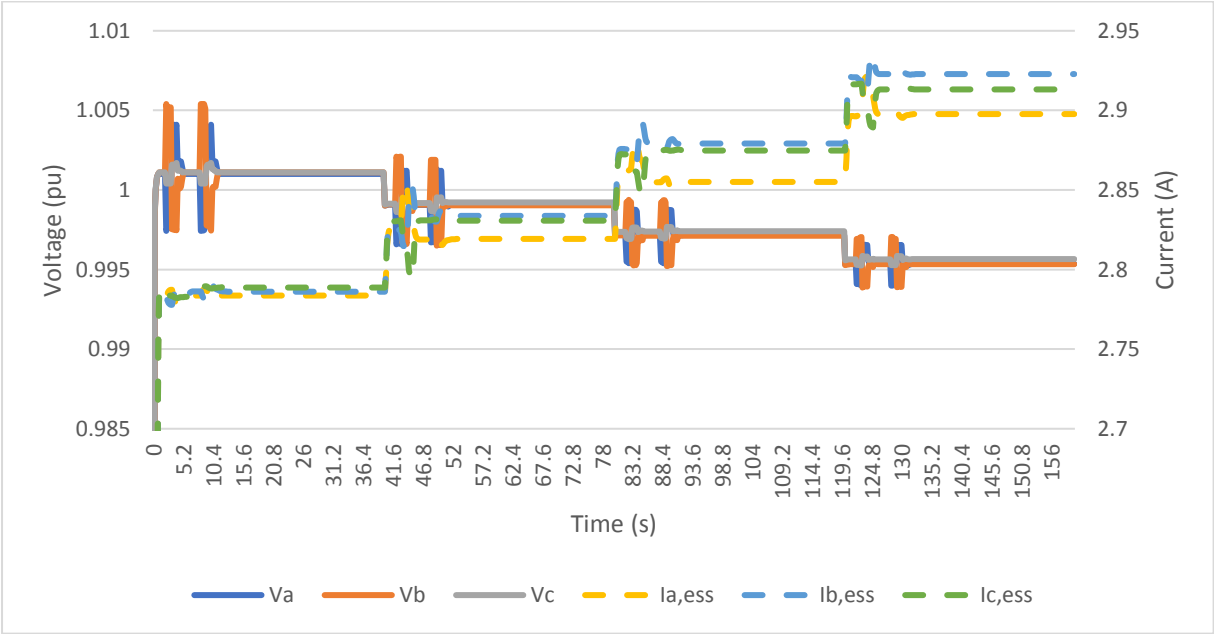

Figure 6-29: A chart showing the voltage per phase at bus 1 and the current from ESS1 (bus 2) per phase

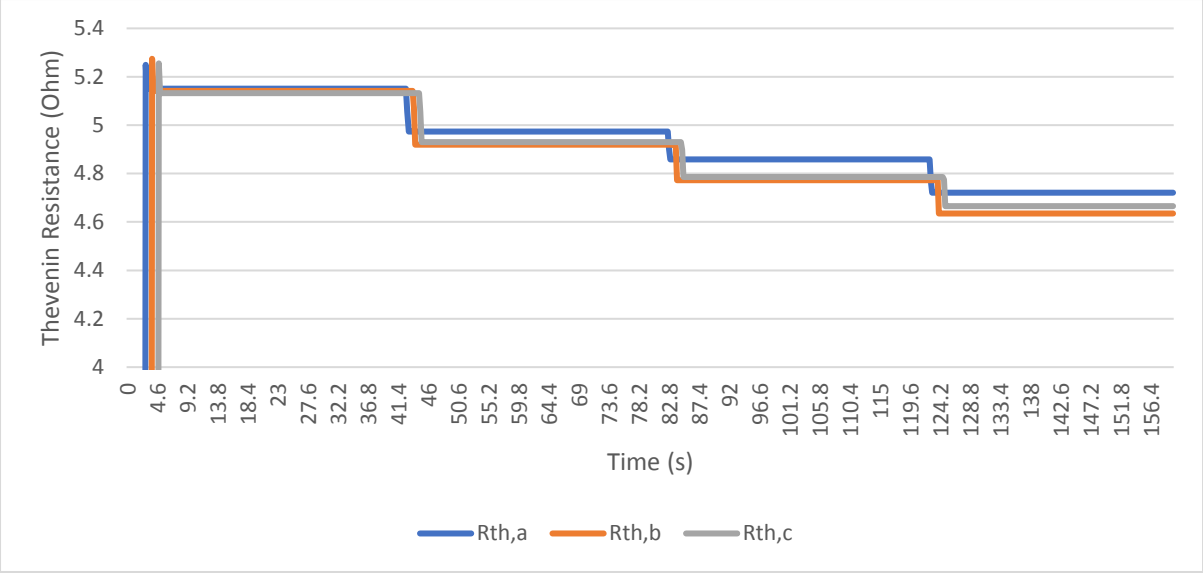

Figure 6-30: The Thevenin resistance measured from bus 2 (ESS1)

6.2.2.1 Discussion and Analysis

Case 2 is a system with increasing load demand, the logical impact of which is a decreasing voltage. While the system was modelled to be balanced, the TEI sensor observes an unbalance in the resistance, but this contradicts the change in load demand as shown in Figure 6-31:

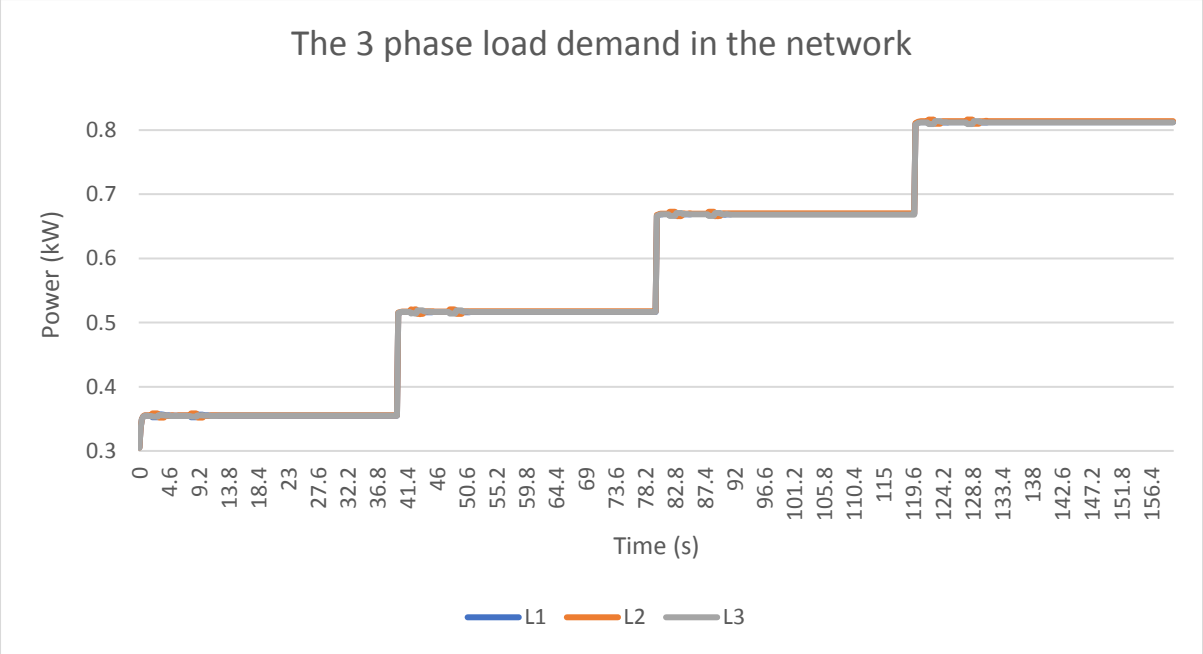

Figure 6-31: The Load demand per phase for case 2

The R_{th} measured decreased as the Load demand (current flowing through the LV network) increased, which makes sense according to Ohms law, but Figure 6-31 shows that the load demand for each phase is equal. It has been discussed in sections 6.1.1.3 and 6.1.2.3 that the performance of the TEI is distorted when the network is under more strain. It is also important to note that the unbalance in R_{th} measured does not exceed 5% but the distortion will increase with more strain on the network as shown in the phase voltage unbalance rate (%PVUR) chart in Figure 6-32.

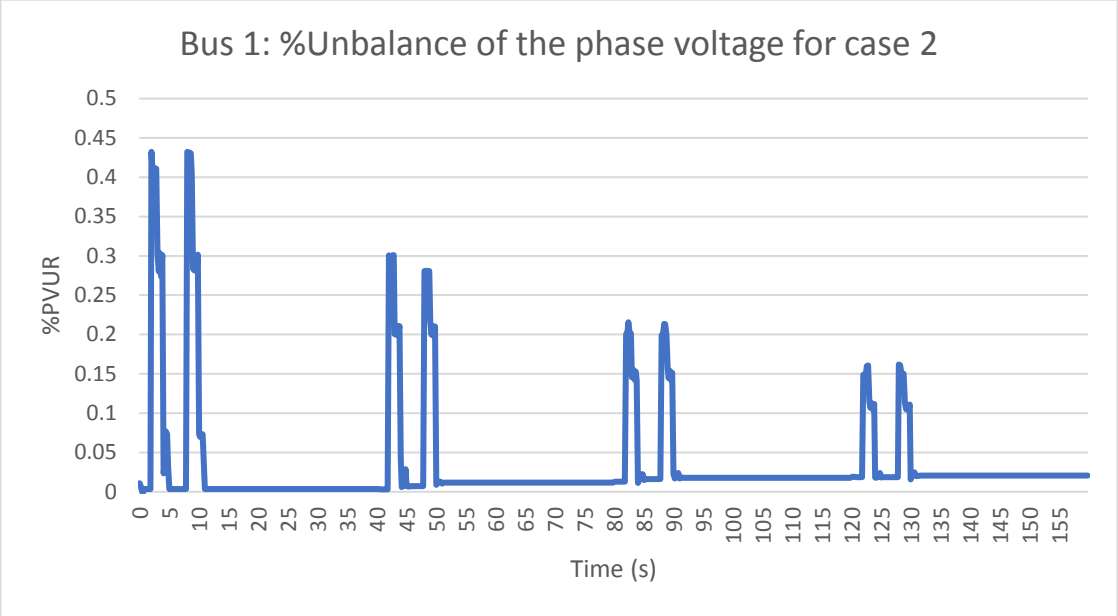

Figure 6-32: Case 2 %PVUR at bus 1.

The voltage unbalance remains low, being less than 0.025% (excluding the impulses due to the TEI modulation). However, there is a slight increase in %PVUR with increased demand, but it is insignificant. The effect of modulation on the test network voltage also decreases with increased demand. This explains the smaller TEI measurements when compared to the hand calculated TEI values presented in section 6.1.1.

6.2.3 Line Impedance fixed, and Load impedance changes percentage unbalance for three stages

Case study 3 has a load of varying unbalance (but constant total demand across 3 phases) changing from 0%, 10%, 15% and 20%. Figure 6-33, Figure 6-34 and Figure 6-35 are the results of the case study.

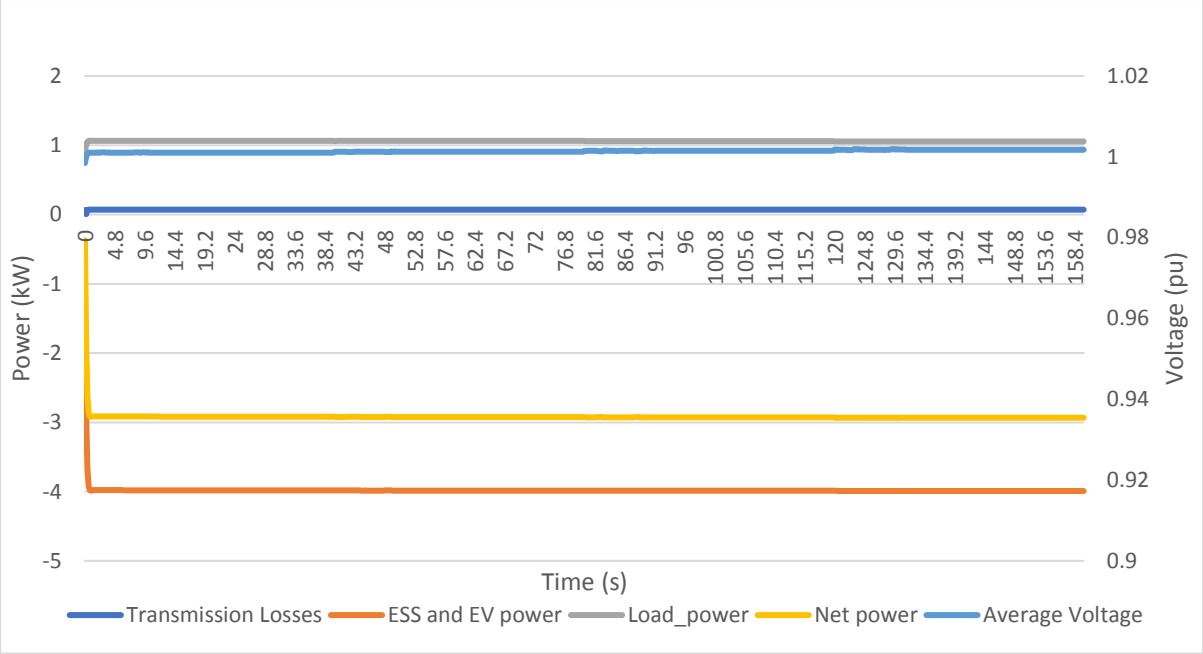

Figure 6-33: The average voltage at bus 1 and the power across each element across the network

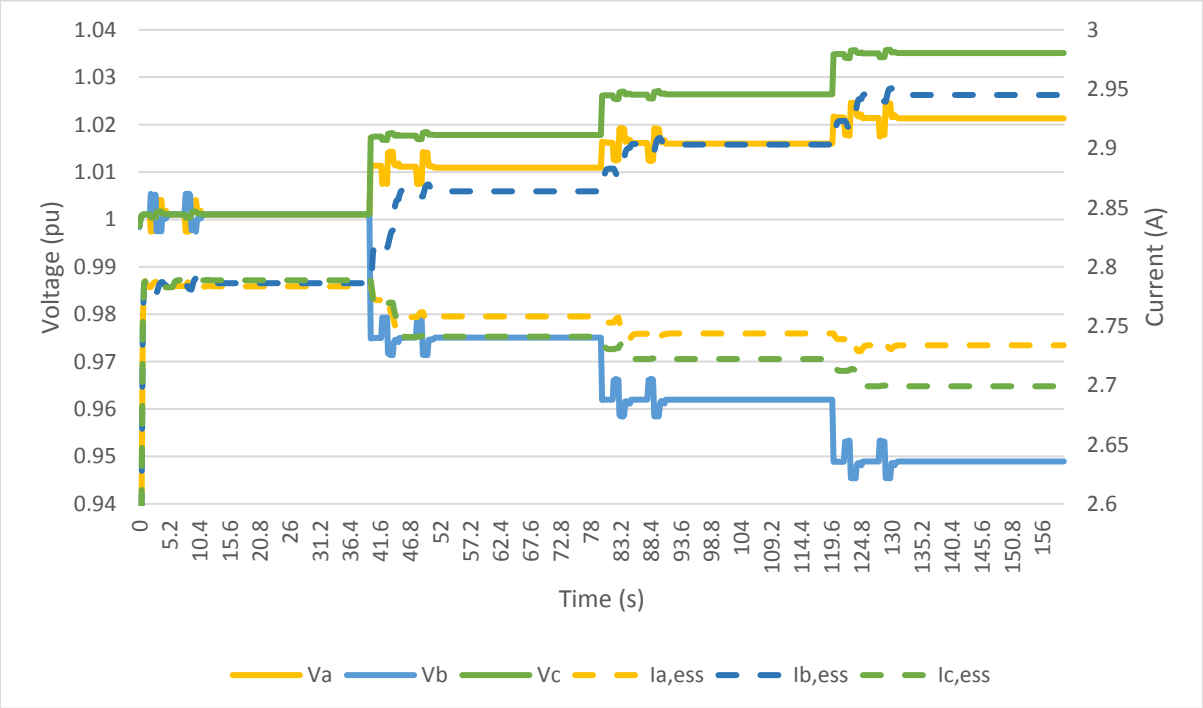

Figure 6-34: The voltage per phase at bus 1 and the current from ESS1 per phase

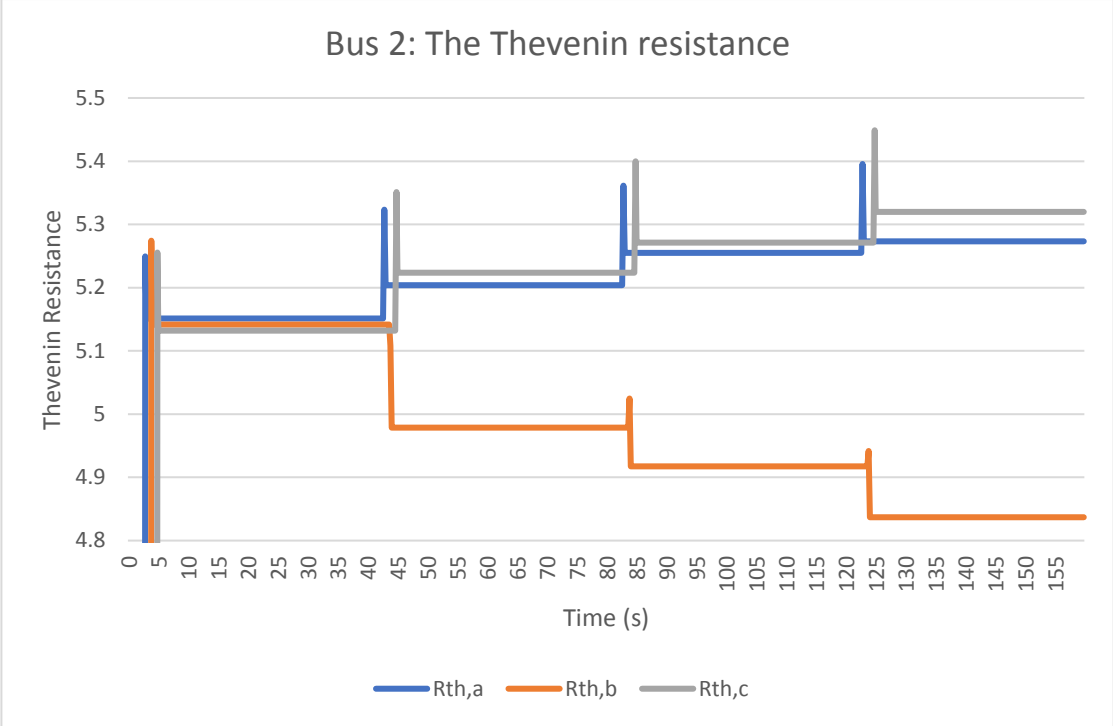

Figure 6-35: The Thevenin resistance measured from bus 2 (ESS1)

6.2.3.1 Analysis and Discussion

Case 3 has a constant 3 phase load (1kW) power with a changing percentage unbalance, changing from 0%, 10%, 15% and 20%. The total load is visible in Figure 6-33 and is constant, resulting in a constant average voltage at bus 1, also shown in Figure 6-33, but the power is not even across the three phases as seen in Figure 6-36. Figure 6-34 indicates that the voltage and the ESS current (current from bus 2) responds accordingly to this unbalance (the ESS is using TEI data to change the current drawn per phase).

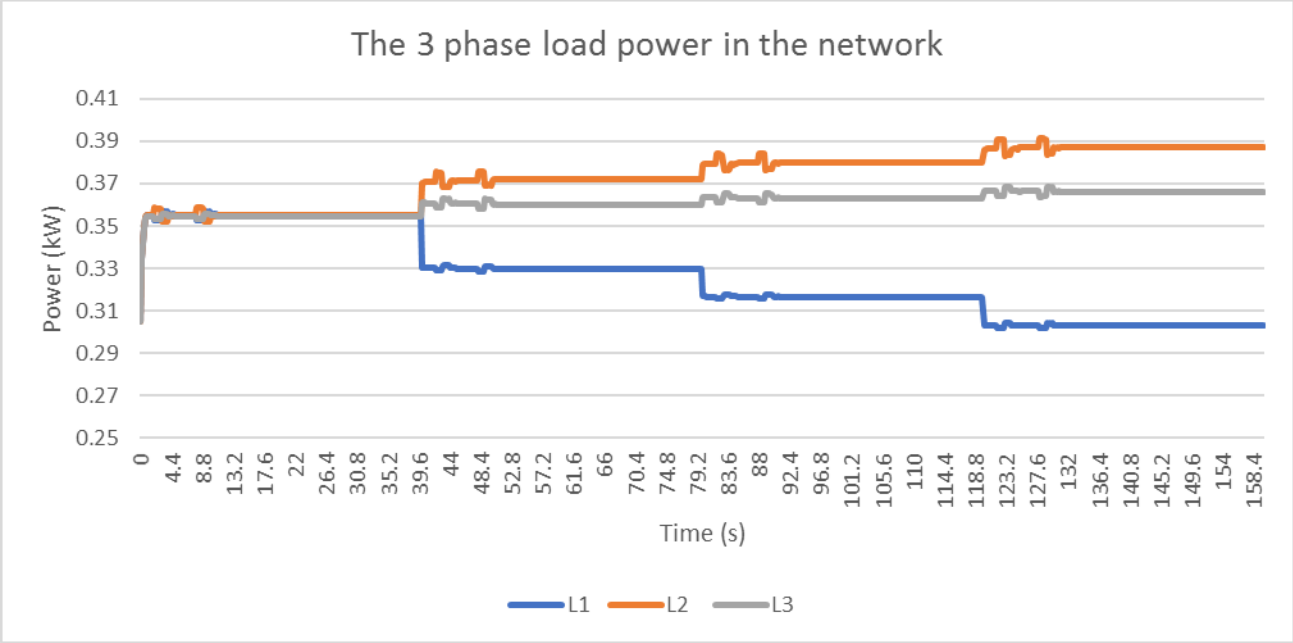

Figure 6-36: The Load demand per phase case 3

There appears to be inconsistency with the load demand per phase compared to the %unbalance that was set. This issue might be due to the inner workings of the RLC load Simulink block in Figure 9-8. Regardless of this inconsistency, there is an expectation of what the TEI measured R_{th} should be, because L_1 has the lowest demand $R_{th,a}$ will be the largest, L_2 being the largest demand will result in $R_{th,b}$ being the smallest and $R_{th,c}$ being in the middle due to L_3 being the middle demand.

This expectation is only partially met with $R_{th,b}$ being the lowest while $R_{th,c}$ and $R_{th,a}$ being more aligned with each other, this correlates with the results in section 6.1.3 (the results observing the TEI's ability to detect unbalances) and the inability of the TEI sensor to detect unbalance accurately. The %PVUR is shown in Figure 6-37.

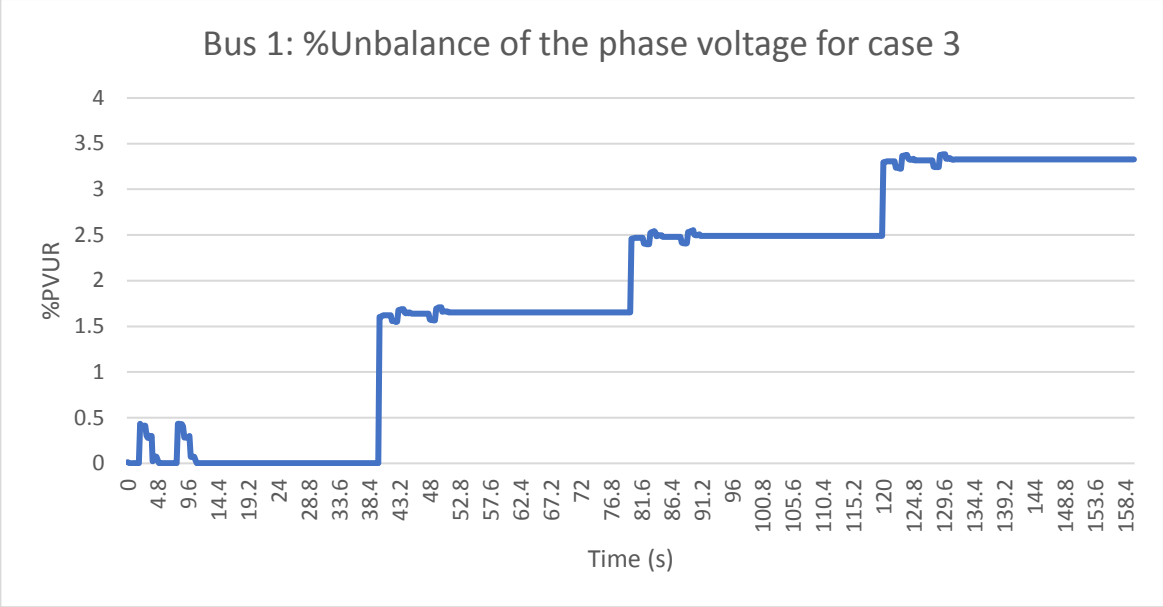

Figure 6-37: Case 3 %PVUR at bus 1.

The phase voltage (of bus 1) unbalance rate (%PVUR) increases with the increased demand unbalance.

6.2.4 Line Impedance changes magnitude three times (balanced) and Load impedance fixed

This case study follows the increasing transmission impedance for three stages going from 5Ω per phase, 7.5Ω per phase, 10Ω per phase and 15Ω per phase. The simulation results are shown in Figure 6-38, Figure 6-39 and Figure 6-40.

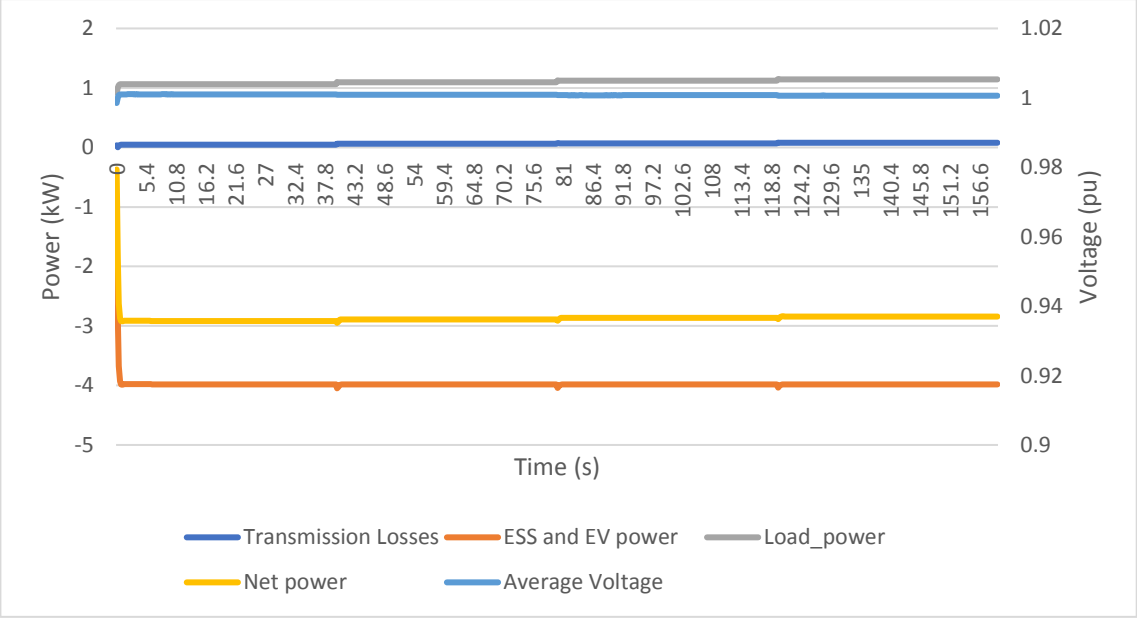

Figure 6-38: The average voltage at bus 1 and the power across each element across the network

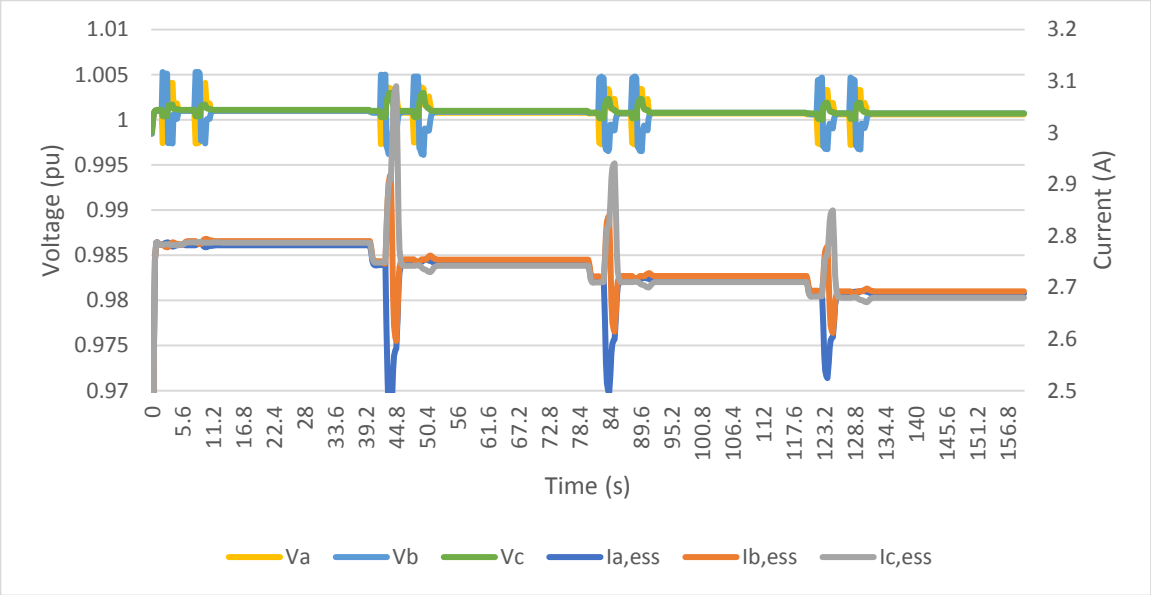

Figure 6-39: The voltage per phase at bus 1 and the current from ESS1 per phase

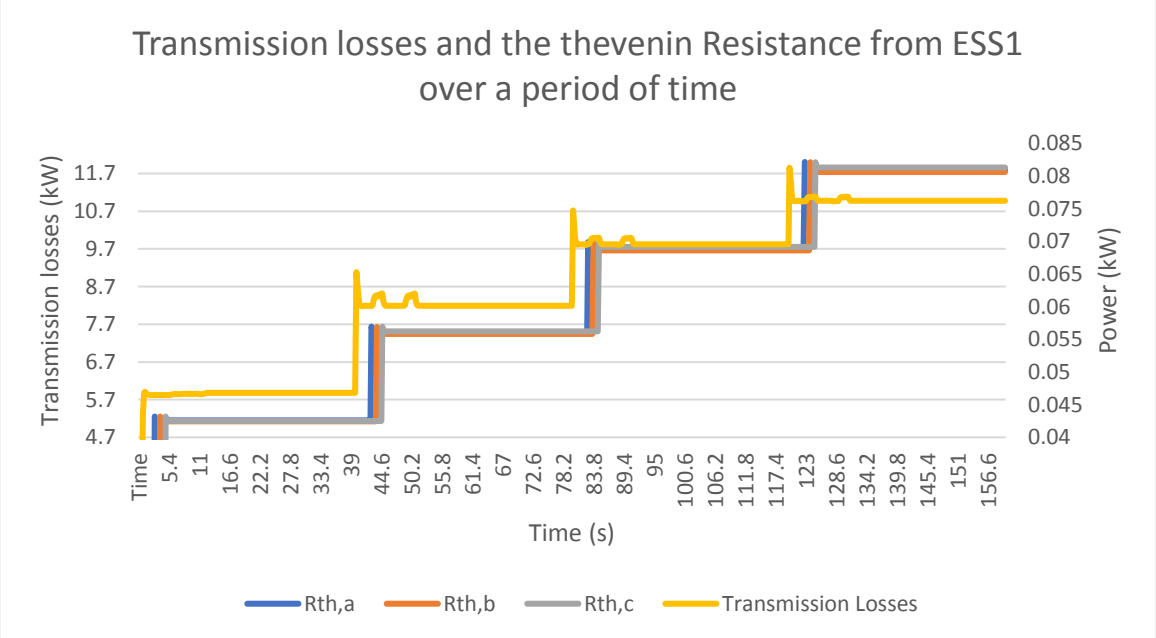

Figure 6-40: The Thevenin resistance measured from bus 2 (ESS1) and the transmission losses of the variable impedance

6.2.4.1 Discussion and Analysis

Case 4 is a network with an increasing transmission impedance. The voltage and current behavior are like the network with a balanced load configuration in section 6.2.2. The distinction is the consistently increasing transmission losses in Figure 6-40 due to the increasing transmission impedance.

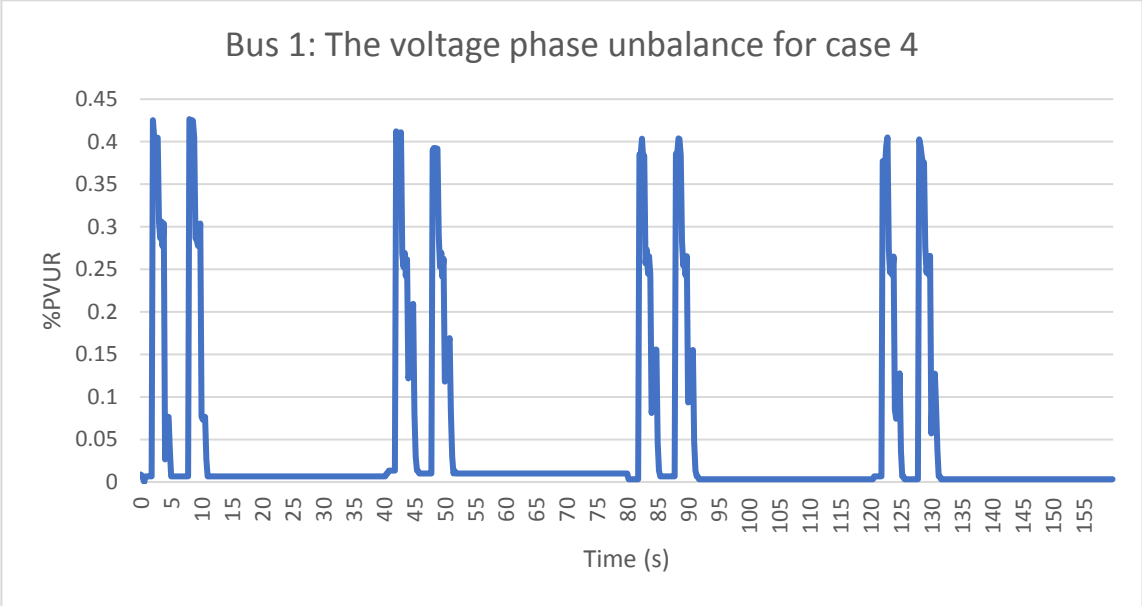

Figure 6-41: Case 4 %PVUR at bus 1

The %PVUR shown in Figure 6-41 remains lower than the %PVUR in Figure 6-37 (when there is no modulation). Still, when compared to the results in Figure 6-32, the impact of the TEI modulation remains high. This is because demand has an impact on the TEI sensor (discussed in sections 6.1.1 and 6.1.2).

6.2.5 Line Impedance changes percentage unbalance three times and Load impedance fixed.

Case study 5 will have a transmission line impedance (resistance) of varying unbalance (but constant impedance sums across 3 phases) changing from 0%, 10%, 15% and 20%. Figure 6-42, Figure 6-43 and Figure 6-44 are the simulation results in case 5.

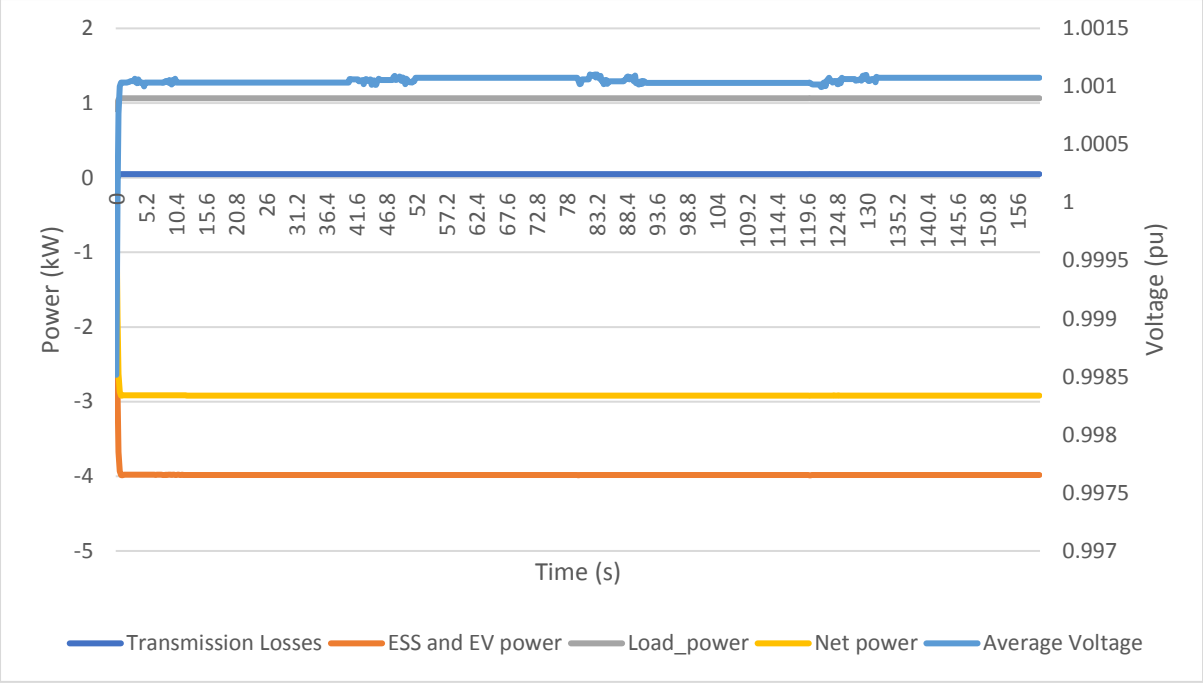

Figure 6-42: The average voltage at bus 1 and the power across each element across the network

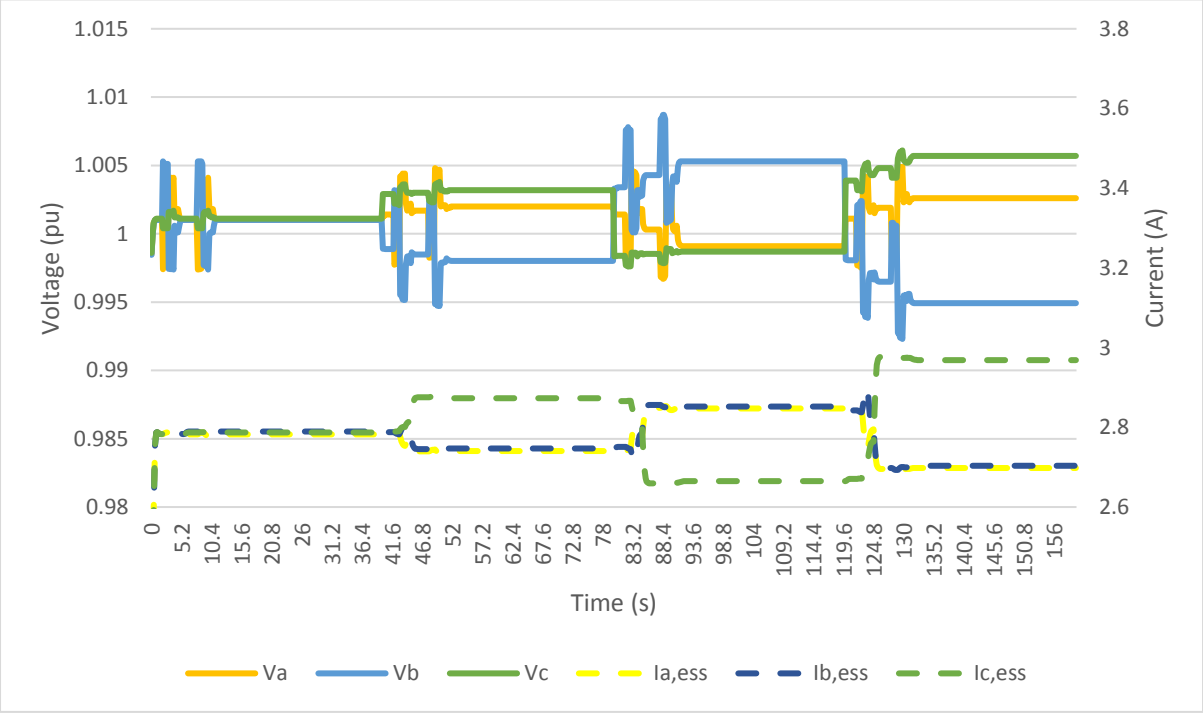

Figure 6-43: A chart showing the voltage per phase at bus 1 and the current from ESS1 per phase

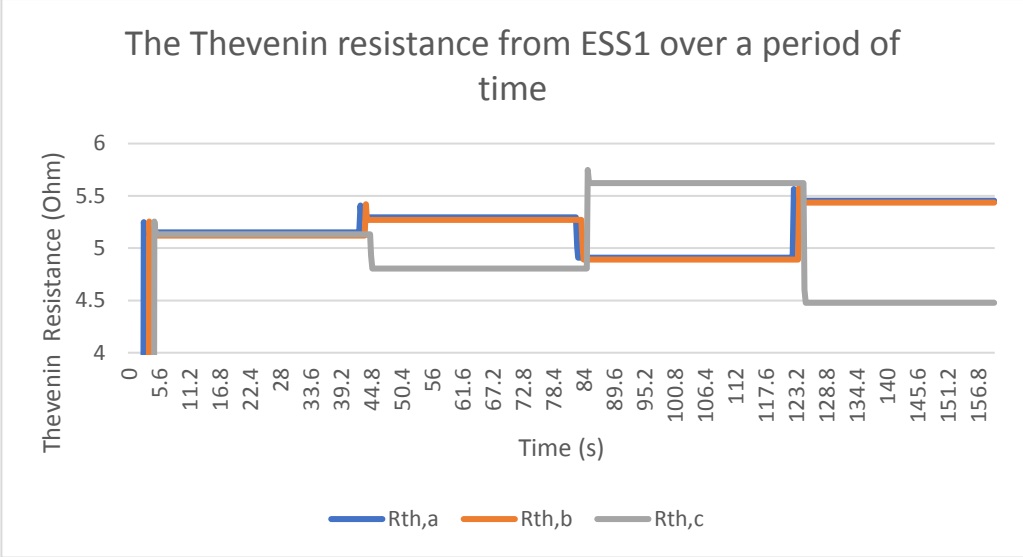

Figure 6-44: The Thevenin resistance measured from bus 2 (ESS1) and the transmission losses of the variable impedance

6.2.5.1 Discussion and Analysis

The results for case 5 (with the changing transmission unbalance) are the results that were expected as seen in case 3 (section 6.2.3, the load with increasing unbalance), the phase voltages (Figure 6-43) moving further apart as the %unbalance increases, the average voltage (Figure 6-42) being constant throughout the simulation and TEI sensor not consistently observing the unbalance as seen Figure 6-44. The results of R_{th} were expected as this was analyzed more thoroughly in section 6.1.3, with the TEI sensor only being able to recognize the unbalance of one phase while equating the median phase and the upper phase (this test stands out as the only time where the phase with median and lower impedance are correlated).

6.3 24 Hour simulation

This section illustrates the impact of Optimal Power Injection (OPI) on the performance of the MAS. It examines the performance of every entity in the network, analyzes the TEI sensor's ability to help minimize losses (even in its limited performance shown in section 6.1.3) and the difference the TEI guided phase power injections (OPI) make on an unbalanced network (how would this alter the voltage quality).

6.3.1 Basic Network assessment

This section shows the network in default operation (no EV or ESS), with the only power, transacting entities being 3-phase PVs and 3-phase RL loads. The demand/generation profiles were borrowed from the Italian network used in [1] and [25]. Figure 6-45 illustrates the load

distribution per phase for the test network and the phase voltage unbalance rate (%PVUR) alongside it, with the peak %PVUR occurring in the evening at 3%. The %PVUR is derived using the equation (2-14) in section 2.6.

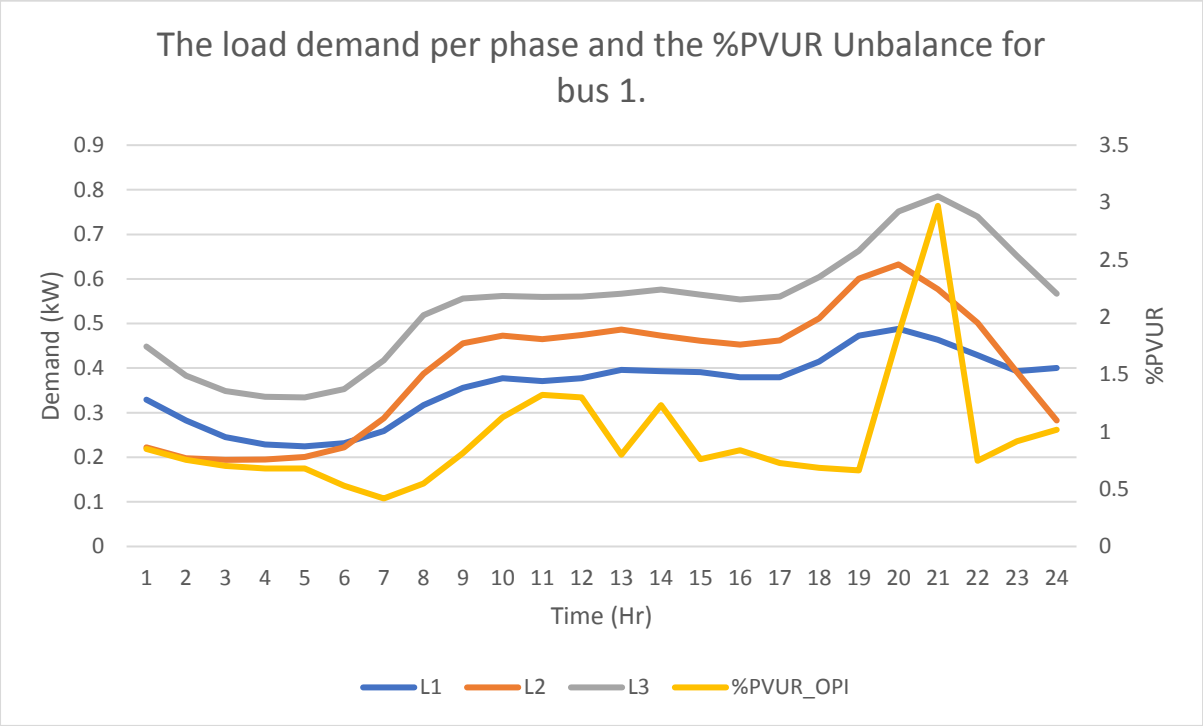

Figure 6-45: 3-phase plot load demand and %PVUR for bus 1

Figure 6-46 illustrates the voltage per phase in the test network at bus 1. The peak voltage occurs at midday (due to PV voltage injection), and the peak voltage unbalance occurs in the evening, as seen in Figure 6-45 with the %PVUR line.

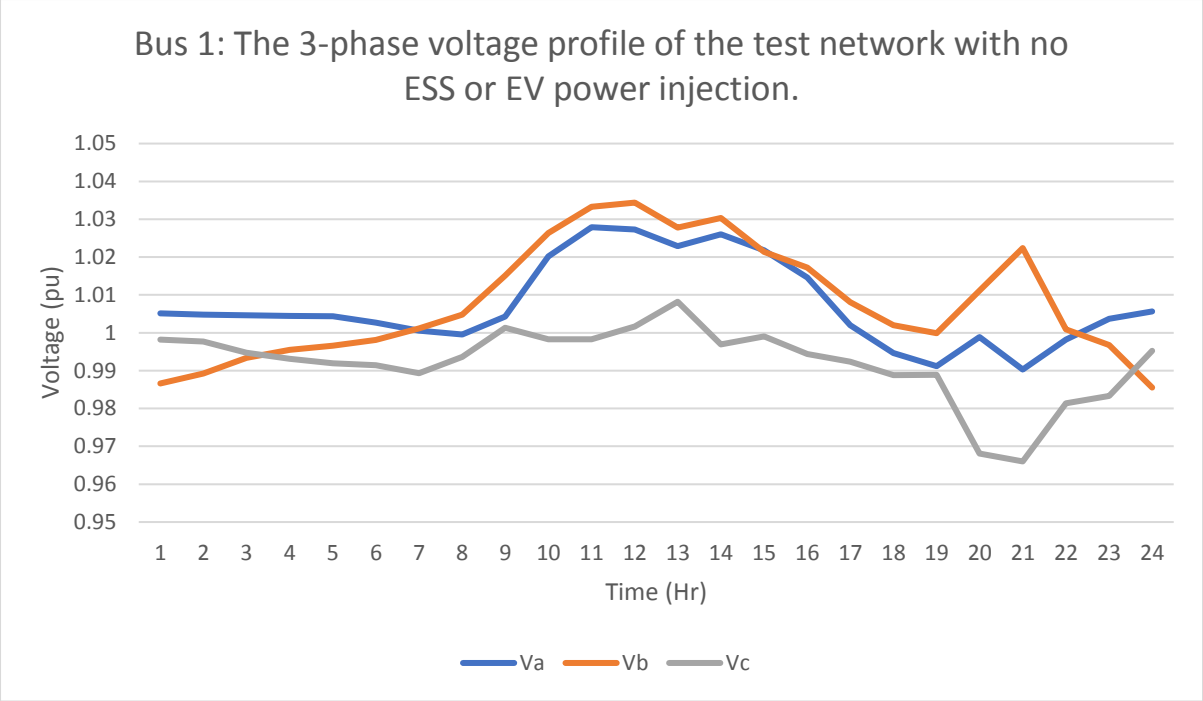

Figure 6-46: The 3-phase voltage profile of the test network with no ESS or EV power injection.

Figure 6-47 illustrates the average voltage profile (of the voltages in Figure 6-46) at bus 1(the low side of the transformer), the load and the photovoltaic power.

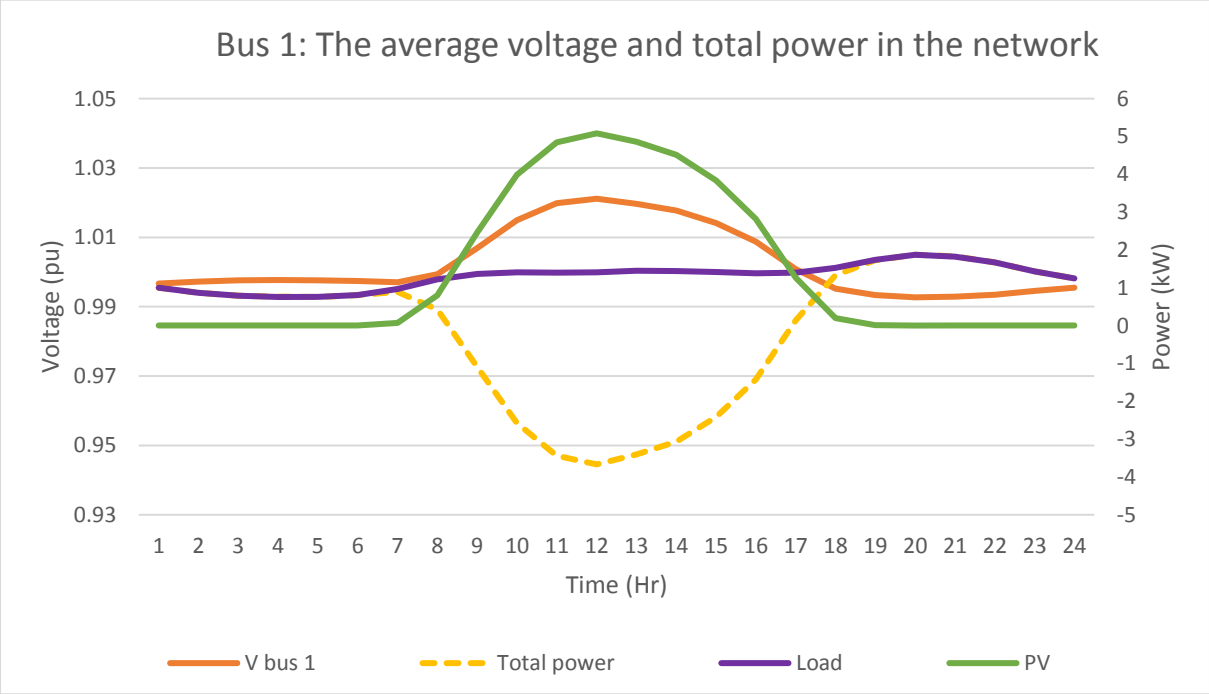

Figure 6-47: Average voltage profile (bus 1) and total power in the LV network

The test network in default has a slight voltage rise due to an increase in PV power injection around midday. Still, it is visible that the load experienced on each line is unbalanced in Figure

6-45, with the %unbalance (IEE definition) shown. There is a need for energy arbitrage at midday by the ESS.

6.3.2 MAS System assessment

The average voltage (at bus 1) with the ESS and EV having unoptimized charging/discharging profiles and with MAS guided charging/discharging is presented in Figure 6-48. V_Dumb is the voltage at bus 1 for uncoordinated charging/discharging (of the ESS and EV), while V_MAS is the voltage of bus 1 with the optimized charging profiles of the ESS and EV (through the MAS algorithm in stage 1 discussed in section 2.5).

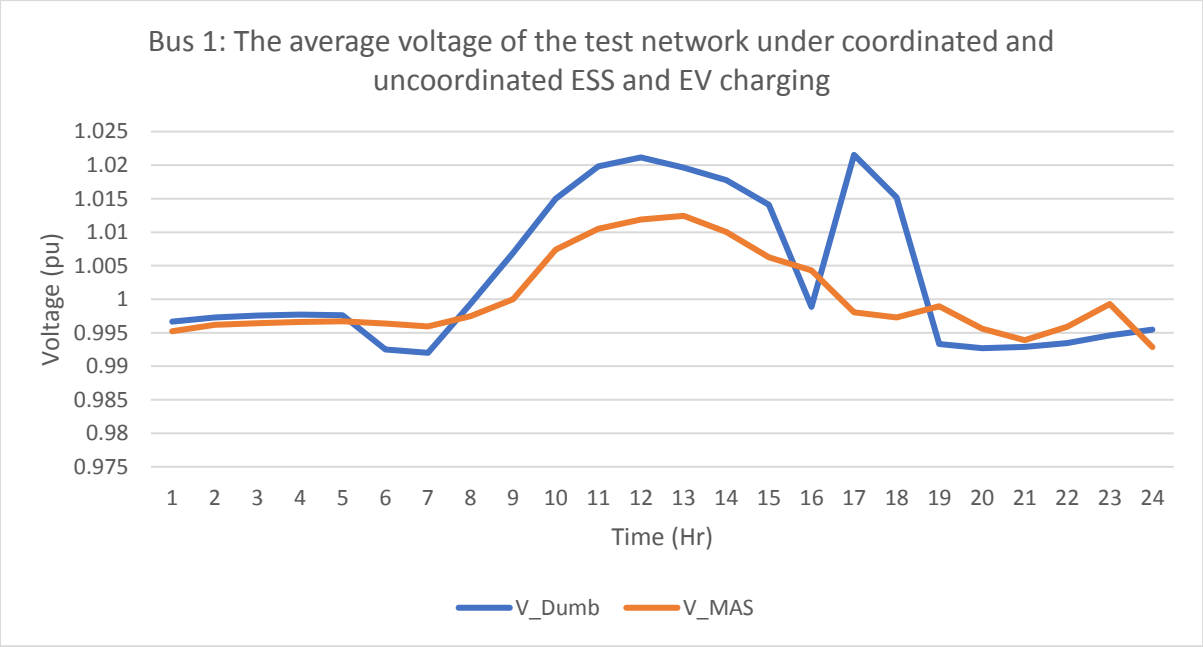

Figure 6-48: The average voltage of the network for MAS and Uncoordinated (dumb) charging

Figure 6-48 shows a massive voltage drop and surge (generating an additional peak in the evening) for the average voltage on bus 1 caused by the ESS for uncoordinated (dumb) charging while still preserving the midday voltage peak caused by the PV power injections. The system with MAS coordination has a much flatter curve with a mitigation of the midday voltage surge.

6.3.3 ESS assessment

The shape of the ESS demand curve (kW) is discussed in this section. A simulation consisting of only a 3-phase voltage source, a MV/LV transformer, and a 3-phase ESS is conducted. The ESS profile was determined on the MAS platform. The ESS charges from morning to afternoon and discharges during the evening to meet the peak load demand seen in Figure 6-45. There is no unbalance in the system as there are no other elements to introduce unbalance.

When a voltage plot has the term BPI (Balanced Power Injection) attached to it, that means the ESS/EV are injecting/sourcing power equally through each phase, while if the voltage plot has OPI (Optimal Power Injection) label on it, it means the ESS/EV are injecting power based on R_{th} determined by the TEI sensor operating on the same bus as the ESS/EV. The label ESS/EV_OPI indicates the power from the ESS/EV under OPI, while the label ESS/EV_BPI is shorthand for the balanced power injection. Figure 6-48 compares the average voltage at bus 1 for BPI and OPI.

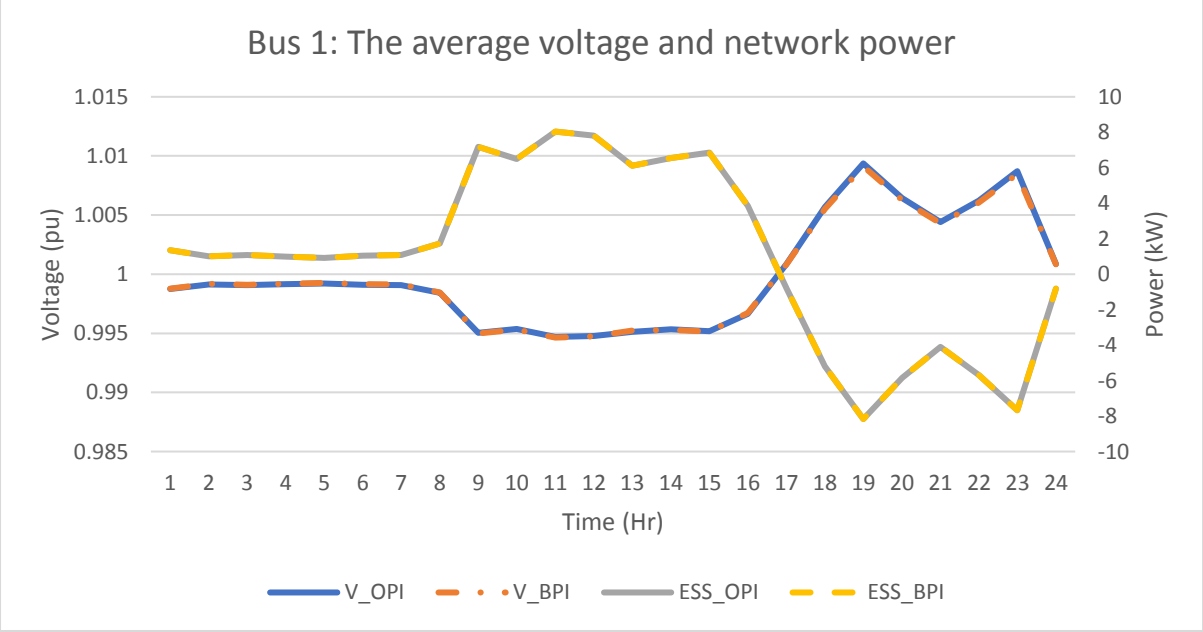

Figure 6-49: The average voltage (bus 1) of the network under OPI and BPI for a single ESS

The ESS takes most of its power from 9 am – 3 pm (early morning and midday), which coincides with the midday voltage surge caused by the solar power injection into the LV network. This shape takes form in the optimization process because the net power demand (not absolute power) is at its lowest (due to the solar discharge), which as a result causes the virtual cost $C(t)$ to be at its lowest; this guides the mono constrained optimization $p(t,T)$ (equation (2-1)) in section 2.5 of the literature review. The evening period (5 pm – 12 midnight) is the

point of EV charge and peak load demand (in Figure 6-45), and this is when the ESS discharges its stored energy from midday to prevent a voltage drop.

Figure 6-49 shows that there is not much difference between BPI and OPI. This is due to the network being balanced which would result in there being equal R_{th} across the three phases, causing the I_{opt} for the OPI to be the same as the current for the BPI resulting in a near-perfect match. The main difference is the phases at which the currents were injected.

6.3.4 ESS and EV assessment

The ESS and EV test excludes the 3-phase PV and 3-phase RL load. Figure 6-50 compares the average voltage at bus 1 for BPI and OPI, it also shows the power for the ESS, EV, and the net sum of their power transferred.

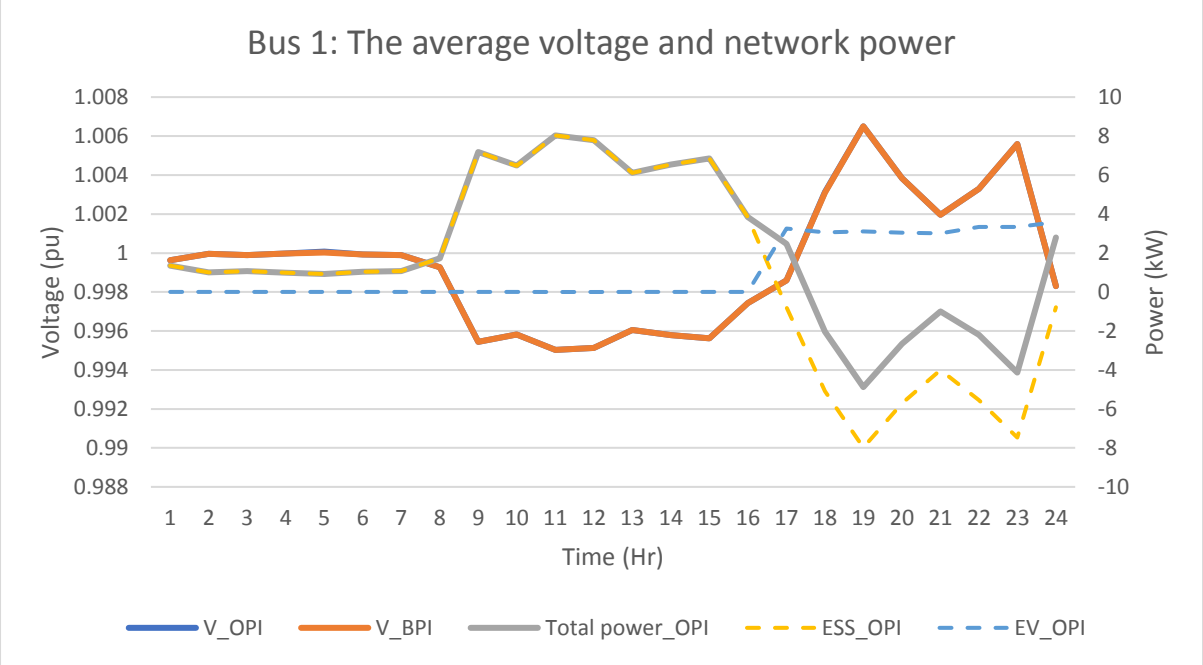

Figure 6-50: The average voltage and power of the network under OPI and none-OPI for ESS1 and EV1

Figure 6-50 shows that in the evening time, EV is consuming power, ESS is injecting more power, and the excess power flows into the grid. The network is balanced and would result in no significant variation in phase voltage waveform. In Figure 6-51, the voltage (bus 1) for each of the phases are presented.

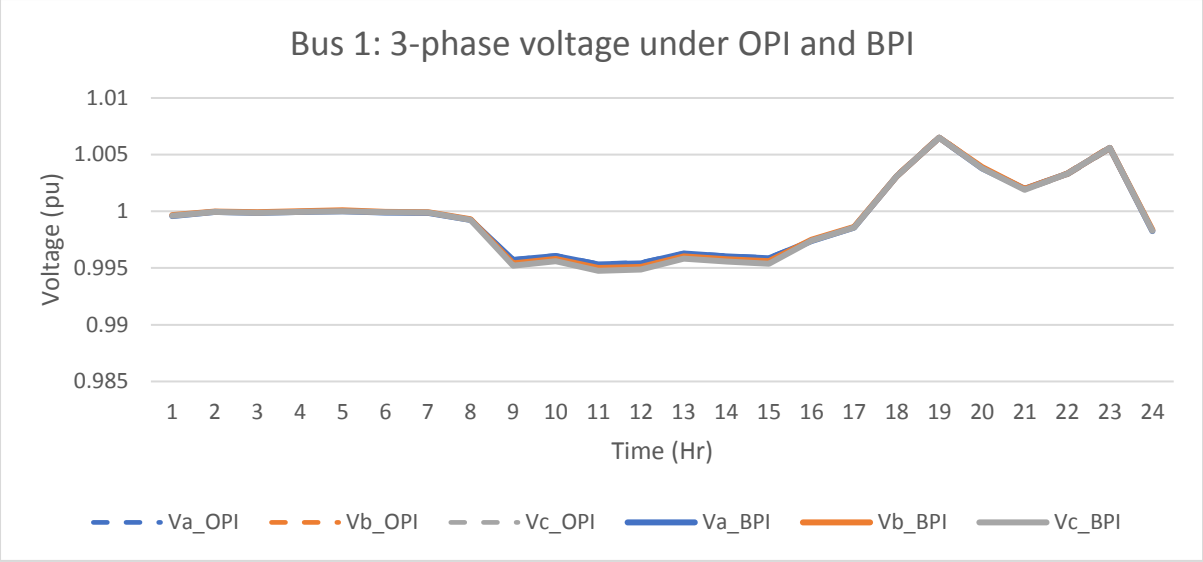

Figure 6-51: 3-phase voltage of bus 1 for a system under BPI and OPI with no PV present in the test network

It can be seen in Figure 6-51 that there is a slight divergence in the phase voltages for the OPI and BPI, but it is not significant, as can be seen from Figure 6-52 comparing the %PVUR (phase voltage unbalance rate) for BPI and OPI. The divergence (however small) is not expected since the system is balanced with all components (transmission lines) being balanced and no insertion of unbalanced entities like the load shown in Figure 6-45.

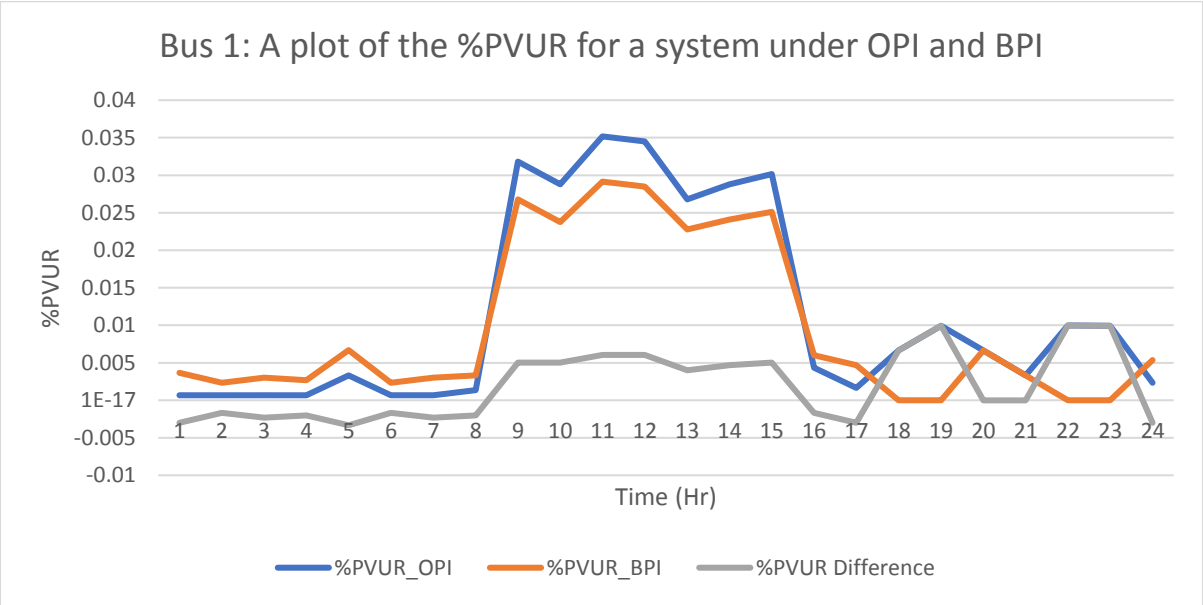

Figure 6-52: The %PVUR of bus 1 for BPI and OPI

Figure 6-52 shows that the %PVUR (phase voltage unbalance rate) is smaller than 0.1%, but there is a slight divergence between the OPI and BPI, with the OPI having a larger %PVUR at midday.

6.3.5 ESS, EV and 3-phase Load assessment

This simulation excludes the 3-phase PV only. Figure 6-53 compares the average voltage at bus 1 for BPI and OPI, it also shows the power for the ESS, EV, 3-phase load, and the net sum of their power transferred.

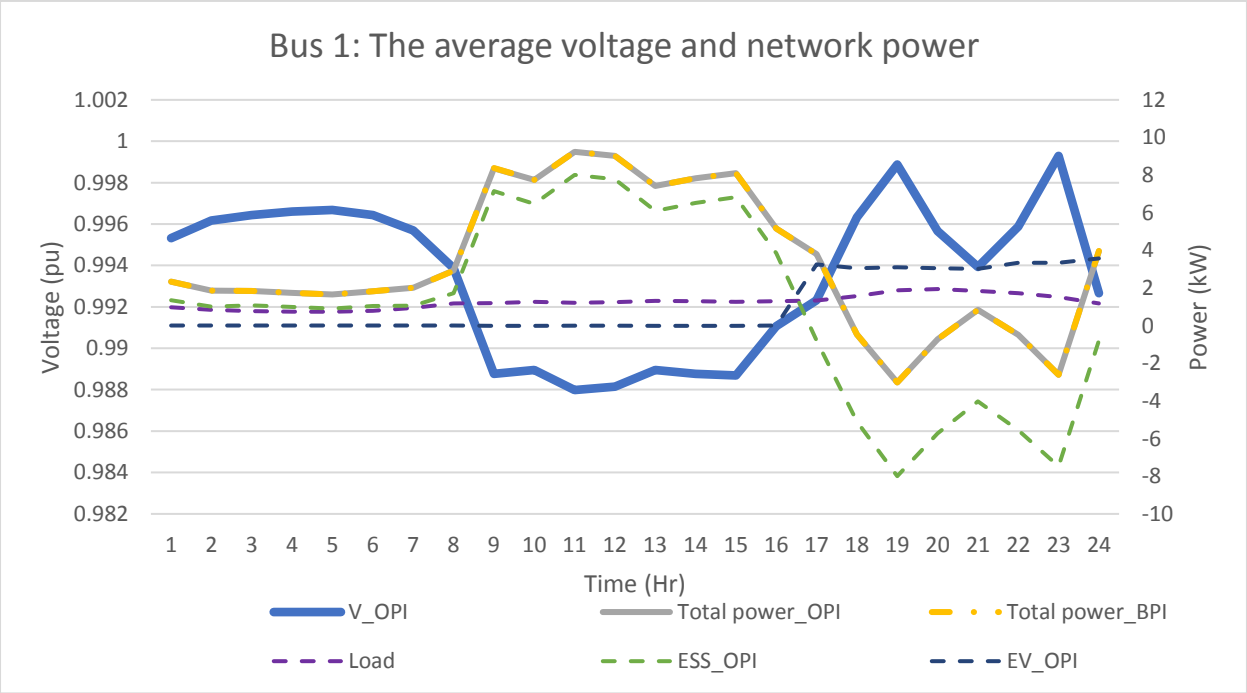

Figure 6-53: The average voltage of the network under OPI and BPI for ESS1, EV1 and L

Figure 6-45 reveals that the load is unbalanced and introduces a voltage unbalance (as seen in Figure 6-46). This means the average voltage profile (Figure 6-53) does not give enough information on the operation of the network. The phase voltage breakdown of bus 1 is shown in Figure 6-54.

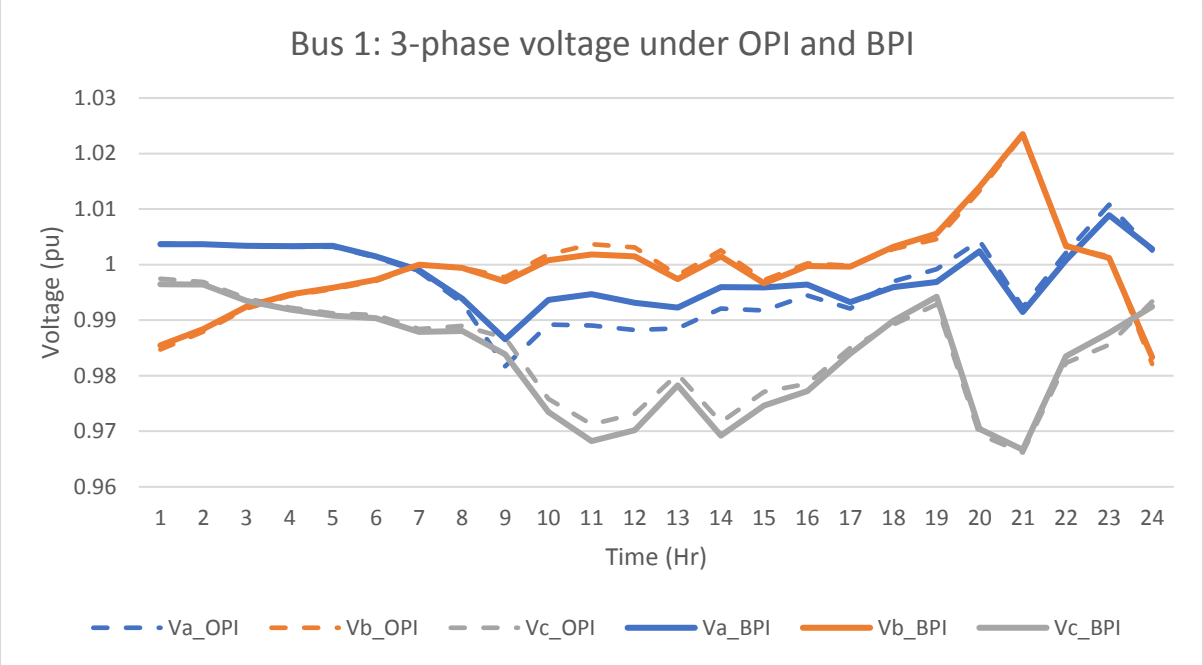

Figure 6-54: 3-phase voltage of bus 1 for a system under BPI and OPI with no PV present in the test network

While the volt (pu) difference is not significant in Figure 6-54, it is far more visible than in Figure 6-51, with the most significant divergence being at midday (maximum ESS power transaction).

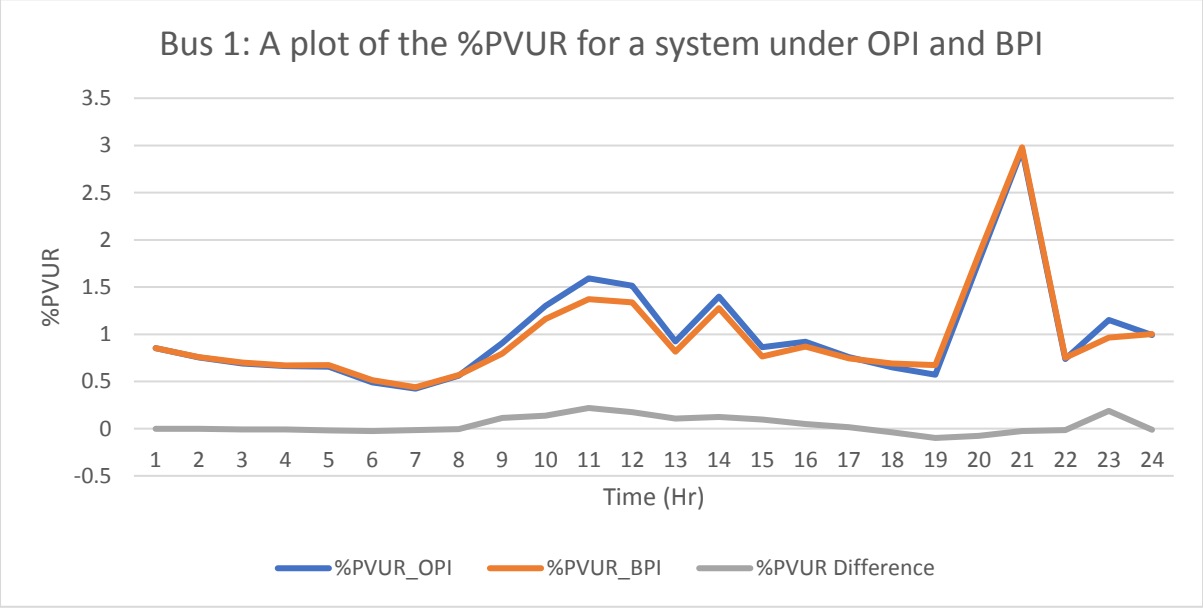

Figure 6-55: The %PVUR of bus 1 for BPI and OPI

It can be seen in Figure 6-55 that the magnitude of the %PVUR (phase voltage unbalance rate) is much higher. Due to the unbalance introduced by the load, there is still a divergence between

the OPI and BPI, which implies the OPI exaggerates the network unbalance. This is to be expected considering that loss minimization is what is being considered during the optimal power transfer of the ESS/EV. This means the voltage unbalance is not being considered. The ESS and EV will try to extract power in the phases with the least R_{th}, meaning the phase with an even lower voltage (lower losses) will have more current being taken from it, resulting in the voltage being dipped more while the phase with a larger impedance (with a larger R_{th}) having a larger voltage due to even less current being synced from that phase. This implies a cost of the overall voltage quality (balance) of the network for the ESS and EV to transfer power optimally.

6.3.6 ESS, EV and 3-phase PV assessment

The ESS, EV and 3-phase PV simulation excludes the 3-phase RL load. Figure 6-56 shows the voltage and power resulting from the interaction of the ESS and EV with the balanced 3-phase PV.

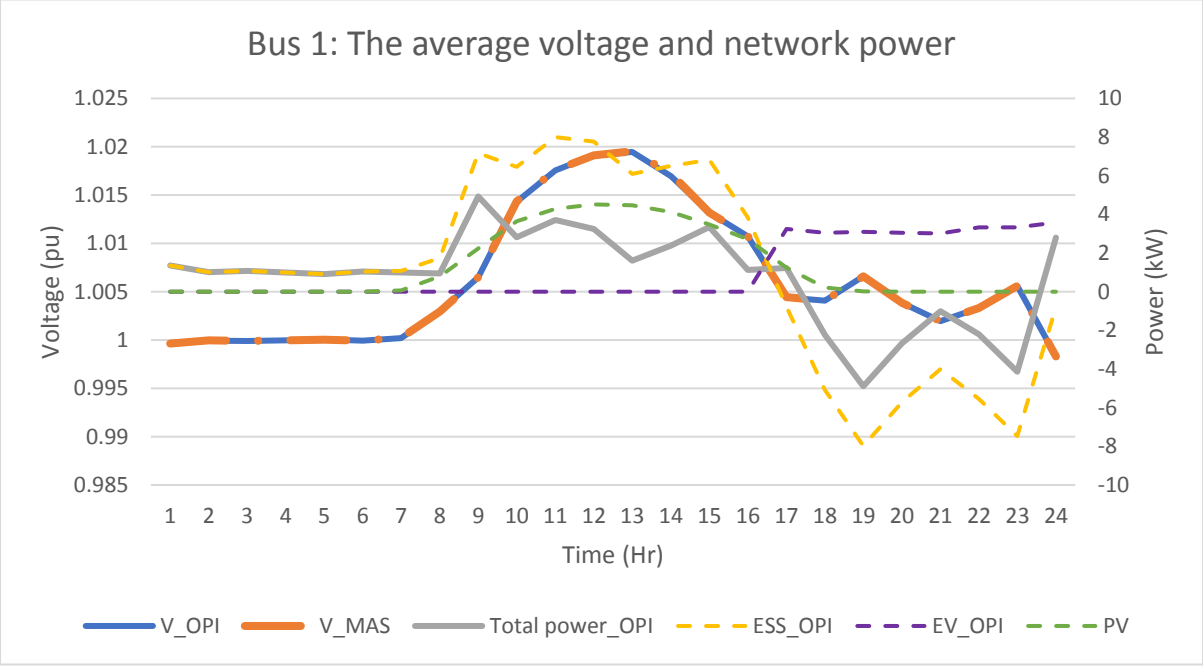

Figure 6-56: the average voltage and power of the network under OPI and BPI for ESS1, EV1 and PV

Figure 6-56 shows that the average voltage has surged due to the PV, with the average voltage curves of the BPI and OPI being similar. It also shows that the phase voltages of the OPI and BPI diverge significantly at the midday peak. Figure 6-57 shows that this happens

regardless of the PV power per phase not diverging significantly (PV has BPI, unlike the 3-phase RL load).

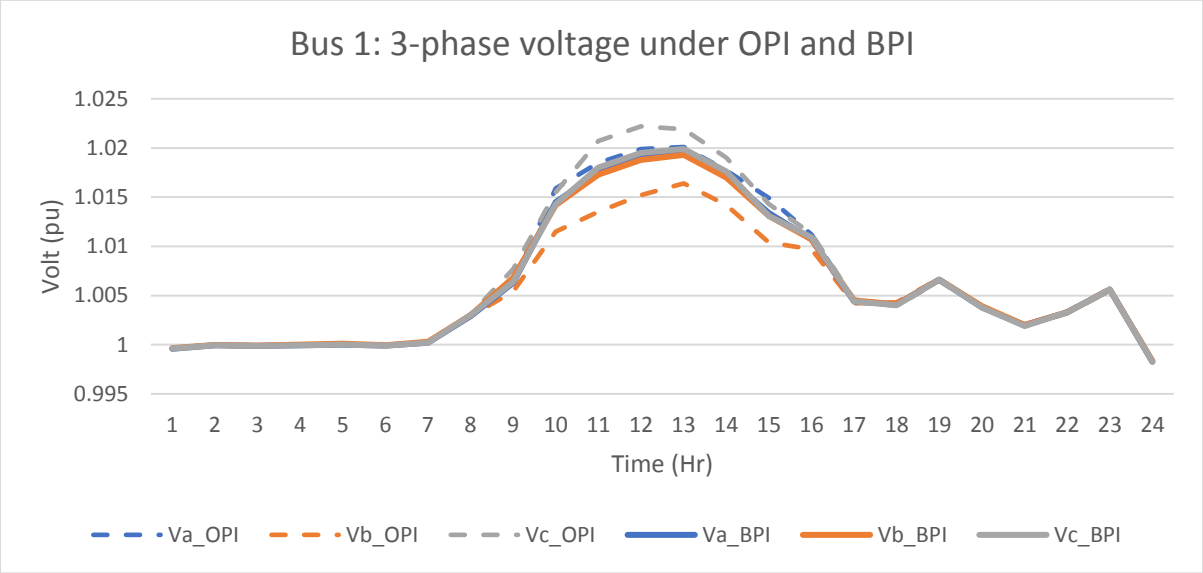

Figure 6-57: 3-phase voltage of bus 1 for a system under BPI and OPI with no PV present in the test network

The PV is shown to have a BPI in Figure 6-58.

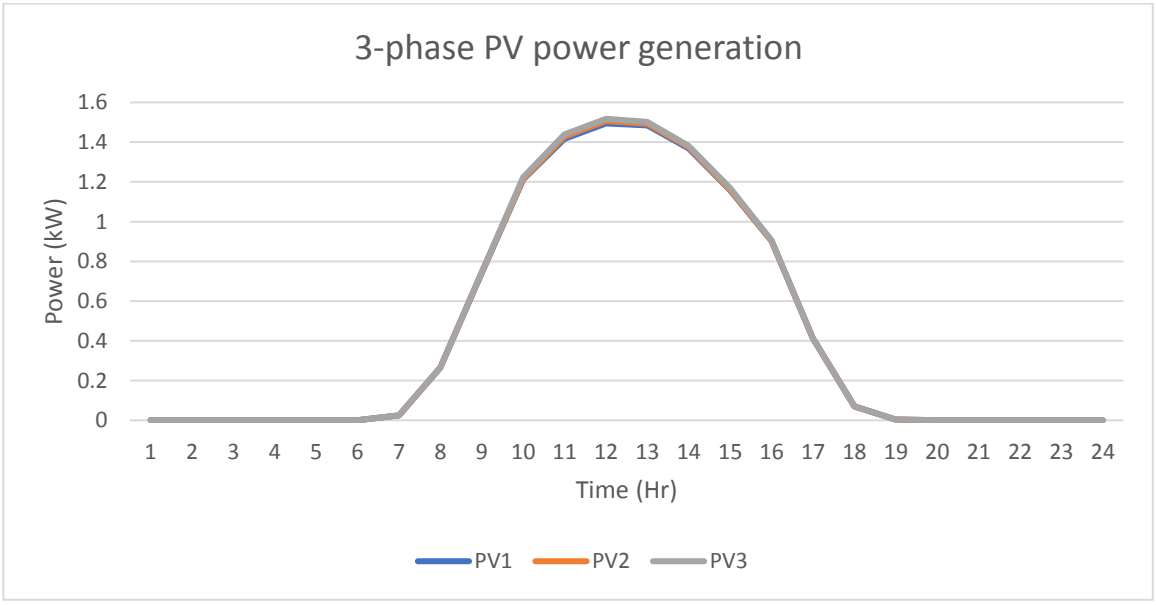

Figure 6-58: PV generation curve

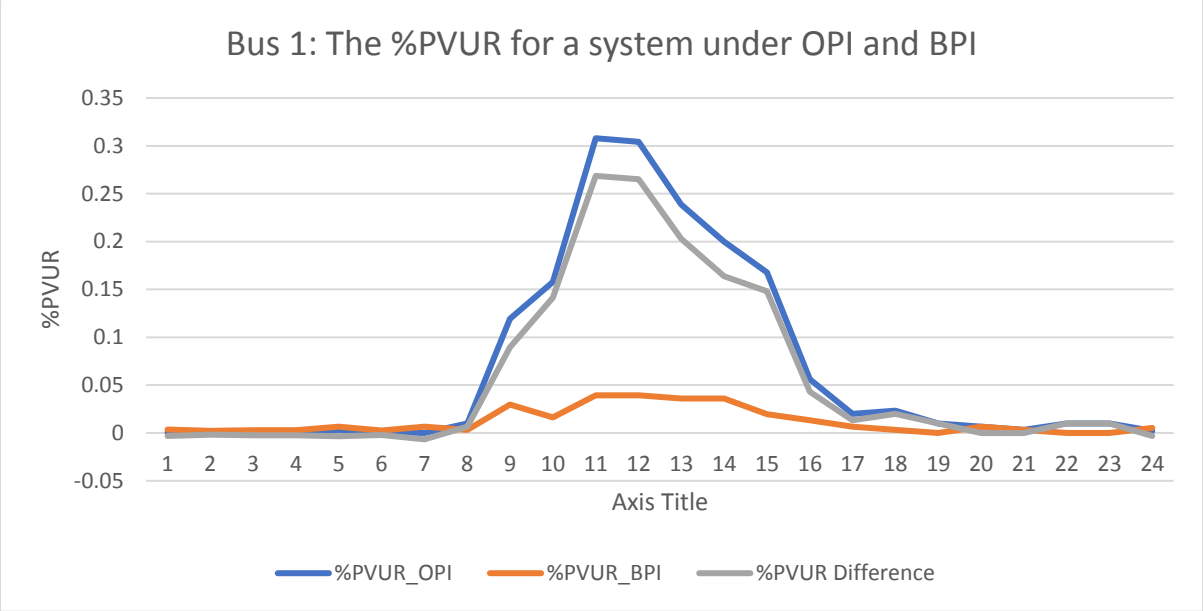

Figure 6-59: The %PVUR of bus 1 for BPI and OPI

Figure 6-59 shows the BPI %PVUR curve being similar to the curve in Figure 6-51 (the test where all external inputs are balanced) for the BPI, but the OPI's diverges. The leading cause of this divergence is the power surge from the 3-phase PV. This further implicates and re-enforces the notion that the TEI's performance depends on the state of the network, as discussed earlier in sections 6.1.1 and 6.1.2.

6.3.7 Full Test network assessment

The full test network simulation consists of all the networks elements in Figure 4-1, such as the 3-phase unbalanced RL load, 3-phase balanced PV, the ESS and the EV. Figure 6-60 shows the voltage and power as a result of the simulation

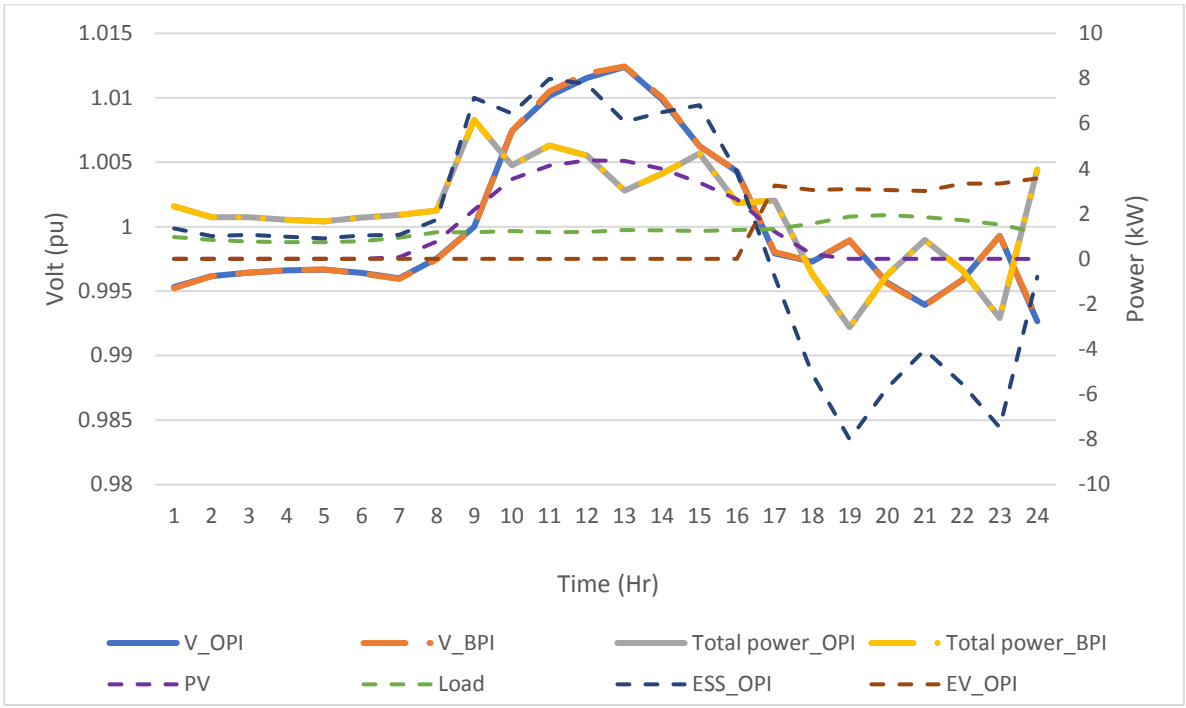

Figure 6-60: A The average voltage of the MAS and OPI simulation

Like the previous simulations, Figure 6-60 shows that the average voltage for the OPI and BPI systems only are the same. Still, the phase voltages diverge similarly to Figure 6-54 (the model excluding the PV) despite the presence of the PV, which had a more pronounced divergence between BPI and OPI, as shown in Figure 6-57. Figure 6-61 presents the phase voltages at bus 1 under BPI and OPI, which is used to derive the %PVUR for the network under BPI and OPI shown in Figure 6-62.

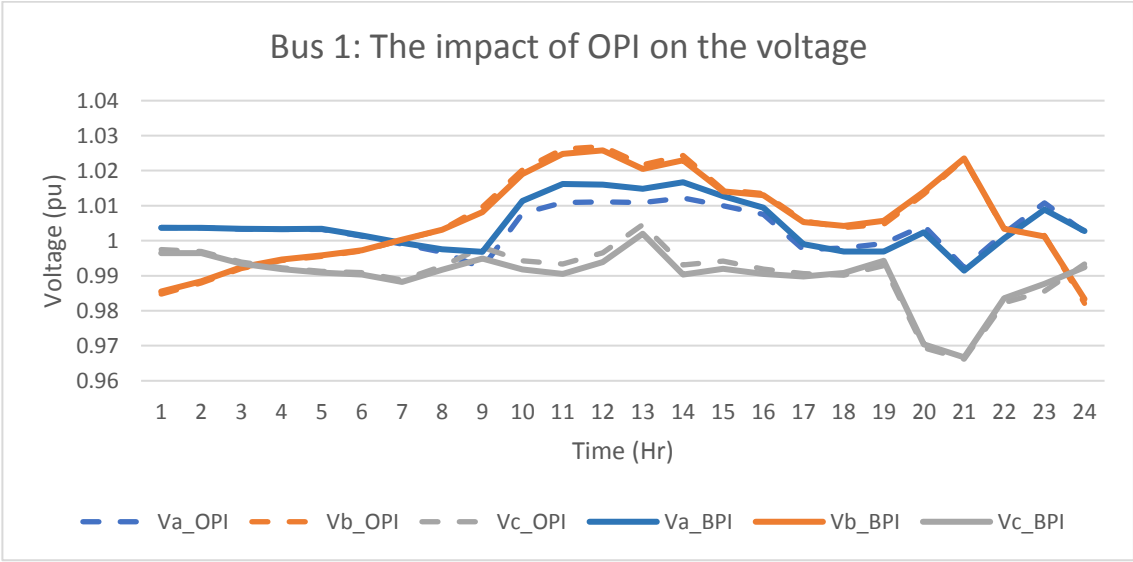

Figure 6-61: 3-phase voltage of bus 1 for a system under BPI and OPI

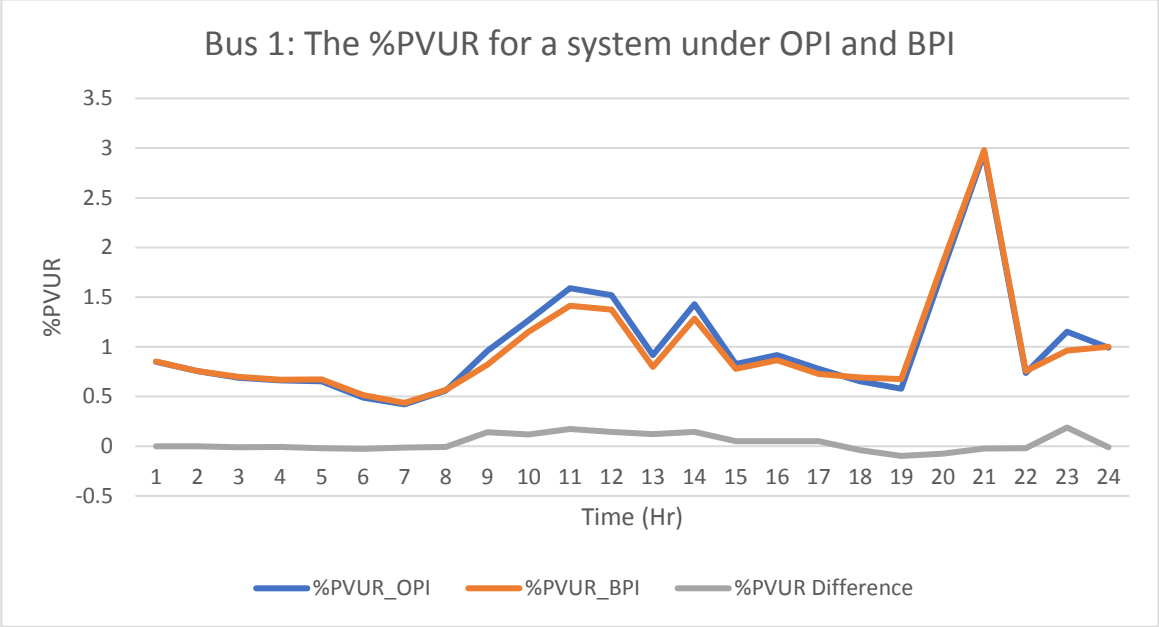

Figure 6-62: The %PVUR of bus 1 for BPI and OPI

It can be seen from Figure 6-62 that the %PVUR is congruent with that of Figure 6-55 (the model excluding the PV), but the scale of divergence between the BPI and OPI (for both phase voltage and %PVUR) is not as significant as Figure 6-57 and Figure 6-59. The PV (external power injection) increases divergence between OPI and BPI. Still, the load (external unbalance) overrides the divergence induced from the PV power surge due to the more significant unbalance caused by the unbalanced 3-phase RL load.

6.3.8 Unbalanced system analysis

This section focuses primarily on unbalance (due to transmission line unbalance), the ability of TEI to minimize losses and what impact this loss minimization has on the network voltage. There is a test with only the ESS and EV transacting power to compare the loss minimization of the BPI and OPI, while the second test will be a replica of the test in section 0 but with a 50% transmission unbalance.

6.3.8.1 Loss minimization of TEI guided injection (OPI)

This section presents a network with changing %unbalance of the transmission lines, an ESS and an EV, with the ESS at bus 2 and EV at bus 3.

The impact of this unbalance on the test network's voltage (with no power injection from the ESS, EV, PV or Load) is shown in Figure 6-63.

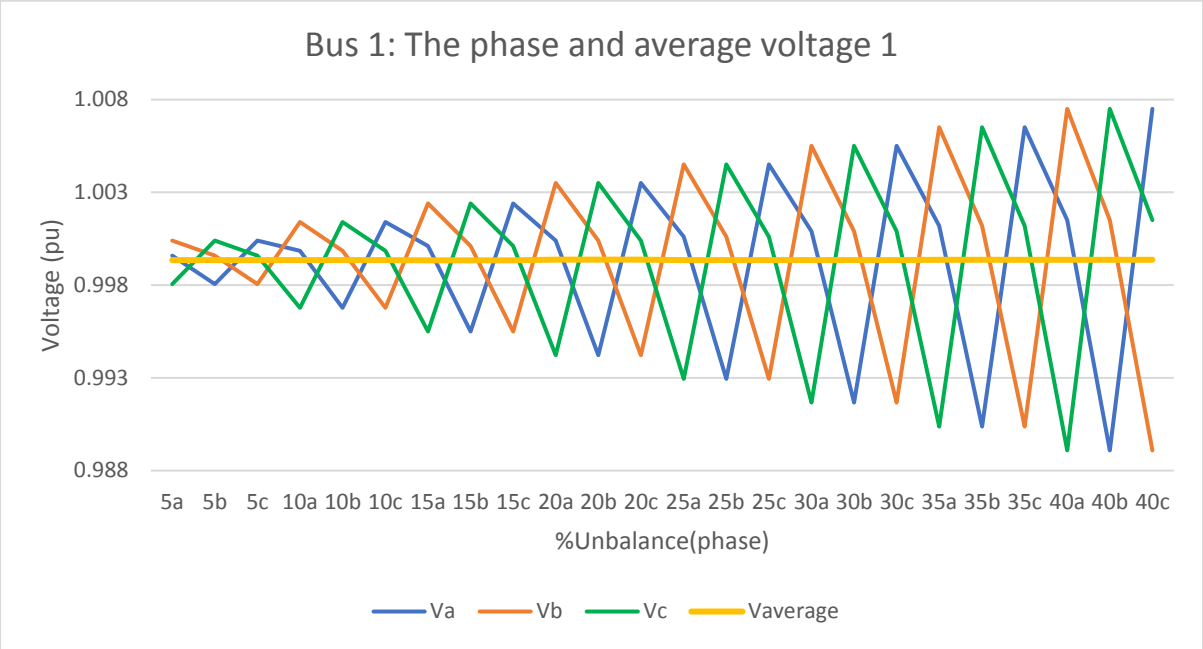

Figure 6-63: The impact of line unbalance (varying from 5%-40%) on bus 12 for the test network.

The phase voltage unbalance rate (%PVUR) is derived from the results in Figure 6-63 and are presented in Figure 6-64 and Table 6-2, with an increasing %PVUR as the transmission unbalance increases.

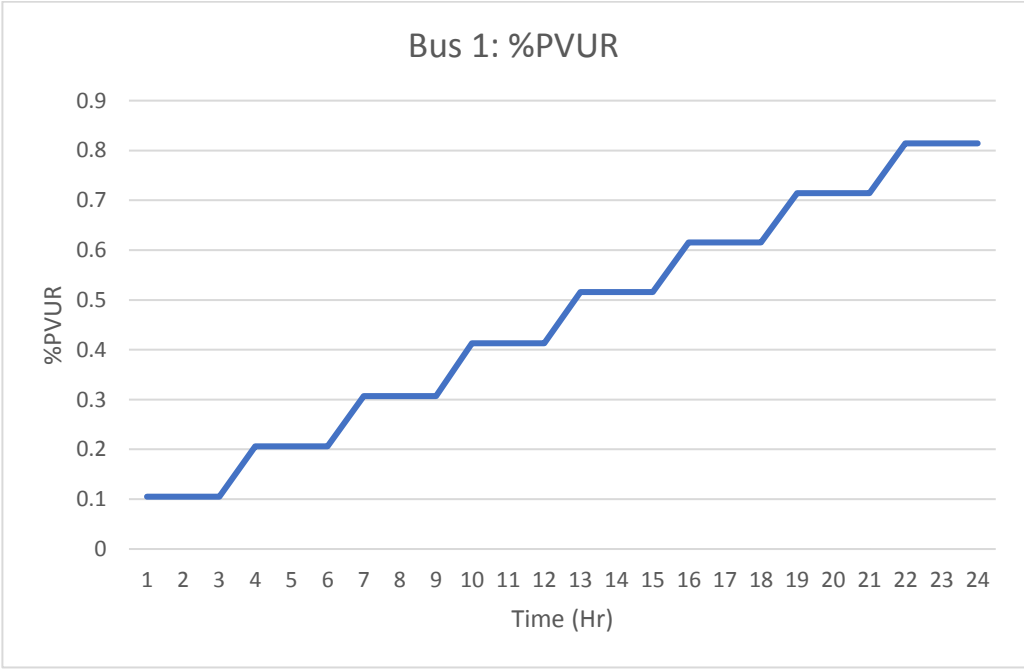

Figure 6-64: %PVUR of bus 1 for a system with no PV, Load, ESS or EV

Table 6-2: : The unbalanced voltage at bus 1

$V_a\ (pu)$	$V_b\ (pu)$	$V_c\ (pu)$	%Unbalance(phase)	%PVUR
0.9995	1.0004	0.9981	5a	0.1051
0.9980	0.9996	1.0004	5b	0.1051
1.0004	0.9981	0.9996	5c	0.1051
0.9998	1.0014	0.9968	10a	0.2061
0.9967	0.9998	1.0014	10b	0.2061
1.0014	0.9968	0.9998	10c	0.2061
1.0001	1.0024	0.9955	15a	0.3069
0.9955	1.0001	1.0024	15b	0.3069
1.0024	0.9955	1.0001	15c	0.3069
1.0004	1.0035	0.9942	20a	0.4129
0.9942	1.0004	1.0035	20b	0.4129
1.0035	0.9942	1.0004	20c	0.4129
1.0006	1.0045	0.9929	25a	0.5157
0.9929	1.0006	1.0045	25b	0.5157
1.0045	0.9929	1.0006	25c	0.5157
1.0009	1.0055	0.9917	30a	0.6151
0.9917	1.0009	1.0055	30b	0.6151
1.0055	0.9917	1.0009	30c	0.6151
1.0012	1.0065	0.9904	35a	0.7145
0.9904	1.0012	1.0065	35b	0.7145
1.0065	0.9904	1.0012	35c	0.7145
1.0015	1.0075	0.9891	40a	0.8142
0.9891	1.0015	1.0075	40b	0.8142
1.0075	0.9891	1.0015	40c	0.8142

Figure 6-64 and Table 6-2 show that the higher the transmission impedance, the higher the voltage is on, the higher the impedance phase (this is due to lower current flowing out of that phase), the inverse is also true. To get a clearer picture, the ESS and EV will inject power based on the TEI values (OPI) and even power injection across each phase (BPI).

The TEI impedances determined from bus 2 (ESS 1) and bus 3 (EV 1) are shown in Figure 6-65:

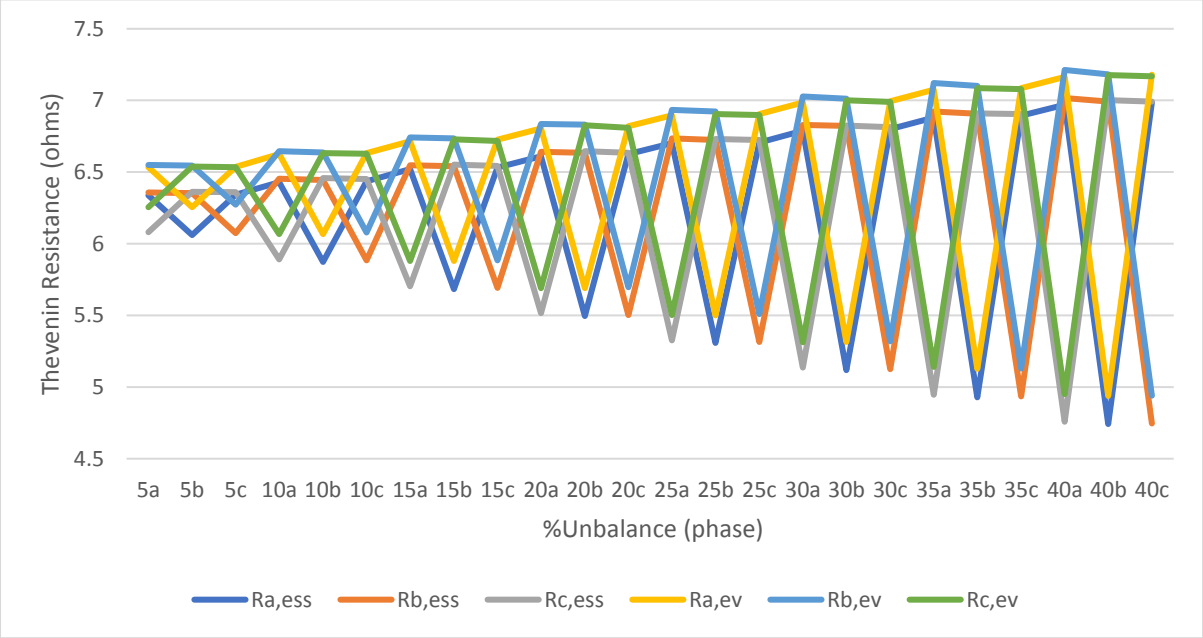

Figure 6-65:The TEI values for bus 2 and bus 3

Figure 6-65 shows that the TEI device is not capable of recognizing the unbalance perfectly, as described in section 6.1.3. Figure 6-66 shows the transmission losses and the average voltage (bus 1) for the system under OPI and BPI.

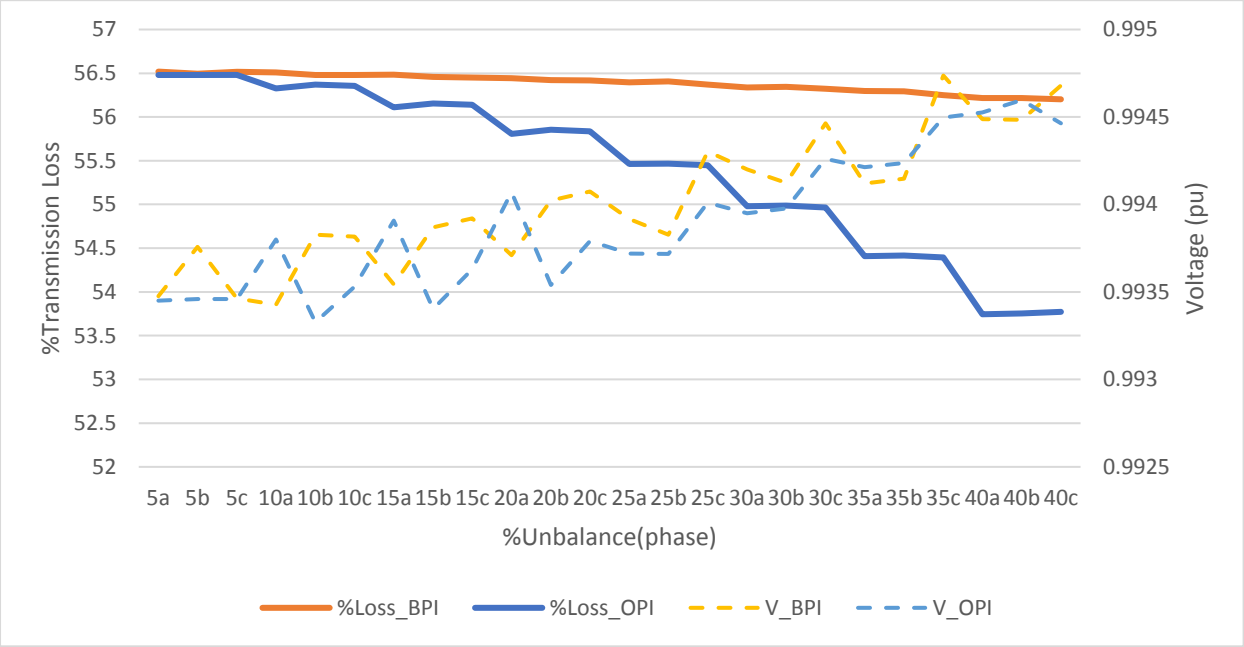

Figure 6-66: The percentage transmission losses of the OPI and BPI implementation.

The percentage losses of the network show that information of the TEI enables for loss reduction, a loss difference of about 2% (at a transmission unbalance of 40%). From the

previous results (presented and discussed in section 6.1.3), it is observed that the TEI does not perfectly recognize unbalance and can barely observe a positive unbalance (when a phase has a higher impedance than the phase with the median impedance) which reveals that those losses are not being fully minimized. The impact on the voltage profile per phase was also analyzed as the average voltage profile hides too much information.

These results are logical because the total transmission impedance remains the same, but the impedance is shifted across the phases, which results in a transmission line having a lower impedance than if it was balanced, leaving room for the TEI sensor to notice this (in its current limited capacity) and help the ESS/EV exploit this by transmitting more power through the line with less impedance and bypass the higher impedance lines.

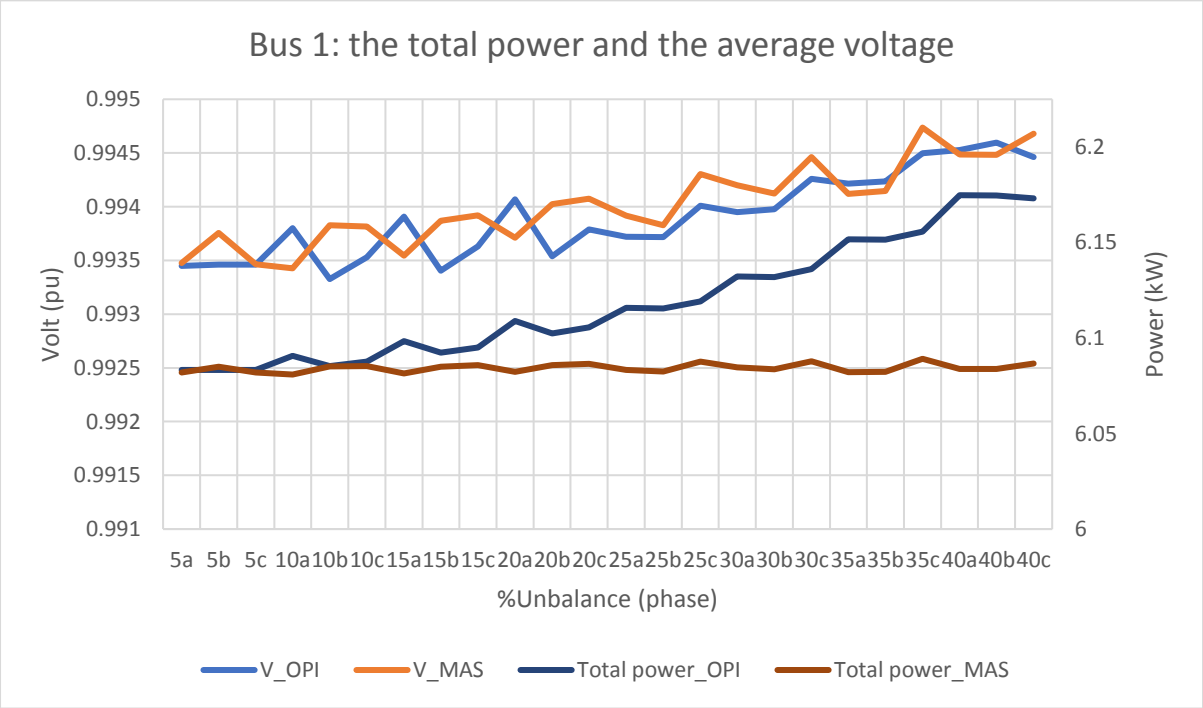

Figure 6-67: The power and the average voltage at bus 1

Figure 6-67 shows a changing average voltage despite the expectation that the average voltage should remain unchanged (due to the total transmission impedance being constant). The change is due to the total power of the ESS and EV increasing as the unbalance increases (an increase of 1% in power for a rise of 0.1% in voltage). This error is due to implementation errors in MATLAB Simulink model and does not disprove or call into question results discussed earlier.

6.3.8.2 Full system with 50% transmission unbalance

This test is a replication of the test done in section 0, but with a transmission unbalance of 50%, the solid lines is the voltage (bus 1) of a balanced transmission, and the dashed lines represent the voltage profile of an unbalanced transmission. Figure 6-68 shows the phase voltages at bus 1, and it shows the impact of transmission impedance unbalance (of 50%) on a system with standard ESS/EV BPI. The level of unbalance is not consistent throughout the day, with the unbalanced system having a larger %PVUR (phase voltage unbalance rate) midday (maximum PV injection) while having a smaller %PVUR in the evening and morning.

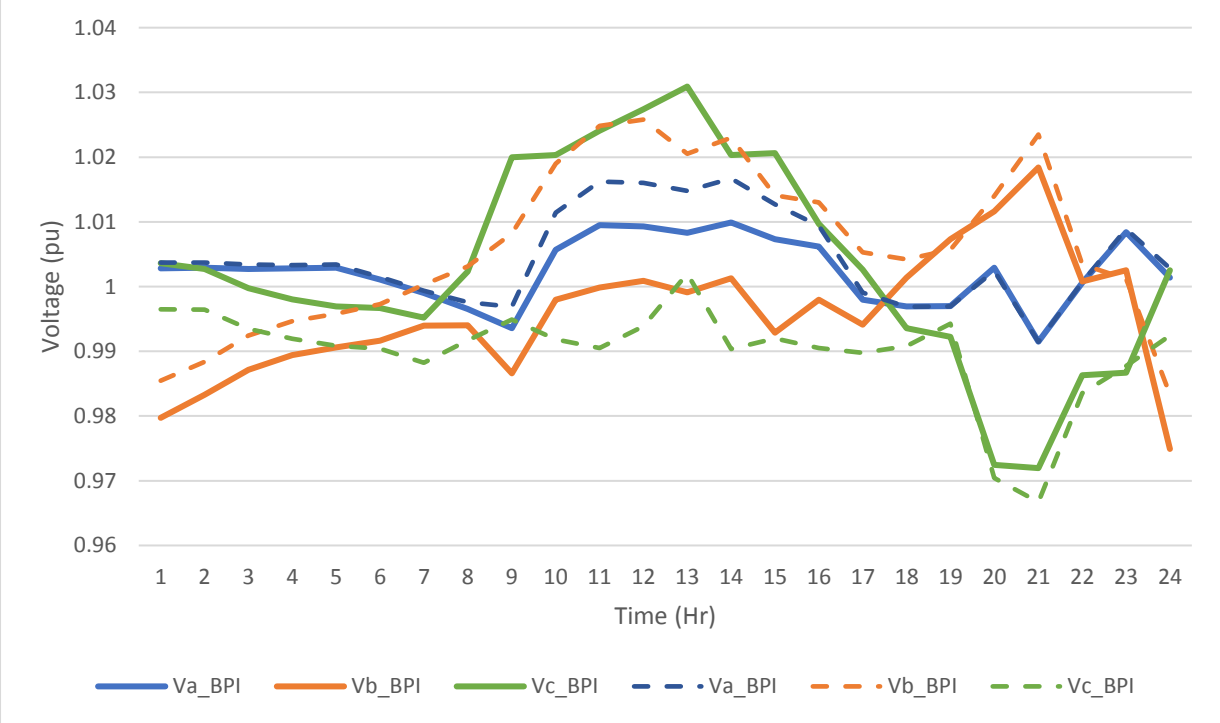

Figure 6-68: The voltage of a network with a balanced transmission line and a network with a 50% unbalanced transmission line with standard power injection

The impact of OPI on an unbalanced system's voltage (bus 1) is presented in Figure 6-69. The maximum variation is less than 0.01 V(pu).

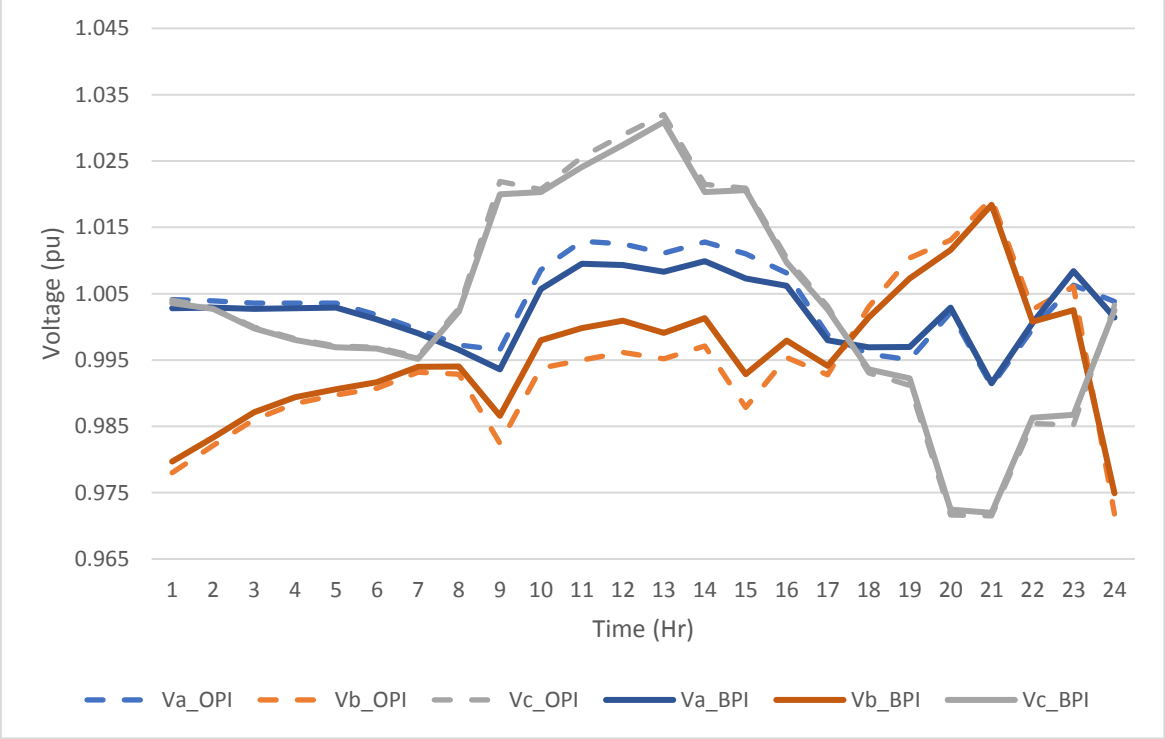

Figure 6-69: The 3-phase voltage of a test network with an unbalanced transmission of 50% at Bus 1

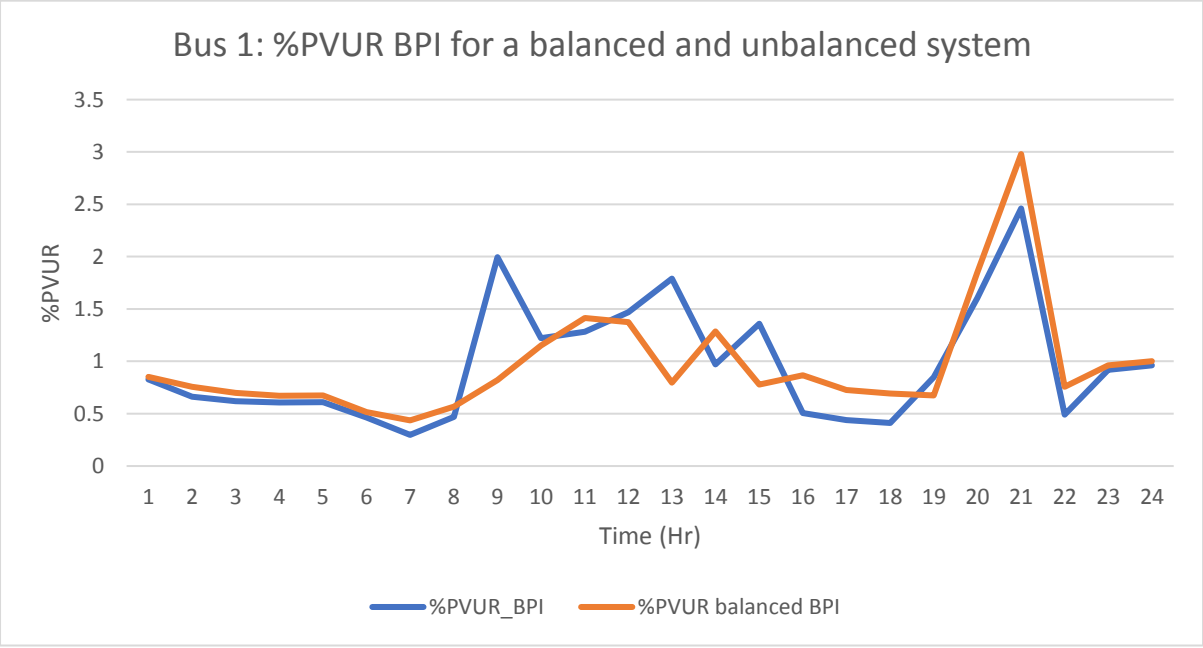

Figure 6-70: The impact of transmission unbalance on %PVUR for a system with BPI

The %PVUR of the voltages in Figure 6-68 is illustrated in Figure 6-70, with the midday unbalance being larger for the unbalanced system and the evening unbalance being lesser. Despite the 50% transmission impedance unbalance, the voltage unbalance is not consistent.

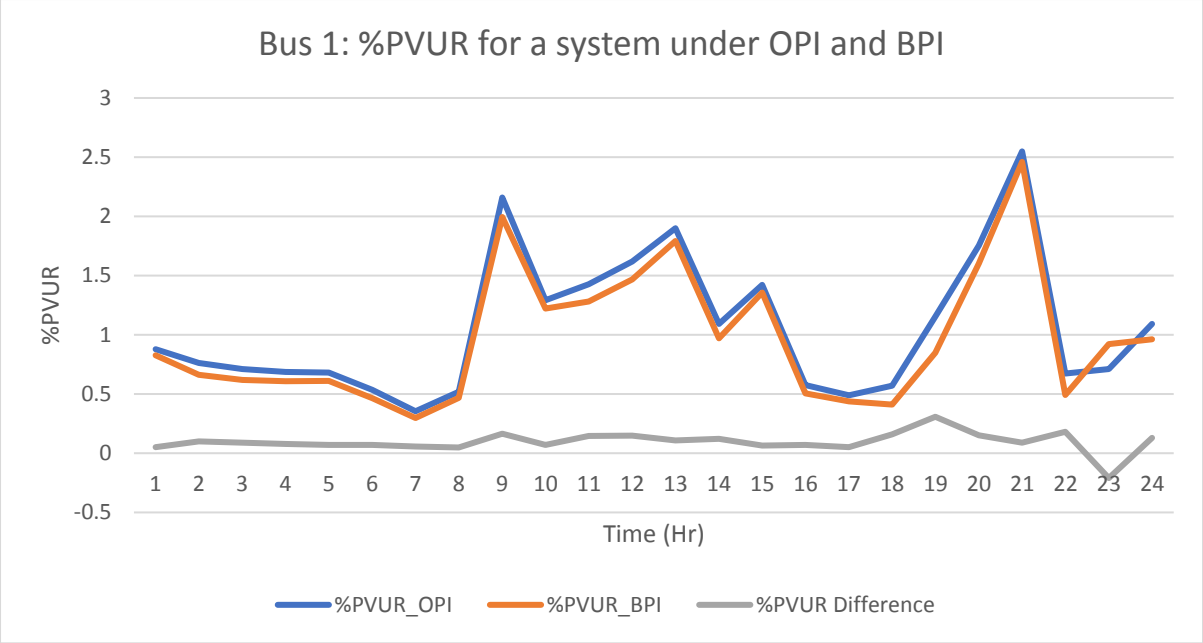

Figure 6-71: %PVUR of a system with a 50% transmission unbalance

Figure 6-71 shows that the OPI does not alter the voltage profile meaningfully but still has a slightly higher %PVUR.

7 Conclusion

The dissertation investigated a novel framework for the regulation of an ever-expanding LV network which will transfer the optimal power from an undefined number of EVs and ESSs into the LV network from various independent nodes. Every aspect of the framework developed for regulation was discussed and tested. The results of the simulation and discussions are presented in chapter 6. Conclusions are drawn for the research questions stated in section 1.6, and the validity of the hypothesis is examined.

7.1 TEI Sensor operation

There were four aspects of the TEI sensor (discussed in section 2.7 of the literature review) that were examined in sections 5.1 and 6.1. These are the accuracy of the TEI sensor, the impact the transformer had on that accuracy, the TEI sensors response to unbalance and how more than one TEI sensor operates simultaneously in the same network. The simulations were carried out on the test network (section 4.1) with the Thevenin impedance (Z_{th}) being determined for bus 2 ($Z_{th,ESS}$) and bus 3 ($Z_{th,EV}$) for each of the test cases.

The accuracy of the TEI was observed by comparing the TEI determined (measured) Z_{th} with the hand calculated Z_{th}. A disparity was found for both the R_{th} and X_{th} (in section 6.1.1.3). With the X_{th} having a disparity of 70% maximum (regardless of the bus examined) while the R_{th} had a less significant disparity of 20% maximum. This test made it clear that the demand on the network, and the strain it causes, has an impact of the determination of Z_{th}. Larger network demand (or more specifically, greater strain on the network) resulted in underestimation of the Z_{th} measured. These results were further validated with the TEI and Transformer analysis.

The tests conducted in the TEI validation (and limitations) are replicated but for a system without the transformer. The transformer used was modelled to be weaker than the transformer used in [1] and [25] to be able to observe a change in network voltage via increased demand, its absence and the direct coupling of the network to the voltage source re-enforces that the accuracy of the TEI depends on the network condition. This is due to none of the Z_{th} measured being smaller than the Z_{th} calculated. The largest impact of the transformer is the accuracy of X_{th}, with the distortion changing from -70% to 25%. The network setup and network conditions have a clear impact on the determination of Z_{th}. This shows that feedback

information should be employed in equations (2-16) and (2-31) to have an adequate estimation of R_{th} and X_{th} .

Unbalance observation of the TEI is limited, with it being better at detecting negative unbalances (lower impedances) than it is at detecting a positive one (higher impedance). This means the TEI sensor has certain limits for its operation. This resulted in the losses observed in Figure 6-66 being larger than they would be ideally; this does not reflect on the algorithm discussed in section 3.3.2.

The results in section 6.1.4 show that on average $Z_{th,simultaneous}$ is at least double the size of $Z_{th,seperate}$. These results make sense once equations (2-31) and (2-32) are analyzed. The main issue being those equations do not account for the increase in current I_{inv} being pulsed in the network (which is double the amount due to two TEI sensors operating). The actual I_{inv} flowing through the network is more than double and results in a V_{inv} doubling in value which causes Z_{th} to double in value.

The analysis reveals the TEI has limited accuracy that depends on the quality of the network components (Transformer), the demand in the network and the X_{th} being drastically altered by the presence of the transformer. It also emerged from the analysis that the TEI sensor's accuracy (R_{th} specifically) is at its best during high network demand (meaning the network is under maximum pressure and is a critical moment) and with a Transformer suited for the network.

7.2 Impact of the OPI on the system

The MAS (stage 1 in section 3.3.1) used in the framework is based on the methods applied in [1], [25] and generates similar results, with a smoother voltage profile (Figure 6-48) than the system that include the ESS and EV in uncoordinated charging. The next stage was to compare systems making use of the same MAS generated charging scheme (for the ESS and EV) but with different modes of phase power injection, BPI and OPI.

It was found that the TEI sensor can be used to minimize transmission losses (through OPI proposed in section 3.3.2), as seen in Figure 6-66, by exploiting the transmission lines with less impedance

The impact of the OPI on the network voltage was minimal, as seen in Figure 6-71 and Figure 6-62 %PVUR (phase voltage unbalance) charts. It can be inferred from this finding that the extra unbalance introduced by OPI is negligible.

Furthermore, the study found that the integration of MAS guided charging with OPI (guided by TEI parameter estimations) is a feasible combination and an improvement on the existing [1], [25] framework as it maintains voltage quality while minimizing losses.

7.3 Answers to Research Questions

A summary of the answers to the research questions formulated in Chapter 1 are presented in the following sections:

7.3.1 What are the similarities and differences between centralized system control and decentralized (MAS) power control?

This was addressed in section 2.2 of the literature review. It can be inferred from the literature review that there are not any similarities between decentralized and centralized control. Still, the decentralized approach allows for a system that is flexible and open to prosumers and can meet their requirements which can vary widely. Also, the decentralized approach is more robust and scalable as it would allow for modification from a hardware and software perspective which is necessary since there will be need for modifications to the system to allow it to handle a more complex active network that is very likely to keep changing over time.

7.3.2 What kind of design strategies have been used for proactive power control using MAS in a LV network?

Ten different proposals were examined, and of these approaches, eight of them made use of the hierarchal multi-agent organization (section 2.4). In contrast, two ([22] and [23]) made use of the flat, decentralized organization. In addition, four of the reviewed hierarchal models ([1], [10], [24] and [25]) made use of very similar principles. This is the Nash certainty equivalence (NCE) principle, which promotes a control scheme that seeks to achieve social optimality by establishing an EV and ESS charging/discharging profiles.

This approach has a straightforward and approachable structure that only requires essential information and very little communication. Other systems such as [11] and [21] require multiple agents for a single physical LV network entity (EV and ESS) that engage in peer to peer optimization, often with the selling and buying of energy from each participant. This added layer (making producing and consuming entities on the network to coordinate with each

other) complicates regulation. It adds an unnecessary layer of control as the largest market participant is the LV network's inelastic demand.

7.3.3 What are the costs of using proactive agents (cognitive) and reactive agents (reflective) in a MAS, and which ones are needed for this task?

While no literature specifically discusses proactive or reactive agents, the concept of multi-agent organization (section 2.4) discusses the different types of agent organization that require different levels of independence from agents. A hierarchal system limits the actions of agents in the MAS (making them more reactive). In contrast, a flat system requires the agents to determine their own tasks and to organize themselves (resulting in them being more proactive). Both structures have their advantages and disadvantages, but the hierarchal organization is more suited to meet the objectives of this thesis. The main reason is that the objective of this project is to regulate the LV network environment and allow it to handle new additions to the system while keeping the performance of the network within regulations. The network has global objectives such as maintaining the voltage while individual (new) actors like EV users have their local objectives such as battery charging. A hierarchal system is optimal because it allows for smaller actors to pursue their own desires ensuring they operate within a regulated body [21]. A fully decentralized system (a system that would require more complex proactive agents) would give too much autonomy to individual actors (which could make setting up a guide or regulations difficult).

The point of the MAS is to help ensure minimal interference in the network's operations, and for other passive users in the network to expect the same service delivery regardless of changes to the network environment. A hierarchy (with more reactive actors) is preferred as it enables the easy introduction of new actors (scalable) while making sure they don't alter or dominated the network.

7.3.4 What are the impacts of network unbalance?

The unbalance caused by transmission lines and unbalanced loads are the focus of this inquiry. Transmission and Load unbalance results in a voltage unbalance. Voltage unbalance has negative impacts on power system equipment. A little unbalance in voltage can result in a larger current unbalance [26]. Power system equipment such as three-phase rectifiers,

transformers, protection devices and inverters [26], [27] are affected because of the unbalance. The excessive current unbalance causes the temperature of the rectifier's diodes to increase, decreases induction motor efficiency, increases transmission losses and increases core losses in power transformers which indicates that network unbalance can cause serious economic loss [26].

7.3.5 What is the impact of trying to determine the Thevenin Equivalent Impendence at different nodes simultaneously?

There was no literature available to discuss this, but the answer to the research question was determined through case studies in section 6.1.4, it is feasible to run multiple TEI sensors together, and there does not appear to be a limit on how many TEI sensors can be active simultaneously. However, the accuracy of the TEI parameters changes drastically (specifically due to how the parameters are determined in section 2.7). The value of the Z_{th} is multiplied by a factor of the number of TEI sensors modulating simultaneously in the network.

7.4 Hypothesis validity

The following hypothesis was formulated to guide the direction of the study:

"A Multi-Agent System (MAS) enabled by Thevenin parameter estimations is a feasible solution for the regulation/control of a distributed and unbalanced LV network to minimize losses in an unbalanced network with multiple independent entities."

Sections 2.2, 2.3.2, 6.3.2, 6.3.8.1, and 6.3.8.2 showed that the hypothesis was valid for answering the research questions posed to test it.

8 References

[1] S. Mocci, N. Natale, F. Pilo and S. Ruggeri, "Exploiting distributed energy storage to increase network hosting capacity with a Multi-Agent control system," University of Cagliari, Cagliari.

[2] M. Lethonen and S. Nye, "History of electricity network control and distributed generation in the UK and Western Denmark," *Energy Policy,* vol. 37, no. 6, pp. 2338-2345, June 2009.

[3] T. Ackerman, G. Andersson and L. Soder, "Distributed generation: a definition," *Electric Power Systems Research,* vol. 57, no. 3, pp. 195-204, 2001.

[4] M. Malengret and C. T. Gaunt, "Using Thevenin Equivalents to Improve Electricity Delivery Efficiency in AC and DC systems," University of Cape Town, Cape Town.

[5] C. A. Sima, M. O. Popescu, C. L. Popescu and G. Lazaroiu, "Integrating Energy Storage Systems and Transmission Expansion Planning in Renewable Energy Sources Power Systems," *2019 54th International Universities Power Engineering Conference (UPEC),* 2019.

[6] Center for Sustainable Systems, University of Michigan, "U.S. Energy Storage Factsheet," University of Michigan, Michigan, 2021.

[7] D. P. Manjure and E. B. Makram , "Impact of unbalance on power system harmonics," *10th International Conference on Harmonics and Quality of Power.,* 2002.

[8] F. Somers, "Hybrid: unifying centralised and distributed network management using intelligent agents," *Proceedings of NOMS '96 - IEEE Network Operations and Management Symposium,* 1996.

[9] K. Saxena and A. R. Abhyankar, "Agent-based decentralised load flow computation for smart management of distribution system," *The Institution of Engineering and Technology,* vol. 11, no. 3, pp. 605-614, 2017.

[10] E. L. Karfopoulos and N. D. Hatziargyriou, "A Multi-Agent System for Controlled Charging of a Large Population of Electric Vehicles," *IEEE Transactions on Power Systems,* vol. 28, no. 2, pp. 1196 - 1204, May 2013.

[11] A. L. Dimeas and N. D. Hatziargyriou , "Operation of a multiagent system for microgrid control," *IEEE Transactions on Power Systems,* vol. 20, no. 3, pp. 1447 - 1455, 2005.

[12] Z. Cheng , J. Duan and M. Chow , "To Centralize or to Distribute: That Is the Question: A Comparison of Advanced Microgrid Management Systems," *IEEE Industrial Electronics Magazine,* vol. 12, no. 1, pp. 6 - 24, 2018.

[13] S. Mocci, N. Natale, F. Pilo and S. Ruggeri, "Multi-Agent Control System for the Exploitation of Vehicle to Grid in Active LV Networks," University of Cagliari, Cagliari.

[14] S. D. J. McArthur, E. M. Davidson, V. M. Catterson, A. L. Dimeas, N. D. Hatziargyriou, F. Ponci and T. Funabashi, "Multi-Agent Systems for Power EngineeringApplications—Part I: Concepts, Approaches,and Technical Challenges," *TRANSACTIONS ON POWER SYSTEMS,* vol. 22, no. 4, pp. 1743-1751, 2007.

[15] Z. Ma, D. Callaway and I. Hiskens, "Decentralised Charging Control for Large Populations of Plug-in Electric Vehicles; Application of the Nash Certainty Equivalence Principle," *2010 IEEE International Conference on Control Applications,* 2010.

[16] S. D. J. McArthur, E. M. Davidson, V. M. Catterson, A. L. Dimeas, N. D. Hatziargyriou, F. Ponci and T. Funabashi, "Multi-Agent Systems for Power EngineeringApplications—Part 2: Technologies, Standards, andTools for Building Multi-Agent Systems," *IEEE TRANSACTIONS ON POWER SYSTEMS,* vol. 22, no. 4, 2007.

[17] "The Foundation for Intelligent Physical AgentsAn Overview," [Online]. Available: https://jade.tilab.com/papers/FIPA%20overview%20Donald.pdf.

[18] F. Ferber, Multi-Agent System: An Introduction to Distributed Artificial Intelligence, London: Addison-Wesley, 1999.

[19] O. Shehory, Architectural Properties of MAS, Pittsburgh: Carnegie Mellon University, 1998.

[20] "FIPA SL Content Language Specification," 3 12 2002. [Online]. Available: http://www.fipa.org/specs/fipa00008/SC00008I.html. [Accessed April 2019].

[21] J. P. Lopes, F. J. Soares and P. M. R. Almeida, "Integration of Electric Vehicles in the Electric Power System," *Proceedings of the IEEE (,* vol. 99, no. 1, pp. 168 - 183, 2011.

[22] R. Belmans, R. Duan, N. Gui, G. Deconinck and Z. F. Qiu, "A Market-based MAS Framework for Microgrids," *IFAC Proceedings Volumes,* vol. 41, no. 2, pp. 11053-11058, 2008.

[23] A. Kulmala , S. Repo and P. Järventausta , "Coordinated Voltage Control in Distribution Networks Including Several Distributed Energy Resources," *IEEE Transactions on Smart Grid,* vol. 5, no. 4, pp. 2010 - 2020, 2014.

[24] S. Mocci, N. Natale, S. Ruggeri and F. Pilo, "Multi-Agent Control System for increasing hosting capacity in Active Distribution Networks with EV," *2014 IEEE International Energy Conference (ENERGYCON),* 2014.

[25] S. Mocci, N. Natale, F. Pilo and S. Ruggeri, "Demand side integration in LV smart grids with multi-agent control system," *Electric Power Systems Research,* 2015.

[26] G. G. Gray and W. J. Martiny, "Efficiency testing of medium induction motors-a comment on IEEE Std 112-1991," *IEEE Transactions on Energy Conversion ,* vol. 11, no. 3, pp. 495 - 499, 1996.

[27] M. G. Davoudi, A. Bashian and J. Ebadi, "Effects of unsymmetrical power transmission system on the voltage balance and power flow capacity of the lines," *2012 11th International Conference on Environment and Electrical Engineering,* 2012.

[28] M. H. Albadi, A. S. Al Hinai, A. H. Al-Badi, M. S. Al Riyami, S. M. Al Hinai and R. S. Al Abri, "Unbalance in power systems: Case study," *2015 IEEE International Conference on Industrial Technology (ICIT),* 2015.

[29] S. Tsau and K. H. Wong, "On-line estimation of thevenin equivalent with varying system states," in *2008 IEEE Power and Energy Society General Meeting - Conversion and Delivery of Electrical Energy in the 21st Century*, Pittsburgh, 2008.

[30] F. Li and H. Yuan, "A comparative study of measurement-based Thevenin equivalents identification methods," in *2014 North American Power Symposium (NAPS)*, Pullman, 2014.

[31] K. Vu, M. M. Begovic, D. Novosel and M. M. Saha, "Use of local measurements to estimate voltage-stability margin," *IEEE Transactions on Power Systems,* vol. 14, no. 3, pp. 1029 - 1035, August 1999.

[32] I. Smon, G. Verbic and F. Gubina, "Local voltage-stability index using Tllegen's theorem," *IEEE Trans. Power Syst.,* vol. 213, pp. 1267-1275, 2006.

[33] S. Corsi and G. N. Taranto, "A Real-Time Voltage Instability Identification Algorithm Based on Local Phasor Measurements," *IEEE Transactions on Power Systems,* vol. 23, no. 3, pp. 1271 - 1279, 2008.

[34] Y. Wang, I. R. Pordanjani, W. Li, W. Xu, T. Chen, E. Vaahedi and J. Gurney, "Voltage Stability Monitoring Based on the Concept of Coupled Single-Port Circuit," *IEEE Transactions on Power Systems,* vol. 26, no. 4, pp. 2154 - 2163, 2011.

[35] G. Wadhwa, A. Kharb, S. Mishra, M. Kumar and S. Srivastav, "A Comprehensive Survey on Real-Time Voltage," in *15th (IEEE) International Conference on Industrial and Information Systems (ICIIS) 2020*, 2020.

[36] X. Mou, W. Li and Z. Li, "A preliminary study on the Thevenin equivalent impedance for power systems monitoring," in *2011 4th International Conference on Electric Utility Deregulation and Restructuring and Power Technologies (DRPT)*, Weihai, 2011.

[37] S. Polster and H. Renner, "Voltage stability monitoring methods fordistribution grids using the Theveninimpedance," in *24th International Conference & Exhibition on Electricity Distribution (CIRED)*, 2017.

[38] G. H. Gabriels, M. O. Windapo, D. T. Oyedokun and S. Ruggeri, "Proposed framework for Integration of Optimal Current Injection and Multi-Agent Control of the LV Distribution network," in *2020 6th IEEE International Energy Conference (ENERGYCon)*, Gammarth, 2020.

[39] South African Bureau of Standards, "The wiring of premises Part 1: Low-voltage installations," *South African Bureau of Standards,,* p. 51, 2001.

[40] G. H. Gabriels and D. T. O. Oyedokun, "Simultaneous Monitoring of the Thévenin Equivalent Impedance at Multiple PCC's on a Network," *IEEE PES/IAS PowerAfrica,* 2018.

[41] P. Penfield, R. Spence and S. Duinker, "A generalized form of Tellegen's theorem," *IEEE Transactions on Circuit Theory (,* vol. 17, no. 3, pp. 302 - 305, 1970.

[42] G. H. Gabriels, D. T. Oyedokun and S. Ruggeri, "“Realtime Thévenin Equivalent Impedance at a PCC in the Italian Power Grid," *2020 International SAUPEC/RobMech/PRASA Conference,* 2020.

[43] A. Mazza, H. Mirtaheri, G. Chicco, A. Russo and M. Fantino, "Location and Sizing of Battery Energy Storage Units," *Energies 2020,* vol. 13, no. 52, 2019.

[44] Spirit Energy, "Understanding Electric Car charging," Spirit Energy, 2020. [Online]. Available: https://www.spiritenergy.co.uk/kb-ev-understanding-electric-car-charging. [Accessed 2 September 2020].

[45] A. V. Adebayo, C. T. Gaunt, K. O. Awodele and M. Malengret, "Online Thévenin Equivalent Impedance Measuring System," in *2019 IEEE PES/IAS PowerAfrica*, Abuja, 2019.

[46] J. Ferber, Multi-Agent System: An Introduction to Distributed Artificial Intelligence, Addison-Wesley Professional, 1999.

[47] J. John and F. Nash, "Equilibrium points in n-person games," vol. 36, no. 1, pp. 48-49, 1950.

[48] M. Malengret and G. C T, "Inverters and Compensators for minimum line losses," University of Capetown, CapeTown.

[49] S. Ruggeri and F. Pilo, *Centralised and decentralised control of active distribution systems: models, algorithms and applications.,* Cagliari.

[50] T. Morstyn, B. Hredzak and V. G. Agelidis, "Control Strategies for Microgrids With Distributed Energy Storage Systems: An Overview," *IEEE Transactions on Smart Grid,* vol. 9, no. 4, pp. 3652 - 3666, 2018.

[51] A. R. Mele, Autonomous Agents, New York: Oxford University Press, 1995.

[52] F. Bergenti, M. Gleizes and F. Zambonelli, Methodologies and Software Engineering for Agent Systems: The Agent-Oriented Software Engineering Handbook, Kluwer Academic Publishers, 2004.

[53] A. Saleem, N. Honeth, Y. Wu and L. Nordström, "Integrated multi-agent testbed for decentralized control of active distribution networks," *2013 IEEE Power & Energy Society General Meeting,* 2013.

[54] Y. Han, K. Zhang, H. Li, E. A. Coelho and J. M. Guerrero , "MAS-Based Distributed Coordinated Control and Optimization in Microgrid and Microgrid Clusters A Comprehensive Overview," *IEEE Transactions on Power Electronics,* vol. 33, no. 8, pp. 6488 - 6508, 2017.

[55] M. Malengret and C. T. Gaunt, "Active Currents, Power Factor, and Apparent Power for Practical Power Delivery Systems," *IEEE Access,* vol. 8, 2020.

[56] "Understanding Electric Car charging," Spirit Energy, 2020. [Online]. Available: https://www.spiritenergy.co.uk/kb-ev-understanding-electric-car-charging. [Accessed 5 September 2020].

9 Appendix

9.1 MATLAB windows

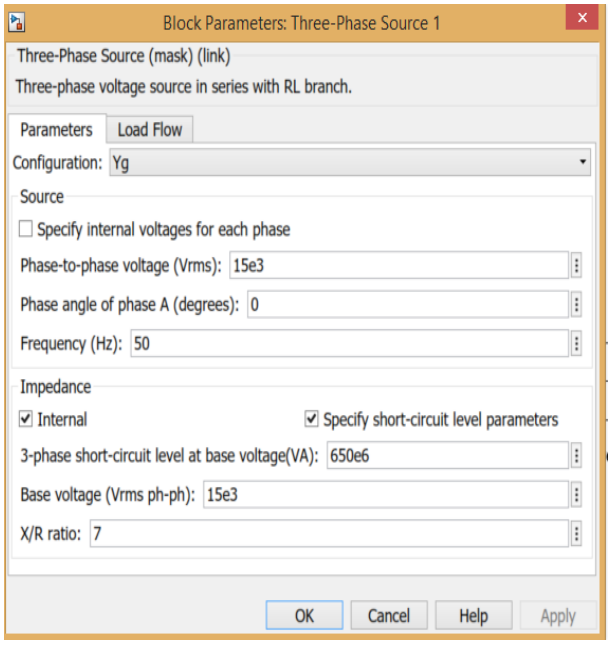

Figure 9-1: 3-phase source parameters 1

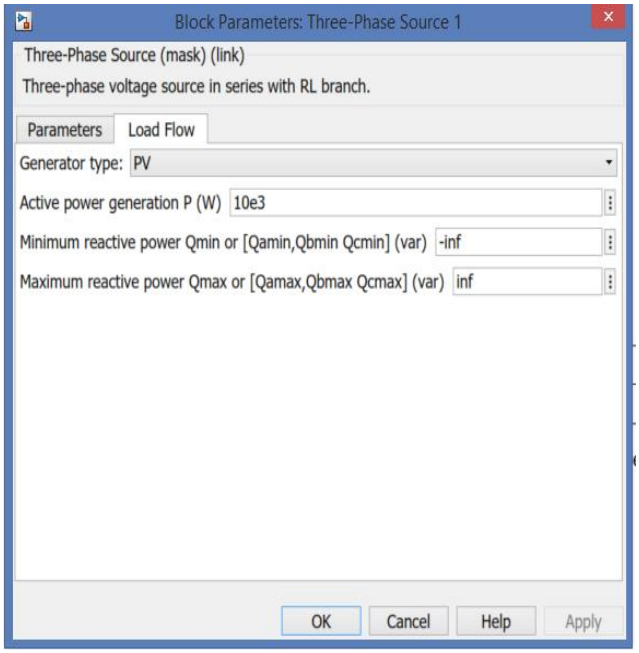

Figure 9-2: 3 phase source parameters 2

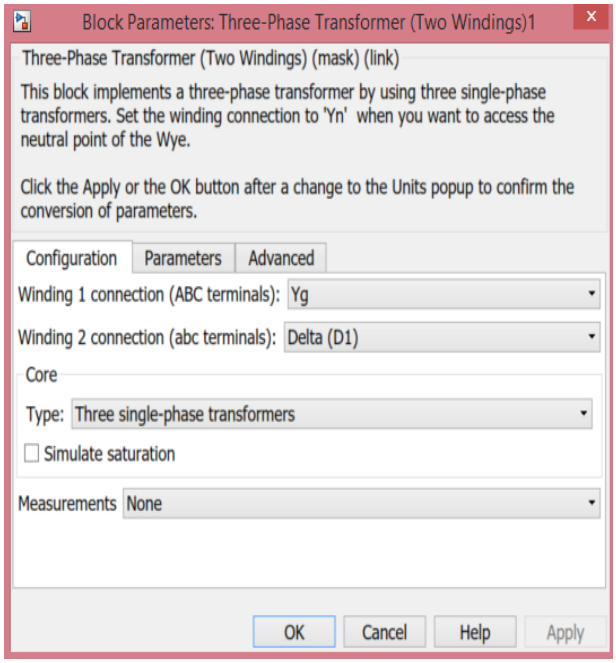

Figure 9-3: 3-phase transformer configuration

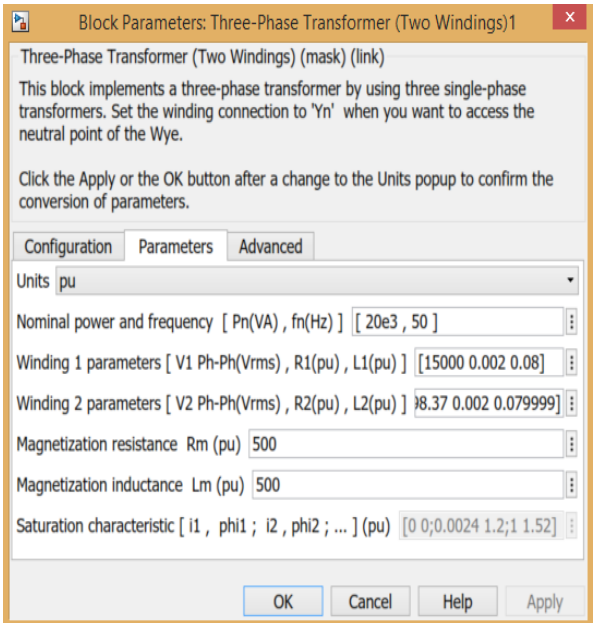

Figure 9-4: 3-phase transformer parameters

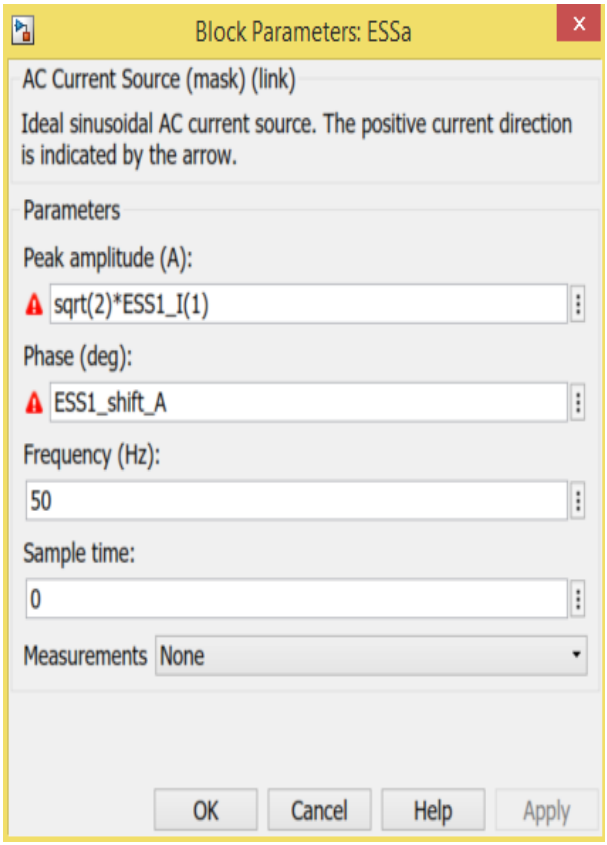

Figure 9-5: AC Current Source setup

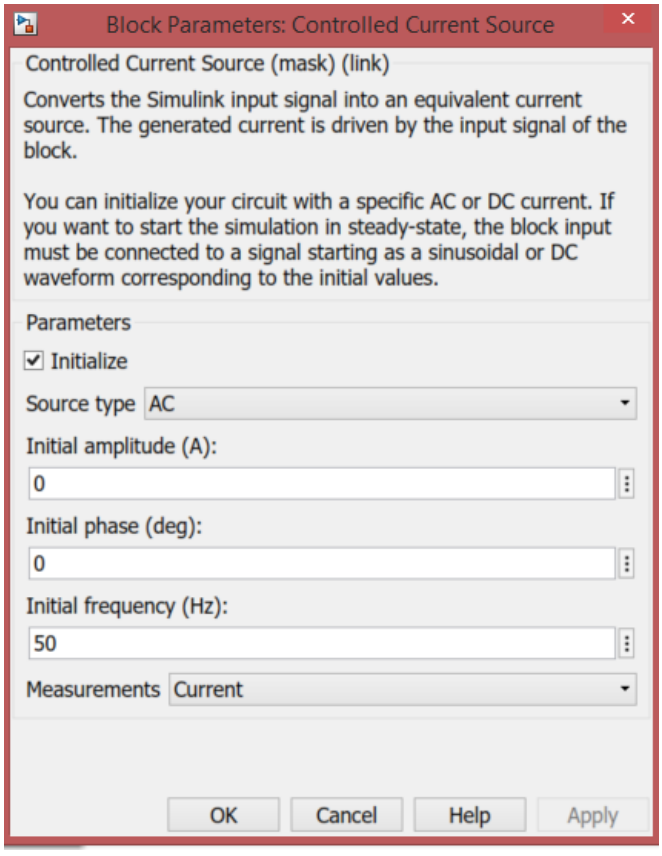

Figure 9-6: Controlled Current Source setup

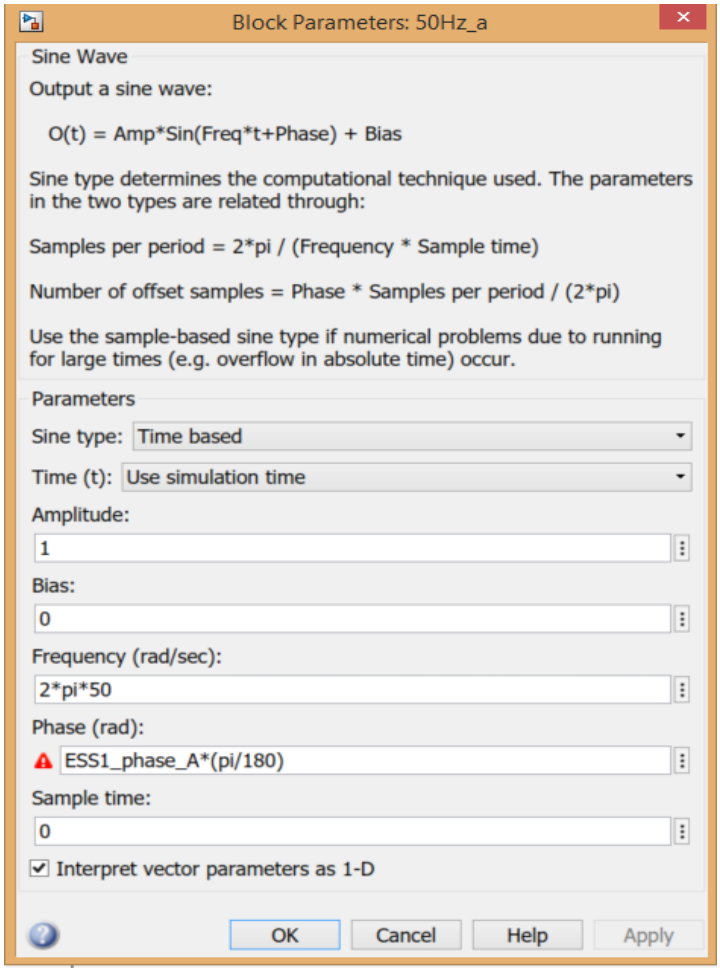

Figure 9-7: Sine Wave block setup

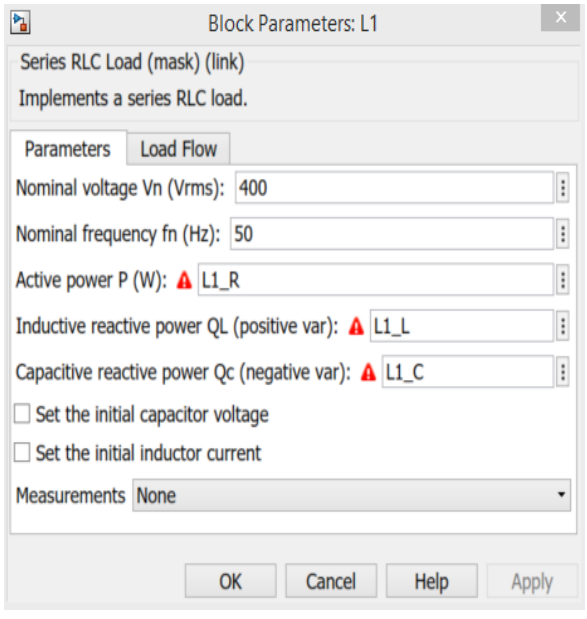

Figure 9-8: RLC Load parameters

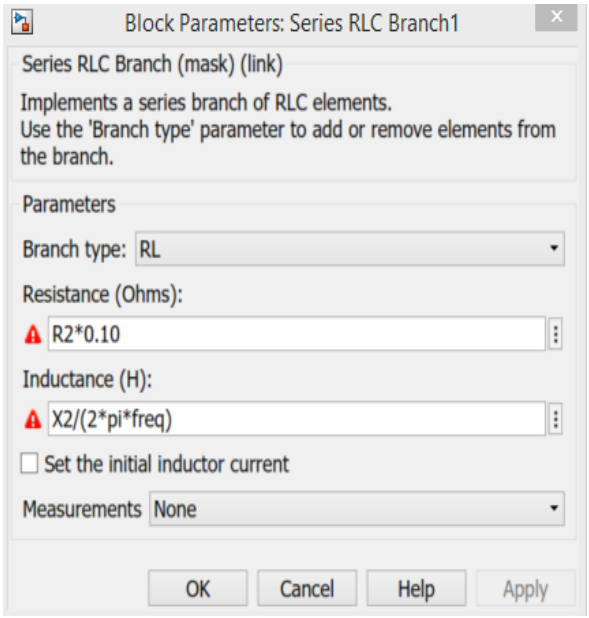

Figure 9-9: RLC Branch parameters

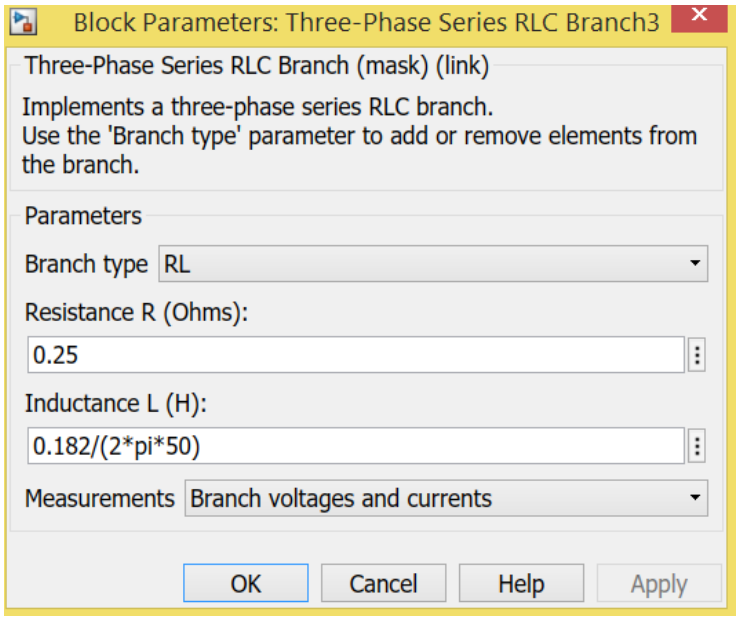

Figure 9-10:Transmission RLC branch parameters

9.2 Tables of TEI verification simulation

Table 9-1: Hand calculated Thevenin impedance at Bus 2 for a variable 3-phase load with a 1 pf

$R_{thh,ess,a}$ (Ω)	$R_{thh,ess,b}$ (Ω)	$R_{thh,ess,c}$ (Ω)	$X_{thh,ess,a}$ (Ω)	$X_{thh,ess,b}$ (Ω)	$X_{thh,ess,c}(\Omega)$	R_{load} (Ω) **(per phase)**
1.649	1.649	1.649	2.041	2.041	2.041	10

1.539	1.539	1.539	2.388	2.388	2.388	20
1.478	1.478	1.478	2.510	2.510	2.510	30
1.443	1.443	1.443	2.571	2.571	2.571	40
1.420	1.420	1.420	2.608	2.608	2.608	50
1.404	1.404	1.404	2.632	2.632	2.632	60
1.392	1.392	1.392	2.650	2.650	2.650	70
1.383	1.383	1.383	2.663	2.663	2.663	80
1.376	1.376	1.376	2.673	2.673	2.673	90
1.370	1.370	1.370	2.681	2.681	2.681	100
1.365	1.365	1.365	2.688	2.688	2.688	110
1.361	1.361	1.361	2.694	2.694	2.694	120
1.357	1.357	1.357	2.698	2.698	2.698	130
1.354	1.354	1.354	2.702	2.702	2.702	140
1.352	1.352	1.352	2.706	2.706	2.706	150
1.349	1.349	1.349	2.709	2.709	2.709	160
1.347	1.347	1.347	2.712	2.712	2.712	170
1.346	1.346	1.345	2.714	2.714	2.714	180
1.344	1.344	1.343	2.716	2.716	2.716	190
1.343	1.343	1.342	2.718	2.718	2.718	200
1.341	1.341	1.341	2.720	2.720	2.720	210
1.340	1.340	1.334	2.721	2.721	2.721	220
1.339	1.339	1.338	2.723	2.723	2.723	230
1.338	1.338	1.337	2.724	2.724	2.724	240

Table 9-2: Hand calculated Thevenin impedance at Bus 3 for a variable 3-phase load with a 1 pf

$R_{thh,ev,a}$ (Ω)	$R_{thh,ev,b}$ (Ω)	$R_{thh,ev,c}$ (Ω)	$X_{thh,ev,a}$ (Ω)	$X_{thh,ev,b}$ (Ω)	$X_{thh,ev,c}$(Ω)	R_{load} (Ω) (per phase)
1.787	1.786	1.787	2.031	2.031	2.031	10
1.692	1.692	1.692	2.418	2.418	2.418	20
1.635	1.635	1.635	2.556	2.556	2.556	30
1.601	1.601	1.601	2.626	2.626	2.626	40
1.578	1.578	1.578	2.668	2.668	2.668	50

1.563	1.563	1.563	2.696	2.696	2.696	60
1.551	1.551	1.551	2.716	2.716	2.716	70
1.542	1.542	1.542	2.731	2.731	2.731	80
1.535	1.535	1.535	2.743	2.743	2.743	90
1.529	1.530	1.529	2.752	2.752	2.752	100
1.524	1.525	1.525	2.760	2.760	2.760	110
1.520	1.520	1.521	2.766	2.766	2.766	120
1.517	1.517	1.517	2.772	2.772	2.772	130
1.514	1.514	1.514	2.776	2.776	2.776	140
1.511	1.511	1.511	2.780	2.780	2.780	150
1.509	1.509	1.509	2.784	2.784	2.784	160
1.507	1.507	1.507	2.787	2.787	2.787	170
1.505	1.505	1.506	2.790	2.790	2.790	180
1.503	1.503	1.504	2.792	2.792	2.792	190
1.502	1.502	1.503	2.794	2.794	2.794	200
1.501	1.501	1.501	2.796	2.796	2.796	210
1.500	1.500	1.500	2.798	2.798	2.798	220
1.499	1.499	1.499	2.800	2.800	2.800	230
1.498	1.498	1.498	2.801	2.801	2.801	240

Table 9-3: Hand calculated Thevenin impedance at Bus 2 for a variable 3-phase load with a 0.9 pf

$R_{thh,ess,a}$ (Ω)	$R_{thh,ess,b}$ (Ω)	$R_{thh,ess,c}$ (Ω)	$X_{thh,ess,a}$ (Ω)	$X_{thh,ess,b}$ (Ω)	$X_{thh,ess,c}$ (Ω)	R_{load} (Ω) (per phase)
1.375	1.375	1.375	2.083	2.083	2.083	11.111
1.371	1.371	1.371	2.385	2.385	2.385	22.222
1.359	1.359	1.359	2.500	2.500	2.500	33.333
1.351	1.351	1.351	2.560	2.560	2.560	44.444
1.345	1.345	1.345	2.598	2.598	2.598	55.555
1.341	1.341	1.341	2.623	2.623	2.623	66.667
1.338	1.338	1.338	2.641	2.641	2.641	77.778
1.335	1.335	1.335	2.655	2.655	2.655	88.889
1.333	1.333	1.333	2.666	2.666	2.666	100
1.331	1.331	1.331	2.675	2.675	2.675	111.111

1.330	1.330	1.330	2.682	2.682	2.682	122.222
1.329	1.329	1.329	2.688	2.688	2.688	133.333
1.328	1.328	1.328	2.693	2.693	2.693	144.444
1.327	1.327	1.327	2.697	2.697	2.697	155.555
1.326	1.326	1.326	2.701	2.701	2.701	166.667
1.325	1.325	1.325	2.704	2.704	2.704	177.778
1.325	1.325	1.325	2.707	2.707	2.707	188.889
1.324	1.324	1.324	2.710	2.710	2.710	200
1.323	1.323	1.323	2.712	2.712	2.712	211.111
1.323	1.323	1.323	2.714	2.714	2.714	222.222
1.323	1.323	1.323	2.716	2.716	2.716	233.333
1.322	1.322	1.322	2.718	2.718	2.718	244.445
1.322	1.322	1.322	2.720	2.720	2.720	255.556
1.322	1.322	1.322	2.721	2.721	2.721	266.667

Table 9-4: Hand calculated Thevenin impedance at Bus 3 for a variable 3-phase load with a 0.9 pf

$R_{thh,ev,a}$ (Ω)	$R_{thh,ev,b}$ (Ω)	$R_{thh,ev,c}$ (Ω)	$X_{thh,ev,a}$ (Ω)	$X_{thh,ev,b}$ (Ω)	$X_{thh,ev,c}$(Ω)	R_{load} (Ω) (per phase)
1.491	1.491	1.491	2.097	2.097	2.097	11.111
1.509	1.509	1.509	2.427	2.427	2.427	22.222
1.505	1.505	1.505	2.554	2.554	2.554	33.333
1.500	1.500	1.500	2.621	2.621	2.621	44.444
1.497	1.497	1.497	2.663	2.663	2.663	55.555
1.494	1.494	1.494	2.691	2.691	2.691	66.667
1.491	1.491	1.491	2.711	2.711	2.711	77.778
1.490	1.490	1.490	2.726	2.726	2.726	88.889
1.488	1.488	1.488	2.738	2.738	2.738	100
1.487	1.487	1.487	2.748	2.748	2.748	111.111
1.486	1.486	1.486	2.756	2.756	2.756	122.222
1.485	1.485	1.485	2.763	2.763	2.763	133.333
1.484	1.484	1.484	2.768	2.768	2.768	144.444
1.484	1.484	1.484	2.773	2.773	2.773	155.555
1.483	1.483	1.483	2.777	2.777	2.777	166.667

1.482	1.482	1.482	2.781	2.781	2.781	177.778
1.482	1.482	1.482	2.784	2.784	2.784	188.889
1.482	1.482	1.482	2.787	2.787	2.787	200
1.481	1.481	1.481	2.790	2.790	2.790	211.111
1.481	1.481	1.481	2.792	2.792	2.792	222.222
1.481	1.481	1.481	2.794	2.794	2.794	233.333
1.480	1.480	1.480	2.796	2.796	2.796	244.445
1.480	1.480	1.480	2.798	2.798	2.798	255.556
1.480	1.480	1.480	2.799	2.799	2.799	266.667

Table 9-5: TEI measured Thevenin impedance at Bus 2 for a variable 3-phase load with a 1 pf

$R_{thh,ess,a}$ (Ω)	$R_{thh,ess,b}$ (Ω)	$R_{thh,ess,c}$ (Ω)	$X_{thh,ess,a}$ (Ω)	$X_{thh,ess,b}$ (Ω)	$X_{thh,ess,c}(\Omega)$	R_{load} (Ω) (per phase)
1.335	1.328	1.329	1.176	1.168	1.170	10
1.362	1.356	1.365	1.362	1.377	1.354	20
1.373	1.382	1.373	1.461	1.452	1.448	30
1.379	1.399	1.386	1.513	1.511	1.510	40
1.391	1.411	1.388	1.555	1.550	1.568	50
1.405	1.416	1.407	1.579	1.586	1.585	60
1.412	1.424	1.424	1.605	1.607	1.597	70
1.421	1.433	1.435	1.626	1.626	1.621	80
1.421	1.442	1.454	1.640	1.640	1.646	90
1.426	1.453	1.456	1.660	1.664	1.664	100
1.430	1.457	1.463	1.667	1.675	1.677	110
1.436	1.462	1.470	1.679	1.683	1.688	120
1.440	1.466	1.477	1.692	1.693	1.699	130
1.447	1.474	1.473	1.712	1.703	1.717	140
1.452	1.478	1.478	1.722	1.712	1.726	150
1.456	1.484	1.481	1.735	1.717	1.741	160
1.465	1.485	1.486	1.756	1.714	1.748	170
1.467	1.490	1.491	1.761	1.721	1.755	180
1.471	1.492	1.495	1.768	1.723	1.761	190
1.476	1.501	1.499	1.776	1.734	1.767	200

1.479	1.499	1.505	1.782	1.736	1.779	210
1.482	1.505	1.503	1.787	1.742	1.769	220
1.485	1.507	1.504	1.796	1.747	1.771	230
1.492	1.510	1.507	1.794	1.751	1.775	240

Table 9-6: TEI measured Thevenin impedance at Bus 3 for a variable 3-phase load with a 1 pf

$R_{thh,ev,a}$ (Ω)	$R_{thh,ev,b}$ (Ω)	$R_{thh,ev,c}$ (Ω)	$X_{thh,ev,a}$ (Ω)	$X_{thh,ev,b}$ (Ω)	$X_{thh,ev,c}$(Ω)	R_{load} (Ω) (per phase)
1.472	1.466	1.471	1.203	1.182	1.197	10
1.517	1.518	1.518	1.411	1.424	1.403	20
1.537	1.543	1.533	1.538	1.514	1.509	30
1.543	1.565	1.551	1.582	1.580	1.593	40
1.556	1.578	1.557	1.625	1.624	1.637	50
1.573	1.587	1.588	1.652	1.677	1.664	60
1.581	1.597	1.596	1.683	1.695	1.679	70
1.591	1.601	1.606	1.705	1.711	1.702	80
1.592	1.611	1.622	1.721	1.724	1.723	90
1.599	1.626	1.636	1.743	1.758	1.748	100
1.606	1.641	1.638	1.758	1.770	1.763	110
1.610	1.639	1.646	1.764	1.766	1.775	120
1.615	1.646	1.654	1.778	1.778	1.787	130
1.624	1.655	1.650	1.805	1.788	1.806	140
1.629	1.659	1.656	1.815	1.797	1.816	150
1.638	1.662	1.661	1.829	1.796	1.839	160
1.642	1.665	1.667	1.846	1.809	1.847	170
1.646	1.670	1.672	1.851	1.816	1.854	180
1.650	1.675	1.677	1.859	1.823	1.861	190
1.655	1.676	1.677	1.867	1.819	1.862	200
1.659	1.680	1.681	1.874	1.825	1.868	210
1.663	1.685	1.684	1.879	1.831	1.871	220
1.667	1.682	1.688	1.890	1.832	1.876	230
1.669	1.686	1.692	1.904	1.837	1.880	240

Table 9-7: TEI measured Thevenin impedance at Bus 2 for a variable 3-phase load with a 0.9 pf

$R_{thh,ess,a}$ (Ω)	$R_{thh,ess,b}$ (Ω)	$R_{thh,ess,c}$ (Ω)	$X_{thh,ess,a}$ (Ω)	$X_{thh,ess,b}$ (Ω)	$X_{thh,ess,c}$(Ω)	Z_{load} (Ω) (per phase)
1.200	1.203	1.204	1.247	1.243	1.247	11.111
1.262	1.264	1.258	1.407	1.409	1.410	22.222
1.286	1.291	1.291	1.487	1.493	1.487	33.333
1.306	1.310	1.308	1.538	1.542	1.539	44.444
1.316	1.315	1.316	1.592	1.577	1.586	55.556
1.330	1.330	1.329	1.627	1.604	1.617	66.667
1.336	1.342	1.342	1.662	1.629	1.642	77.778
1.347	1.360	1.350	1.684	1.656	1.683	88.889
1.357	1.369	1.361	1.704	1.669	1.702	100
1.365	1.381	1.371	1.722	1.690	1.719	111.111
1.374	1.392	1.380	1.729	1.712	1.733	122.222
1.383	1.396	1.389	1.742	1.720	1.749	133.333
1.389	1.402	1.398	1.742	1.738	1.761	144.444
1.397	1.408	1.405	1.752	1.747	1.770	155.556
1.404	1.415	1.423	1.761	1.755	1.769	166.667
1.410	1.428	1.430	1.776	1.768	1.777	177.778
1.416	1.435	1.437	1.793	1.776	1.785	188.889
1.422	1.441	1.444	1.800	1.782	1.804	200
1.427	1.446	1.449	1.806	1.788	1.823	211.111
1.432	1.452	1.455	1.821	1.793	1.829	222.222
1.437	1.463	1.460	1.827	1.803	1.834	233.333
1.442	1.466	1.467	1.832	1.829	1.835	244.444
1.446	1.468	1.471	1.837	1.832	1.823	255.556
1.451	1.473	1.475	1.841	1.836	1.827	266.667

Table 9-8: TEI measured Thevenin impedance at Bus 3 for a variable 3-phase load with a 0.9 pf

$R_{thh,ev,a}$ (Ω)	$R_{thh,ev,b}$ (Ω)	$R_{thh,ev,c}$ (Ω)	$X_{thh,ev,a}$ (Ω)	$X_{thh,ev,b}$ (Ω)	$X_{thh,ev,c}$(Ω)	Z_{load} (Ω) (per phase)
1.323	1.327	1.327	1.290	1.288	1.290	11.111
1.405	1.408	1.401	1.470	1.484	1.474	22.222
1.437	1.444	1.441	1.560	1.572	1.562	33.333

1.462	1.466	1.465	1.621	1.623	1.618	44.444
1.476	1.476	1.475	1.677	1.662	1.669	55.556
1.492	1.491	1.491	1.717	1.686	1.703	66.667
1.500	1.505	1.507	1.749	1.712	1.756	77.778
1.513	1.520	1.516	1.773	1.743	1.773	88.889
1.525	1.545	1.529	1.794	1.771	1.794	100
1.536	1.553	1.540	1.812	1.790	1.812	111.111
1.545	1.561	1.551	1.822	1.799	1.827	122.222
1.556	1.567	1.560	1.831	1.822	1.847	133.333
1.565	1.573	1.571	1.844	1.829	1.856	144.444
1.571	1.582	1.579	1.851	1.839	1.867	155.556
1.579	1.590	1.600	1.861	1.848	1.875	166.667
1.586	1.596	1.608	1.872	1.862	1.883	177.778
1.593	1.603	1.615	1.899	1.871	1.904	188.889
1.600	1.616	1.622	1.906	1.875	1.911	200
1.606	1.622	1.628	1.913	1.881	1.920	211.111
1.611	1.629	1.637	1.925	1.896	1.920	222.222
1.615	1.640	1.643	1.926	1.907	1.926	233.333
1.621	1.650	1.648	1.931	1.916	1.929	244.444
1.626	1.654	1.654	1.936	1.92	1.931	255.556
1.631	1.659	1.656	1.940	1.931	1.926	266.667

Table 9-9: Hand calculated Thevenin impedance at bus 2 for a variable 3-phase load with a 1 pf (no transformer)

$R_{thh,ess,a}$ (Ω)	$R_{thh,ess,b}$ (Ω)	$R_{thh,ess,c}$ (Ω)	$X_{thh,ess,a}$ (Ω)	$X_{thh,ess,b}$ (Ω)	$X_{thh,ess,c}$(Ω)	R_{load} (Ω) (per phase)
1.115	1.115	1.115	0.145	0.145	0.145	10
1.178	1.178	1.178	0.161	0.161	0.161	20
1.201	1.201	1.201	0.167	0.167	0.167	30
1.212	1.212	1.212	0.171	0.171	0.171	40
1.220	1.220	1.220	0.173	0.173	0.173	50
1.225	1.225	1.225	0.174	0.174	0.174	60
1.228	1.228	1.228	0.175	0.175	0.175	70
1.231	1.231	1.231	0.176	0.176	0.176	80

1.233	1.233	1.233	0.177	0.177	0.177	90
1.234	1.234	1.234	0.177	0.177	0.177	100
1.236	1.236	1.236	0.177	0.177	0.177	110
1.237	1.237	1.237	0.178	0.178	0.178	120
1.238	1.238	1.238	0.178	0.178	0.178	130
1.239	1.239	1.239	0.178	0.178	0.178	140
1.239	1.239	1.239	0.179	0.179	0.179	150
1.240	1.240	1.240	0.179	0.179	0.179	160
1.241	1.241	1.241	0.179	0.179	0.179	170
1.241	1.241	1.241	0.179	0.179	0.179	180
1.242	1.242	1.242	0.179	0.179	0.179	190
1.242	1.242	1.242	0.179	0.179	0.179	200
1.242	1.242	1.242	0.179	0.179	0.179	210
1.243	1.243	1.243	0.180	0.180	0.180	220
1.243	1.243	1.243	0.180	0.180	0.180	230
1.243	1.243	1.243	0.180	0.180	0.180	240

Table 9-10: Hand calculated Thevenin impedance at bus 3 for a variable 3-phase load with a 1 pf (no transformer)

$R_{thh,ev,a}$ (Ω)	$R_{thh,ev,b}$ (Ω)	$R_{thh,ev,c}$ (Ω)	$X_{thh,ev,a}$ (Ω)	$X_{thh,ev,b}$ (Ω)	$X_{thh,ev,c}$ (Ω)	R_{load} (Ω) (per phase)
1.240	1.240	1.240	0.203	0.203	0.203	10
1.320	1.320	1.320	0.230	0.230	0.230	20
1.349	1.349	1.349	0.241	0.241	0.241	30
1.364	1.364	1.364	0.246	0.246	0.246	40
1.373	1.373	1.373	0.250	0.250	0.250	50
1.379	1.379	1.379	0.252	0.252	0.252	60
1.383	1.383	1.383	0.254	0.254	0.254	70
1.386	1.386	1.386	0.255	0.255	0.255	80
1.389	1.389	1.389	0.256	0.256	0.256	90
1.391	1.391	1.391	0.257	0.257	0.257	100
1.393	1.393	1.393	0.257	0.257	0.257	110
1.394	1.394	1.394	0.258	0.258	0.258	120

1.395	1.395	1.395	0.258	0.258	0.258	130
1.396	1.396	1.396	0.259	0.259	0.259	140
1.397	1.397	1.397	0.259	0.259	0.259	150
1.398	1.398	1.398	0.259	0.259	0.259	160
1.399	1.399	1.399	0.260	0.260	0.260	170
1.399	1.399	1.399	0.260	0.260	0.260	180
1.400	1.400	1.400	0.260	0.260	0.260	190
1.401	1.401	1.401	0.260	0.260	0.260	200
1.401	1.401	1.401	0.261	0.261	0.261	210
1.401	1.401	1.401	0.261	0.261	0.261	220
1.402	1.402	1.402	0.261	0.261	0.261	230
1.402	1.402	1.402	0.261	0.261	0.261	240

Table 9-11: TEI measured Thevenin impedance at bus 2 for a variable 3-phase load with a 1 pf (no Transformer)

$R_{thh,ess,a}$ (Ω)	$R_{thh,ess,b}$ (Ω)	$R_{thh,ess,c}$ (Ω)	$X_{thh,ess,a}$ (Ω)	$X_{thh,ess,b}$ (Ω)	$X_{thh,ess,c}(\Omega)$	R_{load} (Ω) (per phase)
1.128	1.128	1.126	0.156	0.156	0.157	10
1.207	1.207	1.206	0.181	0.181	0.179	20
1.243	1.244	1.243	0.192	0.191	0.191	30
1.267	1.269	1.266	0.199	0.197	0.196	40
1.286	1.287	1.284	0.207	0.202	0.202	50
1.302	1.300	1.299	0.214	0.204	0.209	60
1.314	1.311	1.311	0.218	0.206	0.212	70
1.325	1.321	1.322	0.222	0.208	0.216	80
1.335	1.330	1.331	0.225	0.209	0.218	90
1.344	1.338	1.340	0.227	0.210	0.225	100
1.351	1.347	1.348	0.229	0.214	0.226	110
1.357	1.353	1.354	0.229	0.213	0.228	120
1.362	1.36	1.361	0.227	0.221	0.229	130
1.368	1.366	1.366	0.228	0.225	0.230	140
1.371	1.371	1.373	0.229	0.222	0.232	150
1.376	1.377	1.378	0.230	0.224	0.233	160
1.382	1.381	1.382	0.232	0.224	0.234	170

1.386	1.385	1.385	0.233	0.225	0.236	180
1.390	1.389	1.389	0.234	0.225	0.236	190
1.394	1.393	1.393	0.234	0.223	0.237	200
1.397	1.397	1.396	0.235	0.225	0.238	210
1.400	1.400	1.399	0.235	0.225	0.238	220
1.404	1.403	1.402	0.233	0.225	0.239	230
1.407	1.406	1.405	0.234	0.226	0.239	240

Table 9-12: TEI measured Thevenin impedance at bus 3 for a variable 3-phase load with a 1 pf (no Transformer)

$R_{thh,ev,a}$ (Ω)	$R_{thh,ev,b}$ (Ω)	$R_{thh,ev,c}$ (Ω)	$X_{thh,ev,a}$ (Ω)	$X_{thh,ev,b}$ (Ω)	$X_{thh,ev,c}(\Omega)$	R_{load} (Ω) **(per phase)**
1.256	1.255	1.253	0.217	0.217	0.219	10
1.354	1.35	1.352	0.258	0.255	0.253	20
1.397	1.398	1.396	0.273	0.271	0.270	30
1.426	1.427	1.425	0.283	0.281	0.282	40
1.448	1.448	1.446	0.291	0.288	0.291	50
1.467	1.465	1.463	0.303	0.293	0.300	60
1.482	1.477	1.478	0.308	0.296	0.304	70
1.494	1.489	1.490	0.314	0.299	0.312	80
1.505	1.500	1.501	0.318	0.303	0.315	90
1.516	1.510	1.511	0.320	0.305	0.318	100
1.525	1.519	1.520	0.323	0.311	0.322	110
1.533	1.526	1.528	0.325	0.312	0.324	120
1.537	1.535	1.535	0.324	0.310	0.326	130
1.544	1.542	1.541	0.326	0.315	0.328	140
1.549	1.548	1.547	0.328	0.316	0.329	150
1.555	1.554	1.553	0.330	0.318	0.331	160
1.559	1.559	1.560	0.326	0.315	0.333	170
1.565	1.563	1.564	0.327	0.316	0.334	180
1.569	1.568	1.569	0.327	0.317	0.335	190
1.574	1.572	1.573	0.330	0.318	0.336	200
1.578	1.576	1.576	0.331	0.319	0.335	210
1.581	1.580	1.579	0.331	0.320	0.336	220

1.584	1.583	1.583	0.332	0.321	0.337	230
1.588	1.586	1.586	0.334	0.321	0.338	240

Table 9-13: TEI measured Thevenin impedance at bus 2 for a variable 3-phase load with a 1 pf

$R_{th,a}(\Omega)$	$R_{th,b}(\Omega)$	$R_{th,c}(\Omega)$	$X_{th,a}(\Omega)$	$X_{th,b}(\Omega)$	$X_{th,c}(\Omega)$	R_l (Ω) (per phase)
2.645	2.625	2.615	2.233	2.233	2.253	10
2.738	2.733	2.730	2.680	2.691	2.677	20
2.806	2.810	2.792	2.930	2.903	2.915	30
2.844	2.867	2.850	3.083	3.051	3.052	40
2.897	2.918	2.886	3.189	3.165	3.214	50
2.940	2.959	2.961	3.260	3.239	3.280	60
2.981	2.998	3.014	3.337	3.358	3.354	70
3.018	3.031	3.040	3.395	3.401	3.417	80
3.038	3.069	3.077	3.467	3.460	3.477	90
3.071	3.102	3.111	3.521	3.513	3.531	100
3.101	3.134	3.142	3.569	3.567	3.578	110
3.122	3.174	3.174	3.601	3.639	3.622	120
3.151	3.191	3.182	3.661	3.672	3.677	130
3.178	3.207	3.208	3.708	3.694	3.715	140
3.206	3.232	3.228	3.766	3.728	3.761	150
3.232	3.265	3.252	3.806	3.772	3.792	160
3.253	3.287	3.273	3.840	3.801	3.830	170
3.268	3.290	3.294	3.854	3.786	3.857	180
3.287	3.308	3.314	3.880	3.810	3.882	190
3.305	3.326	3.334	3.903	3.832	3.921	200
3.321	3.345	3.339	3.945	3.853	3.903	210
3.337	3.354	3.354	3.966	3.880	3.917	220
3.353	3.370	3.370	3.985	3.898	3.936	230
3.3707	3.3847	3.3847	4.019	3.9158	3.9525	240

Table 9-14: TEI measured Thevenin impedance at bus 3 for a variable 3-phase load with a 1 pf

$R_{th,a}(\Omega)$	$R_{th,b}(\Omega)$	$R_{th,c}(\Omega)$	$X_{th,a}(\Omega)$	$X_{th,b}(\Omega)$	$X_{th,c}(\Omega)$	R_l (Ω) (per phase)

2.859	2.837	2.823	2.435	2.440	2.459	10
2.951	2.945	2.941	2.910	2.927	2.910	20
3.019	3.026	3.004	3.181	3.155	3.167	30
3.058	3.085	3.065	3.347	3.316	3.316	40
3.114	3.139	3.102	3.464	3.442	3.493	50
3.161	3.183	3.183	3.543	3.524	3.568	60
3.204	3.223	3.240	3.629	3.656	3.651	70
3.244	3.258	3.268	3.694	3.704	3.721	80
3.265	3.299	3.306	3.773	3.771	3.788	90
3.301	3.336	3.344	3.834	3.831	3.849	100
3.333	3.369	3.377	3.888	3.891	3.902	110
3.355	3.411	3.411	3.925	3.972	3.952	120
3.386	3.429	3.420	3.991	4.009	4.014	130
3.415	3.448	3.448	4.044	4.034	4.056	140
3.445	3.474	3.468	4.109	4.074	4.108	150
3.472	3.510	3.493	4.155	4.124	4.144	160
3.495	3.533	3.516	4.193	4.156	4.188	170
3.512	3.538	3.539	4.210	4.141	4.219	180
3.533	3.558	3.560	4.239	4.169	4.247	190
3.552	3.577	3.581	4.266	4.195	4.291	200
3.569	3.597	3.587	4.312	4.218	4.273	210
3.586	3.608	3.605	4.336	4.249	4.289	220
3.603	3.624	3.622	4.358	4.270	4.311	230
3.622	3.640	3.638	4.396	4.291	4.331	240

Table 9-15: The TEI values for bus 2 and bus 3

$R_{thh,ess,a}$ (Ω)	$R_{thh,ess,b}$ (Ω)	$R_{thh,ess,c}$ (Ω)	$R_{thh,ev,a}$ (Ω)	$R_{thh,ev,b}$ (Ω)	$R_{thh,ev,c}$ (Ω)	**%Unbalance (phase)**
6.338	6.358	6.081	6.534	6.551	6.255	5a
6.060	6.353	6.363	6.255	6.546	6.538	5b
6.342	6.075	6.360	6.537	6.272	6.535	5c
6.430	6.453	5.892	6.626	6.647	6.067	10a
5.872	6.445	6.458	6.067	6.638	6.633	10b
6.437	5.885	6.452	6.632	6.078	6.627	10c

6.521	6.548	5.703	6.716	6.741	5.879	15a
5.684	6.542	6.553	5.879	6.736	6.728	15b
6.531	5.692	6.543	6.726	5.885	6.718	15c
6.611	6.642	5.515	6.805	6.835	5.690	20a
5.496	6.635	6.647	5.690	6.832	6.826	20b
6.625	5.503	6.634	6.820	5.697	6.809	20c
6.702	6.736	5.326	6.896	6.934	5.502	25a
5.307	6.725	6.731	5.501	6.923	6.906	25b
6.707	5.315	6.724	6.905	5.508	6.899	25c
6.790	6.830	5.137	6.986	7.027	5.312	30a
5.118	6.822	6.824	5.315	7.012	7.000	30b
6.801	5.125	6.814	6.994	5.319	6.989	30c
6.880	6.923	4.947	7.075	7.121	5.140	35a
4.928	6.907	6.910	5.126	7.101	7.085	35b
6.893	4.936	6.904	7.087	5.130	7.079	35c
6.969	7.017	4.758	7.165	7.213	4.951	40a
4.742	6.993	7.002	4.938	7.183	7.177	40b
6.986	4.746	6.993	7.180	4.940	7.168	40c

9.3 Detailed unbalanced chart

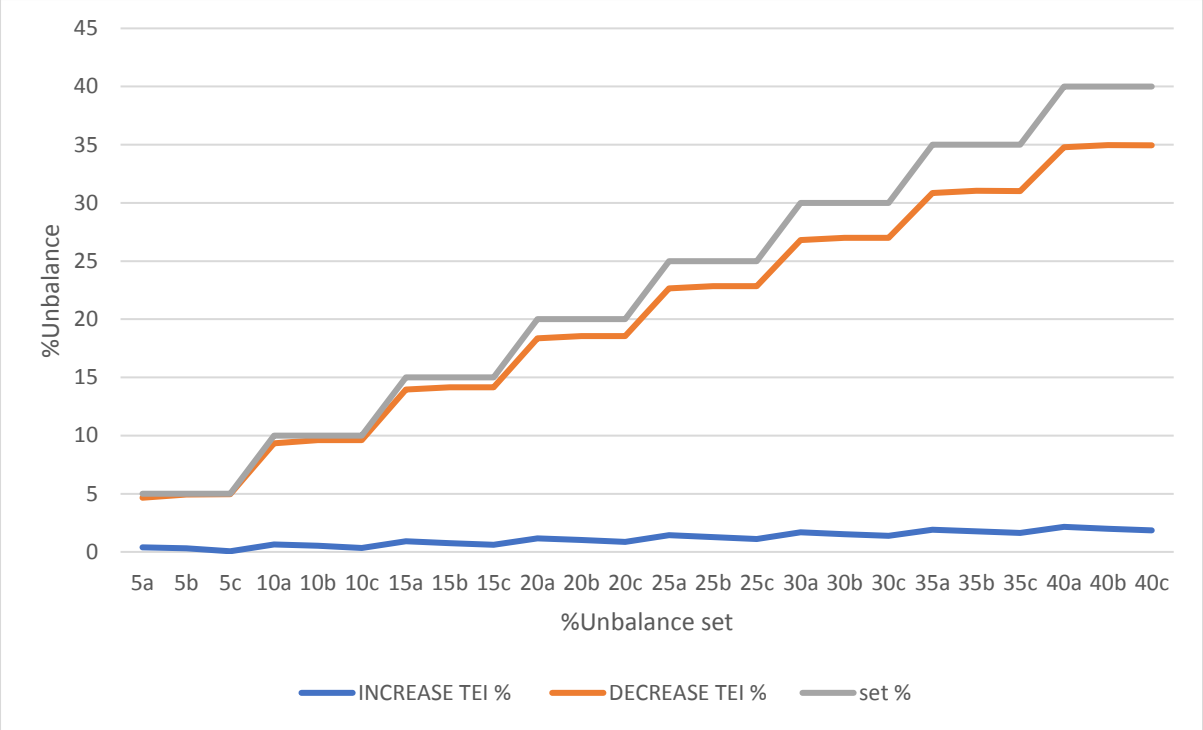

Figure 9-11: A chart showing the TEI sensors response to unbalance of Bus 2